# Transparent Exopolymer Particles and Phytoplankton Nutrient Physiology in the North Pacific and Arctic Oceans

by

Michael Douglas Livingston
B. Sc. Honours, University of Guelph, 2017

A Dissertation Submitted in Partial Fulfillment of the Requirements for the Degree of

DOCTOR OF PHILOSOPHY

in the Department of Biology

## Supervisory Committee

Transparent Exopolymer Particles and Phytoplankton Nutrient Physiology in the North Pacific and Arctic Oceans

by

Michael Douglas Livingston
B. Sc. Honours, University of Guelph, 2017

Dr. Diana E. Varela, Department of Biology & School of Earth and Ocean Sciences
*Supervisor*

Dr. Rana El-Sabaawi, Department of Biology
*Departmental Member*

Dr. Roberta C. Hamme, School of Earth and Ocean Sciences
*Outside Member*

Dr. Jay Cullen, School of Earth and Ocean Sciences
*Outside Member*

## Abstract

The export of organic carbon from the surface to the deep ocean is a key process that regulates the level of carbon dioxide ($CO_2$) in the atmosphere, and is known as the biological carbon pump (BCP). The efficiency of the BCP is largely governed by biological influences in the upper layers of the water column, including the magnitude of primary production, and the sinking rate of particulate organic carbon (POC). However, these processes are still poorly understood in large parts of the ocean. A key factor affecting the BCP is the presence of transparent exopolymer particles (TEP) in the surface ocean. These particles originate from the exudation of organic exopolymeric substances by marine phytoplankton and form sticky carbon (C) gels that facilitate the aggregation of organic matter. These particles are less dense than seawater and affect the sinking of POC from the surface to the deep ocean, and therefore play an important role in the ocean's C cycle. The overall objective of this thesis was to quantify key biological factors that affect surface ocean C cycling and to investigate the effects of variation in environmental conditions on the strengths of these factors. Over a 4-year study, I examined the concentrations and rates of production of TEP, phytoplankton nutrient physiology, and contributions of different sized phytoplankton to nutrient cycling in the Eastern Subarctic North Pacific (ESNP), and Pacific and Central Arctic regions. Measurements of TEP and a variety of biological and environmental variables were made across all regions in the ESNP and Arctic, and total and size-fractionated nutrient uptake rates of C, nitrate ($NO_3^-$) and silicic acid ($Si(OH)_4$) were additionally measured across the ESNP. The concentrations of TEP were largely correlated with the amount of phytoplankton biomass and productivity, but also by environmental variables such as

temperature, mixed layer depth, and nutrient concentrations. We used multivariate models derived from experimental observations measured during this study to produce novel estimates of surface TEP concentrations in the ESNP from 1998 to 2018. Model results show that the concentration of C in the form of TEP (TEP-C) in the surface of oceanic regions of the ESNP is estimated to be between 5-15µg C $L^{-1}$ year-round. We further measured TEP concentrations relative to C fixation by phytoplankton and export potential (i.e., new production), providing the first quantitative comparison among these variables across large spatiotemporal gradients in the ESNP. Results show that low productivity regimes are characterized by higher concentrations of TEP-C (and higher estimates of TEP-C turnover) relative to C uptake and new production, which suggests these regions may undergo less efficient C export. This thesis presents the first field-based connection between excess C consumption by phytoplankton and TEP concentrations. Size-fractionated measurements reveal that small-sized phytoplankton (< 5 µm) are responsible for most of the nutrient uptake and TEP production in the oceanic and less-productive regions of the ESNP. The contribution of the small size-class to nutrient uptake rates did not appear to be influenced by environmental variations. Overall, this work provides new perspectives on surface ocean C cycling in the ESNP by shedding light on the main predictors of TEP, predicting TEP-C concentrations, and by relating TEP-C to total primary productivity and new production. It is also the first of its kind to measure total and size-fractionated Si uptake over large spatiotemporal scales.

# Table of Contents

# List of Tables

# List of Figures

# Acknowledgements

This thesis would not have been possible without the support and assistance from many people in my life. Firstly, I would like to thank my supervisor, Diana Varela. Her guidance, advice, and leadership were invaluable in shaping not only my dissertation, but also my personal and professional development. My time in her lab represents a period of my life that I will never forget and has provided me with lessons and experiences that I will use throughout my career. Diana's guidance will be sorely missed in my future endeavors.

I would also like to specifically thank Shea Wyatt. This thesis would not be of the same quality (or even finished by this date) without his support. I can't recall a single day when we were both working in the student offices where I did not bother him with science questions. Furthermore, he is responsible for taking samples for this work throughout the Arctic. He is truly a knowledgeable scientist and an invaluable contributor to this research.

Becca, Olivia, Nimrod, and Sile – thank you all for your support, sample collection, and most importantly friendship. While I will fondly remember all of our time in the lab, it is our time spent out of the lab that I will remember most. I would also like to thank my family for their continuous support throughout this time of my life – the good days and the bad. I promise it was worth the stress I put on you all.

I would also like to thank the scientists at the Institute of Ocean Sciences. This dissertation was entirely field based, and the multitude of cruises required to construct it would not have been possible without you. Marie Robert – thank you for your patience, excellent leadership, and management of the Line P program that provides the backbone of this work. I also need to thank the captains and crews of the CCGS John P. Tully, CCGS Sir Wilfrid Laurier, and CCGS Louis S. St-Laurent for their contributions to managing the oceanographic programs that make work like this possible.

# Chapter 1: General Introduction

## 1.1 Phytoplankton and the Biological Carbon Pump

Phytoplankton fix large amounts of carbon (C) from the atmosphere via photosynthesis and are responsible for approximately 40-50% of total global C fixation (Field et al., 1998). Carbon is fixed in a phytoplankton cell through the Calvin cycle, where carbon dioxide ($CO_2$) is reduced to carbohydrates using light energy absorbed by photosynthetic pigments. This process provides the necessary organic building blocks for phytoplankton biomass, including glucose, sucrose, starch, cellulose, and other complex polysaccharides (Russell et al., 2010). Approximately 50 Gt $CO_2$ are fixed and incorporated into phytoplankton biomass as particulate C annually owing to this process (Field et al., 1998).

As phytoplankton inhabit the upper layers of the ocean where photosynthetically active radiation (PAR) is available, much of the particulate organic carbon (POC) produced from photosynthesis is originally formed in the euphotic zone of the world's oceans. Gravitationally settling draws POC out of the euphotic zone and transfers it to the deeper regions of the ocean, accounting for a flux of approximately 11 Gt C $yr^{-1}$ (Sanders et al., 2014). This C can be further sequestered in deep sediments for up to several thousand years, effectively removing it from contact with the atmosphere. A world without an operational BCP would result in atmospheric $CO_2$ concentrations approximately 400 ppm higher than they are today (Boyd, 2015). Other contributions to C sequestration in the ocean include the subduction of dissolved inorganic C to depth (known as the solubility pump) and the vertical transfer of organic C via zooplankton migration (Hansell et al., 2012; Steinberg et al., 2008).

## 1.2 Variation in the Efficiency of the Biological Carbon Pump

The BCP is a critically important process for the export and sequestration of C. This process can be fairly inefficient with a large fraction of primary production remineralized and respired by heterotrophic microbial activity back into $CO_2$ or respired by zooplankton grazing in the euphotic zone, with only an average of 10-30% of POC exported below 100 m (Buesseler & Boyd, 2009; Martin et al., 1987; Thomalla et al., 2008). The efficiency of the BCP is influenced by three general processes: the flux of $CO_2$ into POC through primary production in the euphotic zone, the rate of remineralization (or grazing) of POC aggregates in surface and deep waters, and the specific gravity of POC sinking rate (Banse, 1990; De La Rocha & Passow, 2007). Aggregates with higher specific gravities escape remineralization and grazing more than less dense aggregates that undergo greater exposure to heterotrophic activity in the euphotic zone. Thus, factors that control the density of organic aggregates, such as the production and prevalence of highly hydrated buoyant organic gels, and the presence of mineral ballasting agents (such as silica; Si and calcium carbonate), and the porosity of aggregates will impact the overall efficiency of C export. Furthermore, the BCP efficiency is also a product of the size structure of phytoplankton assemblages or communities (Herndl & Reinthaler, 2013). Larger, heavier cells are known to disproportionally contribute to C export compared to their smaller-celled and generally unballasted counterparts due to their faster sinking speeds and higher C content (Passow & Carlson, 2012).

The aggregation and specific density of organic material, phytoplankton productivity, and phytoplankton assemblage structure are all important elements that influence the efficiency of POC export from the euphotic zone (De La Rocha & Passow, 2007). While the BCP is can be inefficient under certain conditions, there are exceptions where its efficiency is considerably

higher, particularly within polar regions where it can range from 30-100% (Buesseler, 1998) or in highly productive continental margins (Jahnke, 1996). The underlying biological mechanisms that influence the efficiency of C export are not yet fully understood and are therefore critical to constrain for a more comprehensive understanding of the ocean C cycle.

## 1.3 The Role of Transparent Exopolymer Particles in Surface Ocean Carbon Cycling

Transparent exopolymer particles (TEP) are a class of organic marine particles composed of exopolymeric substances (EPS) primarily derived from the metabolic exudation of excess C from photosynthesis, or from the degradation of algal cells (Passow & Alldredge, 1995a). TEP is operationally defined as substances greater than 0.4 μm and stainable with Alcian blue dye (Passow & Alldredge, 1995a). The production and formation of TEP is largely attributed to the cellular metabolism of phytoplankton (and to a lesser extent, bacteria), whereas the active or passive excretion of polysaccharides (EPS) produce the necessary dissolved precursor materials that naturally coagulates to form larger TEP particles. TEP is ubiquitous in the world's ocean, with some estimates suggesting 10% of the total dissolved organic C (DOC) inventory in the ocean represents EPS precursors to TEP (Verdugo et al., 2004). It is these particles (TEP), and their inherent characteristics, that have received considerable attention in the last 3 decades owing to their influence on the surface ocean C cycle.

Current literature has established that TEP promotes the aggregation of organic matter, facilitating the formation of POC aggregates that enhances C export from the euphotic zone (Mari et al., 2017; Passow, 2002b; Passow & Alldredge, 1995b; Seebah et al., 2014). Despite being 'sticky', TEP has a lower specific gravity than seawater (densities of 0.7-0.84 g $cm^{-3}$ and

1.03 g $cm^{-3}$, respectively), resulting in a buoyant TEP matrix when unballasted in the water column (Azetsu-Scott & Passow, 2004). These two characteristics have important implications for the downward export of C from surface waters. Efficient C export is dependent on the gravitational settling velocity of an aggregate (Banse, 1990), which TEP can increase through the coagulation of smaller POC particles into larger, heavier, aggregates (Passow & Alldredge, 1995b). However, the positive buoyancy of TEP means than when concentrations of TEP are high relative to the POC generated through primary production (i.e., high TEP:POC ratios), the overall specific gravity and therefore sinking velocity of the aggregate decreases (Azetsu-Scott & Passow, 2004; Mari et al., 2017). As such, TEP plays a dual role in the vertical flux of particulate C in the ocean depending on its concentration relative to other POC (i.e., %TEP-C) (Azetsu-Scott & Passow, 2004). Since TEP is an organic particulate substance, it is possible to directly compare concentrations of TEP based C (TEP-C) with total POC concentrations; this yields the TEP:POC ratio, or the %TEP-C. The dual role of TEP has been directly attributed to the observed decoupling of primary production and C export out of surface waters (Boyd et al., 2000; Kiørboe et al., 1998; Nodder & Waite, 2001; Pitcher et al., 1991), as the relative concentration of TEP-C within POC aggregates influences its sinking velocity, and thus the fraction of primary production that is exported from the euphotic zone before it is remineralized (Mari et al., 2017).

Despite the biogeochemical importance of TEP, little research currently exists into the factors that control its production and standing stocks in the ocean, and in quantifying the impact of such potential predictors on TEP concentrations. It is surprising that no attempts have yet been made at predicting TEP concentrations from its major driving influences, as it has been well established that TEP is primarily driven by phytoplankton biomass and physiology (i.e. C

consumption, nutrient limitation), and that it may be possible to predict TEP using chlorophyll *a* across horizontal gradients at the ocean's surface (Ortega-Retuerta et al., 2017). As such, it may be possible to derive accurate predictions of TEP at the ocean's surface if a modelling approach is used to understand the empirical relationships between concentrations of TEP and commonly measured hydrographic and biogeochemical parameters.

## 1.4 Quantification of Transparent Exopolymer Particles

The quantification of TEP is primarily done via colorimetric methods using the Alcian blue stain (copper-phtalocyanin with four methylene-tetramethylcisothiouronium-chloride sidechains) (Passow & Alldredge, 1995a). Alcian blue, frequently used in medical and biological research to stain mucous layers and extracellular polysaccharides, is a hydrophilic cationic dye that binds with the anionic carboxyl (-COOH) and half-ester-sulfate (O-$SO_3$) groups of acidic polysaccharides. If the pH of the Alcian blue solution is approximately 2.5, it will selectively stain both carboxyl and sulfated polysaccharides, providing the ability for a quantitative colorimetric assessment of the concentration of extracellular polysaccharides in the stained material. Because the dye coagulates with dissolved salt substrates, the stain should only be added to a sample after seawater has been eliminated and salts washed by filtration. Absorption of the dye is determined spectrophotometrically at 787nm, and is linearly related to the amount of stainable material present in a sample (Passow & Alldredge, 1995a).

A reference standard is required to quantify the Alcian blue staining capacity of a given sample. The original method, created by Passow and Alldredge (1995), relies on the commercially available polysaccharide Xanthan Gum (XG) as a standard due to its similar physical and chemical properties to TEP. The Alcian blue staining is directly related to the

amount of XG present, and thus provides a standardized unit for Alcian blue staining capacity. As such, all quantitative measurements of TEP in the literature are expressed in terms of XG equivalents (besides studies that use microscopic enumeration). Recently, an updated version of this method has been developed by Bittar et al. (2018) to account for changes in commercially available XG and to improve the accuracy of the original method. More recently available XG completely dissolves in water, and when Alcian blue is added directly to a dissolved XG solution (of a specific weight), the dye coagulates with the XG particles and forms XG gels that are retained upon 0.4 µm filters. These gels can then be retained on a filter, extracted in a solution of 80% sulfuric acid, and measured spectrophotometrically to relate the measured absorbance to weight of XG. Thus, a XG dilution series can be used to develop a calibration curve for Alcian blue and be used to quantify the amount of TEP on filters in terms of XG equivalents.

It is further possible to quantify the C content of TEP in relation to its Alcian Blue absorption (Engel & Passow, 2001), since the absorption of Alcian Blue is a measure of the weight of the stained EPS (Ramus, 1977). Engel and Passow (2002) observed linear relationships between TEP and C content for a variety of phytoplankton species and natural populations, and derived slopes ranging from 0.51 to 0.81, which implies that TEP consists of 51-81% C. In this thesis (and in other similar studies), a conservative conversion factor of 0.51 is used to estimate C in the form of TEP (TEP-C), in µg C $L^{-1}$ units. This allows for direct comparisons with total particulate organic carbon (POC) concentrations by converting TEP to units of TEP-C, and for estimates of the total fraction of POC composed of TEP (%TEP-C), a biogeochemical important ratio for POC export efficiency (Mari et al., 2017).

## 1.5 Phytoplankton Physiology, TEP production, Carbon Export

The physiology of phytoplankton is another important biological consideration when assessing the efficiency of the BCP. The extent of EPS exudation (as DOC) and the elemental stoichiometry of phytoplankton will impact both the quantity and quality of POC transfer from surface waters to the deep ocean (De La Rocha & Passow, 2007; Polimene et al., 2017). The exudation of DOC precursors that coagulate to form TEP, is inextricably tied to the physiological status of a phytoplankton cell or assemblage. A physiological process known as C overconsumption has been linked to the production of TEP, and is thought to be a major underlying source of TEP production in the ocean (Engel et al., 2002a). This process implies that dissolved inorganic C (DIC) is taken up by a phytoplankton cell at a higher rate than expected from the stoichiometric relationship with nitrate ($NO_3^-$) or phosphate ($PO_4^{3-}$) (Toggweiler, 1993). Typically, this occurs when growth of phytoplankton begins to slow (i.e., due to nutrient limitation) but photosynthesis still proceeds, producing an excess amount of organic C relative to Redfield-Ketchum-Richards Stoichiometry. This results in excess C being exuded as DOC and exopolymeric substances (EPS), which form the precursor material to TEP gels. This extracellular release of C as EPS has been shown to range from 5-50% of gross C fixed by primary production (Karl et al., 1998). Mari et al. (2017) demonstrated the significance of this process through a simple calculation: if a mean extracellular release of EPS of 10-20% of total C uptake is assumed, and 50% of EPS exuded is composed of reactive polysaccharides (TEP precursors) (Benner et al., 1992; Biddanda & Benner, 1997; McCarthy et al., 1996), then the production of TEP precursors represents somewhere between 5-10% of total gross C uptake. Extrapolating this estimate, and assuming a global primary production of 50 Gt C $yr^{-1}$ (Field et al., 1998), ~2.5 – 5 Gt C $yr^{-1}$ would be present in the form of TEP and TEP precursors in the

world's ocean (Mari et al., 2017). Based on these assumptions, C in the form of TEP (TEP-C) clearly represents a major component of the global marine C cycle. Yet, little research exists in comparing TEP-C with estimates of primary production or C export over sufficiently large space and time scales. Currently, we are limited to experimental observations between downward C uptake and TEP or *in situ* studies that often focus on a single point in space or time.

To addresses this, measurements of primary production and C export must be made in conjunction with estimates of TEP-C concentrations ([TEP-C]). This poses some challenges due to the frequency of measurements required to compare TEP-C and primary production / export for comparisons. Primary production rates can be measured relatively easily through daily $^{13}C$ or $^{14}C$ tracer incubations or using other techniques. Carbon export from surface waters can be measured directly using thorium-234 disequilibrium methods, sediment traps, or estimated using new production measurements. New production, defined as the amount of primary production fuelled by oxidized N inputs (typically $NO_3^-$) (Eppley & Peterson, 1979), provides a theoretical estimate of the amount of C available for export from surface waters in a steady-state ocean over relatively large time-scales (days to months), and can be regarded as "C export potential". New production measurements can be performed relatively easily via experimental incubations using $^{15}NO_3$, and provides the distinct logistical advantage of being able to be performed alongside measurements of TEP-C. To my knowledge, no measurements of theoretically available C export (i.e., new production) relative to TEP-C have been made. Comparing C in the form of TEP to total C uptake and C export potential can help to shed light on a major controlling mechanism behind the efficiency of the BCP and help to understand why primary production and export are sometimes decoupled.

## 1.6 Size Structure of Phytoplankton Assemblages in a Changing Ocean

Low-productivity oceanic regions, including oligotrophic and high-nitrate low-chlorophyll (HNLC) regions, are dominated by small celled phytoplankton, including nano (2-20 µm) and pico (<2 µm) phytoplankton. Despite the low overall primary productivity per unit area in these regions, they are nonetheless responsible for ~23% of global net primary productivity owing to their large areal extent (Field et al., 1998). While oligotrophic regions are characterized by macronutrient limitation, HNLC are instead defined as being micronutrient limited, typically by iron (Fe). Both regions are primarily dominated by small celled phytoplankton, which outcompete larger cells under conditions of nutrient limitation owing to their larger surface area to volume ratios (Raven, 1998).

Global warming of the ocean is expected to favour the proliferation of smaller over larger cells due to predicted increases in mixed layer shoaling, thermal stratification, and subsequent increases in nutrient limitation of the surface ocean (Beaugrand et al., 2010; Boyce et al., 2010; Li et al., 2009; Morán et al., 2010; Polovina et al., 2008). A transition to phytoplankton assemblages dominated by small cells is also expected to reduce the efficiency and magnitude of the BCP, as small cells are characterized by slower settling velocities and rapid turnover rate in the microbial loop (Collins et al., 2014; Richardson & Jackson, 2007) compared to larger or denser phytoplankton like diatoms. Predicting the response of phytoplankton communities (and therefore, the BCP) to global ocean change is not straightforward, as phytoplankton growth also depends on light, temperature, and $CO_2$ levels – all of which may have stimulatory effects on phytoplankton communities (Marinov et al., 2010). However, only a limited number of studies have quantified the role of small cells to primary production and nutrient uptake over large gradients in space and time that is required to determine the role of different environmental

drivers on small cell assemblages. Quantifying the role of small cells in primary production, new production, and nutrient dynamics will allow for a better understanding of how hypothesized changes in phytoplankton communities may affect biogeochemical cycling.

## 1.7 The Eastern Subarctic North Pacific and Arctic Regions

The Eastern Subarctic North Pacific (ESNP) can be loosely defined by its governing currents, predominantly the North Pacific Current which splits between 45-50˚N into the northward flowing Alaska Current and the southward flowing California current. The Alaskan current together with the southeastward-flowing Alaskan stream, form the cyclonic central Alaskan gyre (Tabata, 1975). This entire region undergos weak wind driven upwelling (Gargett, 1991), and low water temperatures and salinity (Tabata, 1976). Coupled with high levels of precipitation, low surface salinities promote the formation of shallow haloclines (Tabata, 1975). Closer to shore, seasonal reversals in the direction of coastal winds and currents create upwelling along the coastlines of British Columbia to California, resulting in periodically lower temperatures and higher salinities (Favorite, 1976).

The biological oceanography of the ESNP is largely determined by iron (Fe) and light availability. In general, offshore regions are characterized by consistently low levels of primary production and chlorophyll *a* (chl-*a*), despite high levels of nitrate ($NO_3^-$) and silicic acid ($Si(OH)_4$) (Peña & Varela, 2007). As such, much of the ESNP is characterized as being a HNLC region, where phytoplankton growth is limited by Fe in the spring and summer seasons, and co-limited by Fe and light in the winter seasons (Boyd et al., 1996). Iron-limited waters west of 135˚W are dominated by small-celled phytoplankton (Boyd et al., 1996; Harrison et al., 2004; La Roche et al., 1996). In contrast, the upwelling of deep, nutrient-rich waters closer to shore

induces periodic phytoplankton blooms and nutrient depletion in coastal regions (Harrist et al., 2009). Distinct environmental conditions that extend from the open ocean HNLC regions of the Alaskan gyre to the topographically driven upwelling regions along the continental coastline result in gradients in biological and ecological characteristics across the ESNP.

The Pacific Arctic Region (PAR) differs greatly from the Subarctic, and represents one of the most productive regions in the ocean (Sambrotto et al., 1986; Springer & McRoy, 1993). The environmental and biological characteristics of the region are largely governed by the flow of nutrient-rich Pacific waters from the Northern Bering Sea, through the Bering Strait, and into the Chukchi Sea (Woodgate et al., 2006). An ample supply of nutrients, shallow bottom depths, and sunlight in the spring and summer provide the necessary ingredients for high levels of primary production and sustained phytoplankton growth (Crawford et al., 2015; Varela et al., 2013). In contrast, the Central Arctic regions, including the Canadian Basin, are characterized as being far less productive (Varela et al., 2013; Wyatt et al. 2013; Crawford et al., 2015). The Canada Basin has been undergoing increased sea ice melt, a freshening of the surface layer, a deepening of the nutricline (McLaughlin & Carmack, 2010), and a transition toward small cell dominated phytoplankton communities (Li et al., 2009). Seasonally, the Canada Basin progresses from a highly stratified water column in the spring and summer to a deeper mixed layer with the onset of sea ice during the fall and winter. Nitrate limits phytoplankton growth and new production throughout the Canada Basin, and is particularly limiting in surface waters during spring seasons owing to strong stratification (McLaughlin & Carmack, 2010).

Multiple oceanographic programmes currently stage research expeditions throughout the Subarctic and Arctic regions and provided the opportunities to collect the data included in this thesis. Within the Subarctic, the Line P program are both multi-decadal timeseries. Line P spans

from the southwest coast of Vancouver Island to Ocean Station Papa at 50˚N, 145˚W (in the case of Line P). The La Perouse programs operates along a series of shorter oceanographic transects that span from coastal to off-shelf waters along the west coast of Vancouver Island. The Canada-Three-Oceans (C3O) is a program that provides sampling opportunities across the ESNP (north of the Line P program), from ~48˚N – 54˚N and ~126˚W – 159˚W. In the Arctic, the Distributed Biological Observatory (DBO) and the Joint Ocean Ice Survey (JOIS) programs were set to investigate climate change and sea ice dynamics in the far Arctic. The DBO strategically samples biological 'hotspots' along a series of 5 regions throughout the Bering Strait and Chukchi Seas. In the Canada Basin, the JOIS program conducts oceanographic sampling from the Southernmost Beaufort Slope to 80˚N. Together, these five programs provided ideal opportunities to investigate temporal variations in TEP concentrations and its predictors, phytoplankton productivity and community structure, and influences on upper ocean C cycling and export across strong and distinct gradients in environmental and biological conditions in these vast ocean regions.

## 1.8 Research Objectives

The overarching objective of this thesis is to improve our understanding of biological influences on the marine C cycle in surface waters and the BCP, with particular emphasis on the role of TEP, total primary production and export potential, and small celled phytoplankton. This objective is addressed across three main chapters, with a series of goals and questions within each. These chapters and their questions are addressed below:

1. *Chapter 2: Estimating the concentration of transparent exopolymer particles (TEP) in Arctic and Subarctic Oceans using in situ measurements and model predictions*.

This chapter seeks to address three main objectives: i) how does the concentration of TEP in the surface ocean vary across large gradients in space and time in the Arctic and Subarctic, ii) what are the major biological and environmental predictors of TEP concentrations, and iii) how do surface TEP concentrations vary across large historical datasets using models derived from TEP predictors? This chapter includes measurements for TEP, phytoplankton biomass (chlorophyll-*a*, POC), proxies of phytoplankton production (apparent oxygen utilization rates; AOU), and a series of environmental variables. This includes research performed as part of the Line P, La Perouse, Canada-Three-Oceans (C3O), Distributed Biological Observatory (DBO), and the Joint Ocean Ice Survey (JOIS) programs. This chapter provides one of the largest spatiotemporal studies of TEP ever performed and is the first attempt at using statistical models to predict TEP concentrations.

2. *Chapter 3: Spatiotemporal trends in carbon export potential in the Eastern Subarctic North Pacific estimated from transparent exopolymer particles (TEP), carbon uptake and new production*. The goals of this chapter were to address two main goals i) quantify TEP-based C (TEP-C) concentrations and export estimates relative to total C uptake and export potential, and ii) estimate C overconsumption by phytoplankton relative to TEP-C concentrations. This chapter combines *in situ* TEP measurements with measurements of C uptake and new production, as a proxy for C export potential, over large gradients in space and time in the Subarctic region. It is the first study of its kind to measure TEP-C relative to total C uptake and export potential and provides a new perspective on the predominance of TEP-C sources in the Subarctic,

with important implications for C export. Furthermore, it also builds off work done by Wurl et al., (2011), who measured TEP residence times along Line P. Using these residence times, estimates of TEP-C turnover are also used to directly compare with new production-based C export rates.

3. *Chapter 4: Spatiotemporal trends in small-cell phytoplankton contributions to biogeochemical cycles in the Eastern Subarctic North Pacific.* This chapter focuses on the role of small cells to nutrient uptake and TEP production in the Subarctic Pacific. It combines size fractionated measurements of C, $NO_3^-$, Si, and new production with environmental and biological measurements to determine: i) variability in the contributions of small cells to biogeochemical uptake rates over space and time, ii) the environmental variables that have the greatest impact on small cell dominance to nutrient uptake or new production rates, and iii) the production of TEP by small cells along Line P. This work provides an in-depth analysis as to the role of small cells to biogeochemical cycling in the Subarctic, and how a changing environment may influence their contributions.

Finally, the general conclusions, novelty, and significance of this thesis are presented in Chapter 5.

Appendix A aims to quantify the %TEP-C ratios in different study regions, including the ESNP (both on and off the continental shelf), the Bering and Chukchi Seas, and in the Beaufort Sea/Canada Basin. This appendix supplements Chapter 2.

Appendix B builds off Appendix A, and in a similar fashion to Chapter 1, aims to identify the major biological and environmental predictors behind %TEP-C ratios in the ocean.

Appendix C provides satellite-derived predictions of surface [TEP-C] concentrations across the ESNP using a multivariate modelling approach, using chlorophyll-*a* and temperature as model parameters in a random forest regression model. This appendix supplements Chapter 2, and demonstrates the utility of multivariate approaches in predicting TEP concentrations.

Appendix D provides size-fractionated phytoplankton biomass measurements, specifically biogenic Si and chlorophyll – *a*, across the ESNP and determines statistical variation in size fractionated biomass over space and time.

Appendix E includes measurements of nutrient (C, $NO_3^-$, and Si) uptake by picophytoplankton (<2µm) across Line P in the ESNP for spring and summer of 2021. This data supplements Chapter 4.

# Chapter 2: Estimating the concentration of transparent exopolymer particles (TEP) in Arctic and Subarctic Oceans using *in situ* measurements and model predictions

## 2.1 Abstract

Transparent exopolymer particles (TEP) are marine organic gels that are ubiquitously distributed in the ocean surface and play an influential role in the ocean's carbon (C) cycle due to their tendency to promote aggregation of particulate organic carbon (POC). As TEP has a lower density than seawater, unballasted TEP can prolong the residence time of POC in surface waters, or even induce upward flux, and subsequently decouple surface primary production from POC export to deep waters. In this study, I (i) measured *in situ* TEP and biological and environmental parameters across a multi-year study in Arctic and Subarctic Oceans, (ii) identified major environmental TEP predictors using both multivariate linear regressions (MLRs) and Random Forest Regression (RFR) techniques, and (iii) use TEP predictors to predict surface TEP from commonly reported measurements in historical datasets (1998-2018) in the Subarctic Ocean. Surface water samples for TEP, biological, and environmental measurements were taken throughout the Eastern Subarctic North Pacific (ESNP), Bering and Chukchi Seas (BE-CH), and Beaufort Sea-Canada Basin (BS-CB) from 2019 to 2022. Biological variables, including chlorophyll *a* (chl-*a*), particulate organic carbon (POC) and apparent oxygen utilization (AOU), were identified as important TEP predictors in both MLR and RFR models. Direct (temperature and nutrient concentrations) and indirect (mixed layer depth (MLD), salinity and wind speed (WS)) environmental predictors were also identified as influential, but less important, predictors of TEP concentrations. The inclusion of biological sources, direct, and indirect environmental predictors as model inputs were favoured by both MLR and RFR techniques, with a range of cross validation error on new data from 8 – 16 µg XG eq $L^{-1}$ and explained variance ($R^2$) from 71 – 81%. Statistical models were subsequently applied to long term historical data sets along Line P (consisting of chl-*a*, temperature, AOU, nutrient concentrations, and MLD) to obtain large-

scale spatiotemporal estimates of surface TEP concentrations and to estimate the amount of C present as TEP. In low-productivity oceanic regions of the Subarctic, both models estimated TEP concentrations to be ~35.1 $\pm$ 20.5 µg Xg eq $L^{-1}$ in summer, 30.4 $\pm$ 18.9 µg Xg eq $L^{-1}$ in spring, and 21.3 $\pm$ 8.6 µg Xg eq $L^{-1}$ in winter, projecting that TEP can represent a major source of organic C year-round in this region. These results indicate that while TEP is driven primarily by the amount of phytoplankton biomass and productivity, conditions of increased nutrient limitation, elevated temperature, and shoaling of the mixed layer can drive increases in TEP relative to phytoplankton biomass. Despite their importance to biogeochemical cycling, no large-scale statistical models of surface TEP concentrations currently exist. I present the first predictive model to estimate TEP based C in the ocean's surface and demonstrate its importance to the marine C cycle.

## 2.2 Introduction

Transparent exopolymer particles (TEP) belong to a class of organic polymers derived from extracellular polymeric substances (EPS) and dissolved organic carbon (DOC) precursors that self-assemble into larger, gel like particles (Passow & Alldredge, 1995a). TEP form an organic 'exopolymer matrix' within the surface layers of the ocean, and is considered a critical component of the biological carbon pump (BCP) through its facilitation of organic matter aggregation (Mari et al., 2017). However, the specific gravity of TEP is lower than that of seawater (Azetsu-Scott & Passow, 2004). Therefore, when TEP concentrations ([TEP]) are high relative to total POC concentrations, the density of organic aggregations is low, and sinking rates are reduced (Mari et al., 2017). The ratio of TEP:POC concentrations (%TEP-C), is therefore a moderating factor between the export and retention of POC in the surface ocean. The decoupling

of primary production from POC export has been attributed to elevated %TEP-C (Mari et al., 2017), as high %TEP-C values will delay the timing and magnitude of POC export, resulting in enhanced particle remineralization in the surface layers. The importance of TEP in the marine C cycle is also due to its prevalence in global ocean surface waters, as it has been estimated that approximately 10% of the ocean's DOC pool (~ 70 Pg C) is composed of organic polymers that are precursors to TEP (Verdugo et al., 2004). TEP is produced primarily by phytoplankton (Passow, 2002b; Radić et al., 2006; Zamanillo, Ortega-Retuerta, Nunes, Rodríguez-Ros, et al., 2019), and to a lesser extent by bacteria (Ortega-Retuerta et al., 2010; Yamada et al., 2015), through the extracellular release of TEP precursors (Claquin et al., 2008; Engel et al., 2011). During photosynthesis and growth, phytoplankton typically sequester excess C in the form of polysaccharide material (i.e. chrysolaminarin in diatoms, glycogen in cyanobacteria) (Ball & Morell, 2003; Beattie et al., 1961). These polysaccharides are the predominant form of phytoplankton exudates (known as exopolymeric substances – EPS), and are produced in excess compared to free monosaccharides or amino acids (Mühlenbruch et al., 2018).

Identifying the major biological and environmental predictors of TEP, and accurately predicting [TEP] across large spatial scales, will allow for an under-quantified element of the marine C cycle to be better accounted for in our understanding of ocean C dynamics and change. Major predictors of [TEP] could include a multitude of both biotic and abiotic variables in marine settings. As phytoplankton are the dominant source of marine TEP, the link between TEP and chl-*a* has been shown in a variety of studies (Corzo et al., 2005; de Vicente et al., 2010; Hong et al., 1997; Islam et al., 2021; Ortega-Retuerta, Reche, et al., 2009; Ortega-Retuerta et al., 2017; Passow & Alldredge, 1995a; Prieto et al., 2006; Radić et al., 2006; Ramaiah & Furuya, 2002; Van Oostende et al., 2012; Yamada et al., 2015; Zamanillo, Ortega-Retuerta, Nunes,

Estrada, et al., 2019; Zamanillo, Ortega-Retuerta, Nunes, Rodríguez-Ros, et al., 2019). While chl-*a* concentration has been identified as a good predictor of [TEP] across horizontal gradients in the upper mixed layer (Ortega-Retuerta et al., 2017; Zamanillo, Ortega-Retuerta, Nunes, Estrada, et al., 2019), the relationship between TEP stocks and chl-*a* may become decoupled with depth or during periods of intensified stratification of the water column (Ortega-Retuerta et al., 2017). Other biotic variables, such as dissolved oxygen (DO), POC, and primary production rates, have also been strongly correlated with [TEP] across large spatial scales (Engel et al., 2002b; Kodama et al., 2014; Ortega-Retuerta et al., 2017; Zamanillo, Ortega-Retuerta, Nunes, Estrada, et al., 2019), and may represent useful TEP predictors in conjunction with chl-*a*. The above variables are classified as 'source' predictor variables in this study.

The production of TEP by phytoplankton is linked to the physiological status of the phytoplankton assemblage, and by extension to the direct environmental influences that impact their metabolism and activity (i.e. direct predictors of TEP). The production of TEP precursors are typically enhanced under conditions of nutrient stress in phytoplankton (Corzo et al., 2000; Mari et al., 2005, 2017; Ortega-Retuerta et al., 2018), which promotes cellular C overflow (and thus EPS exudation) (Staats et al., 2000). Increased EPS exudation by phytoplankton has also been linked to increases in temperature in experimental settings via increasing enzymatic activities and photosynthetic rates (Biermann et al., 2014; Claquin et al., 2008; Engel et al., 2011; Fukao et al., 2012; Goldman & Mann, 1980; Guo et al., 2022; Piontek et al., 2009; Seebah et al., 2014; Taucher et al., 2012; Wohlers et al., 2009). Strong evidence of these relationships have been shown across large spatial scales, including significant positive correlations between surface [TEP] and temperature (Ortega-Retuerta et al., 2019; Van Oostende et al., 2012; Zamanillo, Ortega-Retuerta, Nunes, Estrada, et al., 2019), and negative correlations with nutrient

concentrations (Van Oostende et al., 2012; Zamanillo, Ortega-Retuerta, Nunes, Estrada, et al., 2019). In addition to the physiological effects that warmer temperatures and nutrient limitation have on TEP production and accumulation, strong thermal stratification in the upper mixed layer can act to trap the positively buoyant TEP matrix (Mari et al., 2017) and TEP accumulation in surface waters has been frequently observed in late summer months (Mari et al., 2001; Mari & Burd, 1998; Ortega-Retuerta, Passow, et al., 2009a; Ortega-Retuerta et al., 2018; Wurl et al., 2011). Similar studies (that did not measure TEP directly) have also found strong correlations between the surface accumulation of dissolved organic carbon (DOC) (a TEP precursor) and both, higher temperatures and the development of seasonal thermoclines (Hansell & Waterhouse, 1997).

Major TEP sinks from the surface ocean include wind-driven mixing, gravitational settling, heterotrophic consumption, and photolysis by UV radiation (Ortega-Retuerta et al., 2009; Zamanillo, Ortega-Retuerta, Nunes, Rodríguez-Ros, et al., 2019). While heterotrophic bacteria have been identified as a potential source of TEP, it is well understood that bacteria actively colonize and consume TEP matrices (Busch et al., 2017; Zamanillo, Ortega-Retuerta, Nunes, Estrada, et al., 2019; Zamanillo, Ortega-Retuerta, Nunes, Rodríguez-Ros, et al., 2019; Zäncker et al., 2019), and that heterotrophic consumption and associated respiration would likely be a sink rather than a source of TEP in marine environments.

The goals of this study were to i) collect *in situ* measurements of [TEP] and related biological and environmental parameters across a multi-year study in the Arctic and Subarctic, ii) identify the major predictors of [TEP] in surface waters across the Subarctic and Arctic regions using Multiple Linear Regression (MLR) and Random Forest Regression (RFR) modelling techniques, and iii) validate these models on new input data from historical data sets to predict

changes in surface TEP in the ESNP. Based on evidence from previous studies, I hypothesized that surface TEP concentrations ([TEP]) could be predicted over large spatial scales from statistical models with primary driving forces of TEP as input variables. This includes biological sources (i.e., phytoplankton biomass and productivity), environmental conditions that promote EPS release (i.e., temperature, nutrient concentrations), and indirect environmental conditions that act to promote surface TEP retention or degradation (i.e., stratification, solar irradiance, wind-driven turbulence, net community respiration). These inputs were included based on i) the availability of their corresponding measurements (i.e., feasibility of field sampling, availability in datasets and remote sensors), ii) observational and experimental evidence for an inherent relationship with TEP in the literature, and iii) significant *in situ* correlations with marine TEP.

## 2.3 Methods

### 2.3.1 Sampling Regime

Discrete samples for particulate organic matter (TEP and POC), chl-*a*, dissolved oxygen (DO), dissolved nutrients (nitrate ($NO_3^-$), silicic acid ($Si(OH)_4$), and phosphate ($PO_4^{3-}$)), and measurements of environmental conditions (mixed layer depth (MLD), temperature, density, salinity, daily photosynthetically active radiation (PAR), solar radiation dose (SRD), wind speed (WS), depth), were taken from the Eastern Subarctic North Pacific (ESNP), the Bering and Chukchi Seas (BE-CH), and the Beaufort Sea/Canada Basin (BS-CB) (Figure 2.1, Table 2.1). Sampling in the ESNP was conducted during spring, summer, and winter from 2019 to 2022 as a part of the Line P and La Perouse programs onboard the *CCGS John P Tully*; sampling in the BE-CH was conducted during summers of 2021 and 2022 as part of the Canada-3-Oceans (C3O)/Distributed Biological Observatory (DBO) programs onboard the *CCGS Sir Wilfrid*

*Laurier*; and sampling in the BS-CB was done during the fall of 2022 as a part of the Joint Ocean Ice Study/Beaufort Gyre Observing System (JOIS/BGOS) onboard the *CCGS Louis S. St-Laurent*. All research cruises were operated by Fisheries and Oceans Canada (DFO). Samples were collected using a Sea-Bird rosette (SBE-911plus) equipped with 24 10L Niskin bottles and a conductivity-temperature-depth (CTD) sensor, with additional sensors for DO and *in situ* fluorescence. At each station, samples were taken from 1 to 2 depths at 5m and the chlorophyll max.

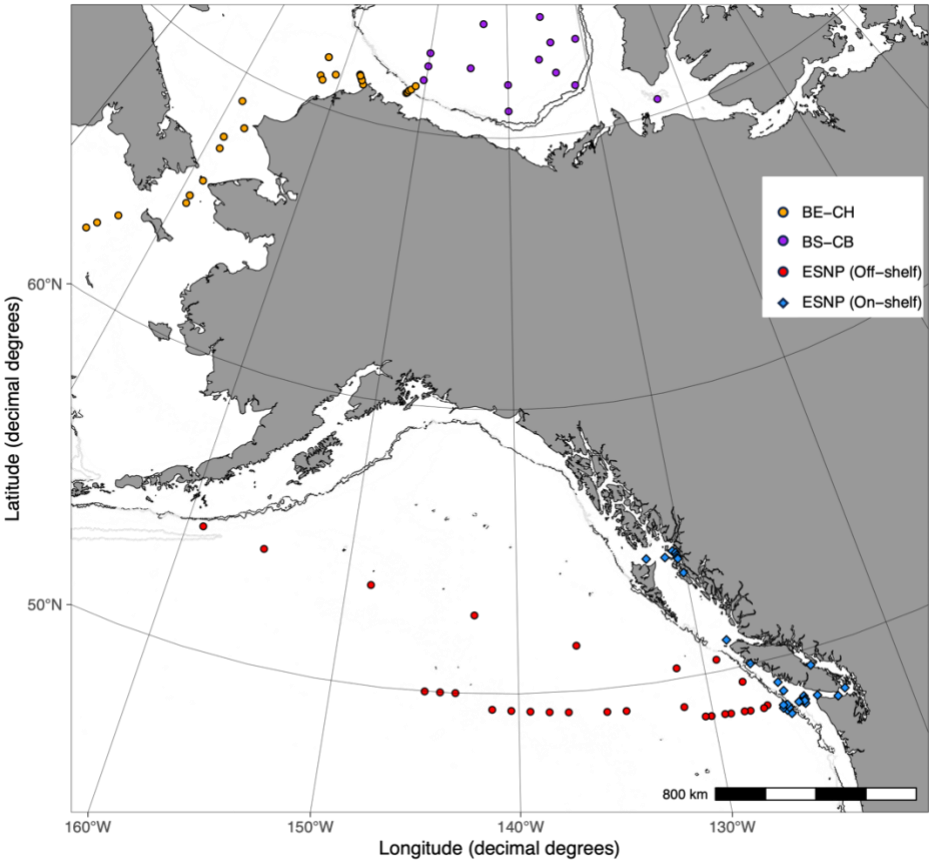


**Figure 2.1.** Sampling stations in the Eastern Subarctic North Pacific (ESNP), Bering and Chukchi Seas (BE-CH), and Beaufort Sea/Canada Basin (BS-CB) during 12 oceanographic cruises, covering spring, summer, fall, and winter from May 2019 – October 2022 (Table 2.1). Regions were defined as in Carmack and McLaughlin (2011) and Varela et al. (2013). Seawater samples were collected from 1-2 depths, at 5m and the chlorophyll max. Many of the stations were sampled repeatedly across years (2019-22), particularly within the ESNP. The BE-CH region was sampled in 2021 and 2022, while and BS-CB region was only sampled in 2022 (see Table 2.1). ESNP stations located north of 50˚N and west of 130˚W were sampled as part of the DBO/C30 cruise program. Grey contours indicate shelf breaks at 1500m depth. The ESNP is considered as a Sub-Arctic region while Arctic regions in this study refer to both BE-CH and BS-CB. 'OFF-shelf' stations are defined as stations that were located off the continental shelf in waters >1500 m depth, as denoted by the gray contour line; 'ON-shelf' stations are located in near-shore regions in waters <1500m depth.

**Table 2.1.** Information about sampling programs, regions covered, dates and season, and number of samples taken per cruise used during this study. ESNP stations located above 50˚N and west of 130˚W were sampled as part of the DBO/C3O cruise program (Figure 2.1). Number of samples (n) represents the total amount of individual samples taken per cruise, including a maximum of 2 depths per station but not including replicate samples. Cruise ID refers to the program, year, and cruise number. 'OFF-shelf' stations are defined as stations that were located off the continental shelf in waters >1500 m depth, as denoted by the gray contour line; 'ON-shelf' stations are located in near-shore regions in waters <1500m depth.

| **Cruise (ID #)** | **Region** | **Date Range** | **Seasonal categorization** | **# of stations** | **n** |
|---|---|---|---|---|---|
| Line P (2019 -006) | ESNP (ON + OFF) | June 2 - 18, 2019 | Spring | 5 | 13 |
| La Perouse (2019 – 005) | ESNP (ON + OFF) | May 24 - June 2, 2019 | Spring | 6 | 10 |
| Line P (2019 – 008) | ESNP (ON + OFF) | Aug 13 – 29, 2019 | Summer | 5 | 10 |
| La Perouse (2019 – 009) | ESNP (ON + OFF) | Aug 31 – Sept 11, 2019 | Summer | 6 | 12 |
| Line P (2020 – 001) | ESNP (OFF) | Feb 7 – 25, 2020 | Winter | 5 | 13 |
| Line P (2021 – 006) | ESNP (ON + OFF) | May 2 -19, 2021 | Spring | 24 | 39 |
| Line P (2021 – 008) | ESNP (ON + OFF) | Aug 24 – Sept 7, 2021 | Summer | 18 | 24 |
| C3O/DBO (2021) | ESNP (OFF) + BE-CH + BS-CB | July 9 – 30, 2021 | Summer | 11 | 13 |
| Line P (2022 – 001) | ESNP (OFF) | March 1 – 20, 2022 | Winter | 6 | 6 |
| C3O/DBO (2022) | ESNP (OFF) + BE-CH + BS-CB | July 9 – 30, 2022 | Summer | 22 | 37 |
| La Perouse (2022 - 009) | ESNP (ON + OFF) | Aug 27 – Sept 7, 2022 | Summer | 9 | 17 |
| JOIS (2022) | BE-CH + BS-CB | Sept 24 – Oct 11, 2022 | Fall | 27 | 27 |

### 2.3.2 Regional Categorization

The broad oceanographic domains classified in this study were determined according to the physical and environmental properties that distinguish each region, primarily temperature and salinity (Carmack & McLaughlin, 2011; Varela et al., 2013). The dataset was analyzed in two groups: i) Subarctic (ESNP), and ii) Arctic (BE-CH and BS-CB). The Subarctic was further split into two categories, 'On-shelf' (ESNP – ON) and 'Off-shelf' (ESNP – OFF), where 'Off-shelf' stations are defined as stations located off the continental shelf in waters >1500 m depth and 'On-shelf' stations defined as being in waters <1500 m, and include stations positioned above the continental slope.

### 2.3.3 Particulate Organic Matter (TEP and POC)

TEP concentrations were determined using the updated method for TEP quantification (Bittar et al., 2018), based on the original TEP quantification method (Passow & Alldredge, 1995a). Seawater samples (100 – 500 ml) were filtered through 0.4 µm polycarbonate filters under low filtration pressure (<150 mm Hg). Before removing the filters from the filtration unit, they were stained with 0.5 ml of Alcian blue (AB) dye (0.02%, pH 2.5) for <5 s, rinsed with deionized water to remove any excess dye, and frozen at -20 ˚C until laboratory analysis (within 1 month). Blank samples (empty filters stained with AB dye and measured as described above) were taken each sampling day. The TEP samples from the BE-CH were the exception to this method; instead of immediately filtering and staining the filters, 125-300 ml of seawater were preserved in 1% formalin and stored at 4˚C until analysis on shore. The preserved samples were then filtered and stained on shore in the same fashion as above; this methodology has been verified as an accurate approach to estimating [TEP] (Passow & Alldredge, 1995a). Filters were

then placed in 6 ml of extraction solution (80% $H_2SO_4$) for 2.5 hours and the solutions were analyzed on a Beckman DU530 spectrophotometer at 787 nm. Values were expressed as µg Xanthan Gum Xanthan equivalents (XGeq.) $L^{-1}$. Filter blanks did not vary significantly throughout any of the cruises and were consistently well below detection limits. Calibration curves for the AB dye were made using Xanthan gum as a standard, and calibration factors were calculated as described in Passow and Alldredge, (1995) and Bittar et al., (2018). The calibration factors fell within the range of the calibration factors in the above studies (88-139) but varied slightly for each new batch of AB dye. The detection limit for calibration standards was determined to be 4 µg (XGeq.) $L^{-1}$, similar to the values described by Bittar et al., (2018). Error estimate for TEP quantification was estimated at $\pm$ 13% based on the mean coefficient of variation (standard error divided by the mean), based on triplicate measurements collected throughout the study (n = 57 triplicates). TEP carbon content (TEP-C) was calculated by multiplying [TEP] by a conservative conversion factor of 0.51 (Engel & Passow, 2001) to estimate TEP-C in terms of µg C $L^{-1}$.

The C content in TEP (TEP-C) was calculated by multiplying [TEP] by a conservative conversion factor of 0.51 (Engel & Passow, 2001). The fraction of total POC composed of TEP-C (%TEP-C) was then calculated using equation 2, in accordance with Engel and Passow (2001):

$$TEP - C = [TEP] * 0.51 \quad [1]$$

$$\%TEP - C = \frac{TEP-C}{Total\ POC} * 100 \quad [2]$$

Samples for POC were collected by filtering 500 – 1000 ml of seawater through pre-combusted (6h, 450°C) glass fibre filters (GF75, 0.7 µm nominal porosity) under low filtration pressure (<150 mm Hg), and immediately frozen at -20˚C. Frozen filters were dried at 60°C for

at least 48 h on-shore. Filters from the BS-CH region were immediately dried on board. Dry filters were acidified (to remove inorganic carbon) in a desiccator saturated with HCl fumes for 12h. After acidification, the filters were dried again and analyzed on an elemental analyzer at the Department of Earth and Ocean Sciences, University of British Columbia. Triplicate samples for both TEP and POC were taken a minimum of twice per cruise to estimate variation in sample analysis.

### 2.3.4 Phytoplankton biomass (chlorophyll *a*)

Chlorophyll *a* (chl-*a*) analyses were performed by filtering ~500 ml of seawater under low filtration pressure (<150 mm Hg) through a GF75 glass fiber filter (0.7 µm nominal porosity) and immediately freezing the filter at -20˚C. Once onshore, chl-*a* was extracted in 90% acetone at -20˚C for 24 h and measured on a Turner Designs 10AU fluorometer (Parsons, 1984). Triplicate samples were taken a minimum of twice per cruise to estimate variation in sample analysis.

### 2.3.5 Dissolved Oxygen and Apparent Oxygen Utilization (AOU)

Total dissolved oxygen (DO; ml $L^{-1}$) samples were taken throughout the Subarctic and Arctic regions in accordance with Department of Fisheries and Oceans (DFO) protocol. Briefly, [DO] was measured at sea after seawater collection from Niskin bottles using an automated Winkler titration system (Metrohm Dosimat model) with modifications according to Carpenter (1965). In some instances, CTD measurements of [DO], taken from a DO sensor attached to the CTD was used when discrete (bottle) DO measurements were not available (CTD sensors were calibrated with the Winkler DO measurements). DO concentrations were converted to estimates

of Apparent Oxygen Utilization (AOU) as a rough proxy of phytoplankton productivity. AOU values were calculated as follows:

$$AOU = DO_{equilibrium} - DO \quad [1]$$

where $DO_{equilibrium}$ is the calculated DO at equilibrium with the atmosphere based on temperature and salinity values (Emerson & Hamme, 2022).

### 2.3.6 Dissolved inorganic nutrients

Samples for dissolved inorganic nutrients ($NO_3^-$, $Si(OH)_4$, and $PO_4^{3-}$) were taken directly from Niskin bottles, and syringe-filtered through 0.2 µm polycarbonate filters into 15 ml centrifuge tubes. Filtered samples were frozen immediately at -20˚C until analysis onshore on an Astoria Nutrient Analyzer following the procedures of Barwell-Clarke et al. (1996). Additional samples for $Si(OH)_4$ measurements were collected and filtered as above but stored at 4°C until analysis onshore following the manual protocol by Brzezinski and Nelson (1986).

### 2.3.7 Environmental parameters

Water temperature, salinity, and density were measured throughout the water column from sensors on the Seabird CTD package at every station. Mixed layer depth (MLD) was defined as the depth in the water column at which the density increased by more than 0.03 $kg/m^3$ from the average surface density (1-5 m) (de Boyer Montégut et al., 2004).

Wind speed data, collected 24 h average prior to sampling, was obtained from the Goddard Earth Sciences Data and Information Services Centre (GES DISC) using an hourly

time-averaged 2-dimensional data collection in Modern-Era Retrospective analysis for Research and Applications version 2 (MERRA-2). Wind speed data was obtained with a 0.5˚ x 0.625˚ spatial resolution. Photosynthetically active radiation (24 h surface PAR) (µE $m^{-2}$ $s^{-1}$) was obtained from the NASA Aqua MODIS Satellite at Level 3, km daily resolution. Solar radiation dose (SRD), as an estimate of irradiation in the water column, was calculated using daily average PAR and MLD, as described in Zamanillo et al, 2019, and by the equation:

$$SRD = \frac{I}{Kd\ (PAR) \times MLD} \times \left(1 - e^{(-Kd(PAR) \times MLD}\right) \quad [2]$$

where *I* is the average surface daily PAR in the 24 h prior to sampling, *Kd (PAR)* is the average PAR diffuse attenuation coefficient in the euphotic zone, and MLD is the mixed layer depth (m). Average diffuse attenuation coefficients (*Kd (PAR)*) was determined as the slope of the linear regression between CTD profiles of logarithmic PAR and depth.

### 2.3.8 Statistical Approach: Determining TEP Predictors

The measurements described in sections *2.3.3 – 2.3.7* were included in this study based on strong support for a relationship with TEP concentrations, observed correlations in the literature, and availability in historical datasets and remote sensors (Table 2.2). These variables were subsequently used as input parameters in two statistical techniques, Multiple Linear Regression (MLR) and Random Forest Regression (RFR) models to identify the most significant large-scale predictors of [TEP] (and [TEP-C]).

**Table 2.2.** Predictor variables used in the Multiple Linear Regression (MLR) and Random Forest Regression (RFR) models in this study. Each predictor variable was grouped into a broad 'predictor' category of (i) sources for TEP production, (ii) direct environmental influences (responsible for increasing EPS excretion in phytoplankton), and (iii) indirect environmental influences (associated with TEP retention and degradation in the surface ocean). Available regions refer to the regions where explanatory variables were collected during this study. Supporting literature refers to previous studies that provided evidence of the links between marine TEP concentrations and the explanatory variables.

| Predictor Category | Predictor variables | Regions sampled in this study | Supporting Literature |
|---|---|---|---|
| Biomass | Chlorophyll *a* (chl-a) | All | Ortega-Retuerta et al. 2017; Ramaiah & Furuya, 2002; Yamada et al., 2015; Zamanillo et al., 2019a; Zamanillo et al., 2019b; Prieto et al., 2006; Van Oostende et al., 2012; Radić et al., 2006; Corzo et al., 2005; Ortega-Retuerta et al. 2009; Corzo et al., 2000*; Ortega-Retuerta et al., 2010; Ortega-Retuerta et al., 2009b; Hong et al., 1997; Passow and Alldredge, 1995; Islam et al., 2021; de Vicente et al., 2010 |
| | Particulate organic carbon (POC) | All | Ortega-Retuerta et al. 2017; Zamanillo et al., 2019a; Zamanillo et al., 2019b; Yamada et al., 2015; Ortega-Retuerta et al., 2019 |
| Productivity/respiration | Dissolved oxygen (DO); Apparent oxygen utilization rate (AOU) | All* | Ortega-Retuerta et al. 2017; Kodama et al., 2014; Ortega-Retuerta et al., 2019; Ramaiah & Furuya, 2002; Yamada et al., 2015; Ortega-Retuerta et al., 2010; Ortega-Retuerta et al., 2009b |
| | Carbon uptake ** | Subarctic | Engel et al., 2002*; Zamanillo et al., 2019a; Zamanillo et al., 2019b |
| Direct environmental influences (EPS excretion) | Temperature | All | Zamanillo et al., 2019b; Ortega-Retuerta et al. 2018; Van Oostende et al., 2012; Claquin et al., 2008; Guo et al., 2022; Taucher et al., 2012; Yamada et al., 2015; Ortega-Retuerta et al., 2019; Engel et al., 2011 |
| | $[NO_3^-]$ | All | Ortega-Retuerta et al. 2017; Zamanillo et al., 2019b; Van Oostende et al., 2012; Corzo et al., 2005; Corzo et al., 2000; Mari et al., 2005 |
| | $[Si(OH)_4]$ | All | Ortega-Retuerta et al. 2017; Zamanillo et al., 2019b; Ortega-Retuerta et al. 2018 |
| | $[PO_4^{3-}]$ | All | Ortega-Retuerta et al. 2017; Zamanillo et al., 2019b; Van Oostende et al., 2012; Mari et al., 2005 |
| Indirect environmental influences (TEP retention, degradation, export) | Mixed layer depth | All | Ortega-Retuerta et al. 2018; Van Oostende et al., 2012 |
| | Salinity | All* | Zamanillo et al., 2019b; Ortega-Retuerta et al. 2018; Yamada et al., 2015; Ortega-Retuerta et al., 2019; Islam et al., 2021 |
| | Season | All | Ortega-Retuerta et al. 2018 |
| | 24 h-averaged PAR | Subarctic | Zamanillo et al., 2019b; Ortega-Retuerta, et al., 2009 |
| | Solar radiation dose (SRD) | Subarctic | Zamanillo et al., 2019b; Ortega-Retuerta, et al., 2009 |
| | Wind speed | All | Zamanillo et al., 2019b; Wurl et al., 2011; Burns et al., 2019 |
| | Depth | All | Wurl et al., 2011; |

*Indicates data from the DBO/C3O 2021 cruise was not available.

**Carbon uptake measurements collected but analyzed as part of Chapter 3.

### 2.3.9 Multiple Linear Regression (MLR) analysis

MLR is frequently utilized to identify the predictor variables that capture the greatest amount of variance in the dependant variable (Graham, 2003). First, statistically significant relationships between *in situ* measurements and TEP were identified via independent linear regression analyses. Only significantly correlated variables ($p < 0.05$) were considered for MLR analyses, as non-linear or insignificant variable relationships would violate linear regression assumptions and potentially introduce overfitting. As this strategy relies on multiple statistical tests, a Bonferroni correction was utilized, and an alpha value of 0.01 was utilized to reduce the chances of Type 1 error. A MLR was derived and further evaluated in terms of the statistical importance of each variable. Akaike Information Criterion (AIC), a commonly used scoring technique for evaluating model parameters, was then used to remove unnecessary variables that did not significantly contribute to the model. This was done using the R package *stats*; models consisting of different variables combinations were compared with AIC selection criterion with the lowest scoring models with the least number of variables used for predictor variable selection. Variables that introduced excessive multicollinearity or a violation of linear modelling assumptions were also removed as determined through variance inflation factors using the R package *vif*. As such, the final optimal MLRs for both the Subarctic ($MLR_{Subarctic}$) and Arctic ($MLR_{Arctic}$) regions were composed of primary TEP predictors that (i) had strong mechanistic and literary evidence for a relationship with [TEP], (ii) were correlated with TEP in the respective dataset, (iii) were selected by AIC criteria, and (iv) were statistically valid and satisfied all linear modelling assumptions.

Cross validation techniques were further used to assess the performance of MLRs on predicting TEP from new input data. This involved randomly splitting the input data into an 80%

'training' group and a holdout 20% 'testing' group. MLRs were first derived using the training datasets, and subsequently applied to new data inputs from the holdout testing data. MLRs were evaluated by comparing measured to predicted TEP values. Evaluation metrics were expressed in terms of mean absolute error (MAE), or the average error rate between predicted and measured values. The R software packages *ggplot2*, *olsrr*, *caret*, and *car* (RStudio v1.3.1093) were used to create, validate, and visualize MLRs in this study, and to select relevant predictor variables of surface TEP.

### 2.3.10 Random Forest Regression (RFR) analyses

RFR is an ensemble learning method, which combines the predictions from multiple models to make more accurate predictions than any single model. It operates by building a series of decision trees (DT) that are composed of a random sample of explanatory input variables (*mtry*) and built from a random subset of the data. Each DT generates an output based on iteratively progressing through a series of decision nodes. Finally, the resulting predictions are averaged across each DT to generate more accurate predictions and to reduce overfitting (Breiman, 2001). RFRs applied to both Subarctic and Arctic datasets were built as an ensemble of 1000 trees (to ensure each sample row is predicted multiple times) and with an *mtry* = 4 (i.e., 4 variables were randomly subsampled for each DT). Once the most influential predictor variables were identified, new RFRs were derived for each region composed of only the most significant predictors ($RFR_{Subarctic}$, and $RFR_{Arctic}$).

In contrast to MLR, RFR techniques do not rely upon linear relationships between explanatory and response variables (Breiman, 2001) or specific data distributions; as such, they may be able to identify TEP predictors that may not be recognized by MLRs. Like MLRs, RFR

techniques allow for the estimation of variable importance (VI) from a set of explanatory (input) variables. A commonly reported metric for estimating VI in RFRs is the mean square increase in error (% MSE increase) attributed to the removal of a specific predictor variable. Cross validation techniques were performed in the same fashion as MLRs. The *randomForest* package of the statistical programming language R (v 4.2.3) was used to compute all RFR modelling.

### 2.3.11 Predicting Spatiotemporal Trends in Historical TEP (and TEP-C) Concentrations

MLR and RFR models (consisting of only the most influential predictors) were applied to large historical datasets from the ESNP to estimate spatiotemporal trends in surface (5 m) TEP. The historical datasets of explanatory variables are available from DFO for the Line P transect. The model was applied to the dataset from the following two decades: 1998 to 2018, for spring, summer, and winter cruises. Predicted historical [TEP], in µg XG eq $L^{-1}$, were converted to C units (µg C $L^{-1}$, expressed as [TEP-C]) using the conservative conversion factor of 0.51 as described by Engel and Passow (2001).

## 2.4. Results

### 2.4.1 Biological and environmental characterization of surface waters

There were distinct variations in the biological and environmental properties of each study region (Figure 2.2). Across the entire scope of the study, [TEP] ranged from 2 – 137.6 µg XG eq $L^{-1}$, [Chl *a*] from 0.03 – 26.4 µg $L^{-1}$, [POC] from 46.78 – 1253.97 µg C $L^{-1}$, and AOU from -4.80 – 11.50 and ml $L^{-1}$, respectively (Fig 2.2A-D). Concentrations of TEP were highest during the spring and summer in the ESNP (ON shelf) and BE-CH regions, while significantly lower [TEP] were observed in winter and fall across all regions (Figure 2.2A). TEP

concentrations did not vary significantly between years, or between surface (5 m) and the Chl *a* max depth if region is accounted for (Two-Way ANOVA, $p > 0.05$).

Chl-*a* and POC concentrations had generally similar patterns to [TEP] in all regions, with highest ranges observed in the spring/summer in the ESNP-ON and BE-CH, and the lowest in the fall and winter throughout each region (Figure 2.2B, C). Particularly low values for TEP, chl-*a*, and POC were observed throughout the BS-CB. Unsurprisingly, there were significant physical variations between regions, including temperature (-1.9 – 17.7 ˚C), mixed layer depth (3-114 m), wind speed (2.3 – 14.7 m $s^{-1}$), and salinity (24.2 – 34.8) (Figure 2.2E-G). Solar Radiation Dose (SRD) was highest in summer months, followed by spring and winter (Figure 2H). Nutrient concentrations ($NO_3^-$, $PO_4^{3-}$, $Si(OH)_4$) were variable, with generally higher concentrations in the ESNP (OFF and ON), particularly in the winter (Figure 2.2J-L).

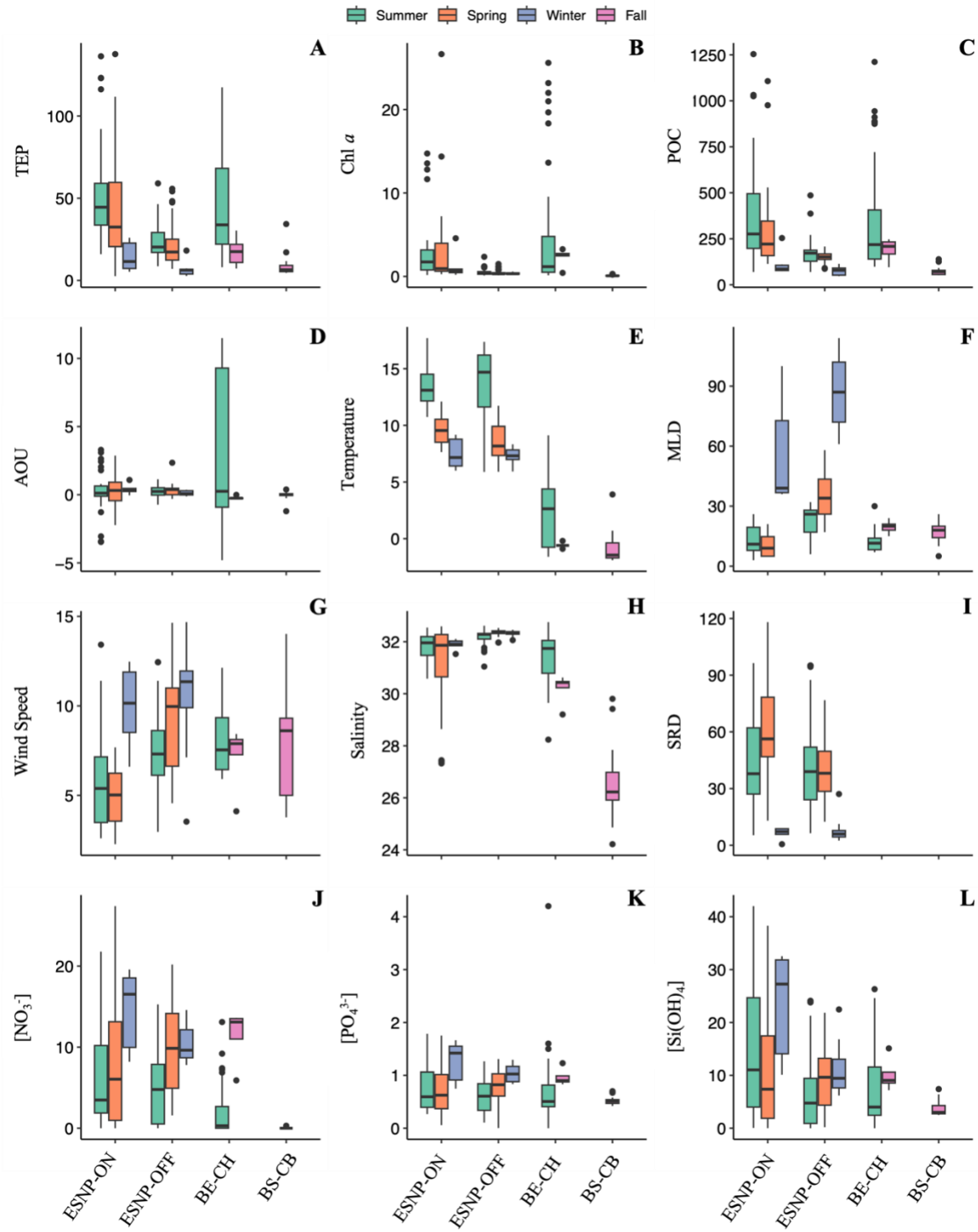
Summer
Spring
Winter
Fall
A
TEP
B
Chl a
C
POC
D
AOU
E
Temperature
F
MLD
G
Wind Speed
H
Salinity
I
SRD
J
[NO3-]
K
[PO43-]
L
[Si(OH)4]
ESNP-ON
ESNP-OFF
BE-CH
BS-CB

**Figure 2.2.** Boxplots displaying median and ranges in TEP concentrations (µg XG eq $L^{-1}$) (**A**), chlorophyll *a* (µg $L^{-1}$) (**B**), particulate organic carbon (POC; µg C $L^{-1}$) (**C**), apparent oxygen utilization (**D**) (AOU; ml $L^{-1}$), temperature (˚C) (**E**), mixed layer depth (MLD; m) (**F**), wind speed (m $s^{-1}$) (**G**), salinity (psu) (**H**), solar radiation dose (SRD; W $m^{-2}$) (**I**), nitrate ([$NO_3^-$]; µM)(**J**), phosphate ([$PO_4^{3-}$]; µM) (**K**), and silicic acid ([$Si(OH)_4^-$]; µM) (**L**), in the the Eastern Subarctic North Pacific (ESNP, ON = ON-shelf and OFF = OFF-shelf), Bering and Chukchi Seas (BE-CH), and Beaufort Sea/Canada Basin (BS-CB). Samples were collected at various times of year (summer, spring, winter, and fall), from 2019-2022. Boxes represent the 50% interquartile range, while the vertical lines indicate the range in values outside the interquartile range, and black dots indicating outliers. 'OFF-shelf' stations are defined as stations that were located off the continental shelf in waters >1500 m; 'ON-shelf' stations are defined as near-shore regions in waters <1500m depth.

### 2.4.2 Biological and environmental relations with TEP

*Proxies of biomass*

Surface [TEP] were significantly positively correlated with all proxies of phytoplankton biomass (chl-*a*, POC, and AOU) across each oceanographic region during all seasons and years (Figure 2.3). In the Subarctic, linear regressions between TEP and chl-*a* ($R^2$ = 0.62, $p$ < 0.001) and POC ($R^2$ = 0.68, $p$ < 0.001) yielded strong significant results. Similarly, in the BE-CH, TEP was strongly correlated with chl-*a* ($R^2$ = 0.54, $p$ < 0.001) and POC ($R^2$ = 0.25, $p$ < 0.001). In contrast, TEP was not well correlated with chl-*a* in the BS-CB but was with POC ($R^2$ = 0.52, $p$ < 0.001); this result is likely due to the small number of observations in the region coupled with the consistently low measured TEP and chl-*a* concentrations (Figure 2.2A-B).

There was little evidence of seasonality in the relationships between TEP and phytoplankton biomass in the Subarctic (data not shown). Summer seasons consisted of a slightly stronger covariance between TEP and chl-*a* ($R^2$ = 0.65, $p$ < 0.001) compared to spring ($R^2$ = 0.59, $p$ = 0.001) and winter ($R^2$ = 0.42, $p$ = 0.005) seasons; however, statistical significance was only observed in lower average winter values compared to spring/summer. Seasonal variation between TEP and biomass proxies in the BE-CH were not significant.

*Proxies of productivity/respiration*

AOU displayed a weak, but significant statistical correlation ($R^2$ = 0.02, $p$ = 0.03), while total dissolved oxygen concentrations (DO) were not significantly correlated with TEP across the entirety of the study regions (Figure 2.3). In the Subarctic, DO was significantly positively correlated with TEP ($R^2$ = 0.08, $p$ < 0.001), however the relationship is significantly improved if AOU is used instead ($R^2$ = 0.22, $p$ < 0.001) (Figure 2.3). TEP was also more highly correlated with AOU concentrations in the summer ($R^2$ = 0.34, $p$ < 0.001) compared to spring ($R^2$ = 0.25, $p$ < 0.001) and winter (*n.s*) seasons (not shown in Figure). TEP was similarly significantly correlated with AOU ($R^2$ = 0.15, $p$ = 0.03) in the BS-CB (Figure 2.3).

*Direct environmental predictors*

Concentrations of TEP were significantly correlated with temperature across the entire dataset, particularly within the Subarctic ($R^2$ = 0.07, $p$ = 0.002) and BS-CB regions ($R^2$ = 0.1, $p$ = 0.01) (Figure 2.3). In contrast, within the Subarctic, chl-*a* and POC were not significantly correlated with temperature (data not shown).

Over the entire study, TEP was significantly negatively correlated with [$NO_3^-$] ($R^2$ = 0.02, $p$ = 0.01, $n$ = 217), and to a lesser degree, [$PO_4^{3-}$] ($R^2$ = 0.01, $p$ = 0.05, $n$ = 217), but not [$Si(OH)_4$] concentrations (Figure 2.3). However, there was large regional variation in the relationship between TEP and nutrient concentrations, as shown in Figure 2.3. While TEP was significantly negatively correlated with both [$NO_3^-$] ($R^2$ = 0.09, $p$ = 0.0002, $n$ = 148) and [$PO_4^{3-}$] ($R^2$ = 0.06, $p$ = 0.002, $n$ = 148), in the ESNP, TEP was not correlated with any nutrients within the Arctic regions (besides a slightly positive correlation with [$PO_4^{3-}$] in the BS-CB) (Figure 2.3).

*Indirect environmental predictors*

Concentrations of TEP were negatively correlated with the depth of the mixed layer (MLD) across the entire study ($R^2$ = 0.12, $p$ < 0.001, $n$ = 217); this trend was preserved across Subarctic ($R^2$ = 0.17, $p$ < 0.001, $n$ = 148), and Arctic ($R^2$ = 0.23, $p$ = <0.001, $n$ = 69) regions (Figure 2.3). Similarly, TEP concentrations were significantly negatively correlated with WS across the entire study scope ($R^2$ = 0.02, $p$ = 0.03, $n$ = 217), although the correlation strength and significance were not particularly strong. This result is explained by the stark regional differences in the correlations between TEP and WS, with weak negative correlations observed in the Subarctic, and strong positive correlation observed in the BE-CH. Average 24-h PAR and SRD were uncorrelated with TEP concentrations in the Subarctic (with no data available for the BE-CH and BS-CB), although a general positive relationship was observed between both variables and TEP concentrations (Figure 2.3). TEP was strongly correlated with salinity in both the BS-CB and BE-CH (Figure 2.3).

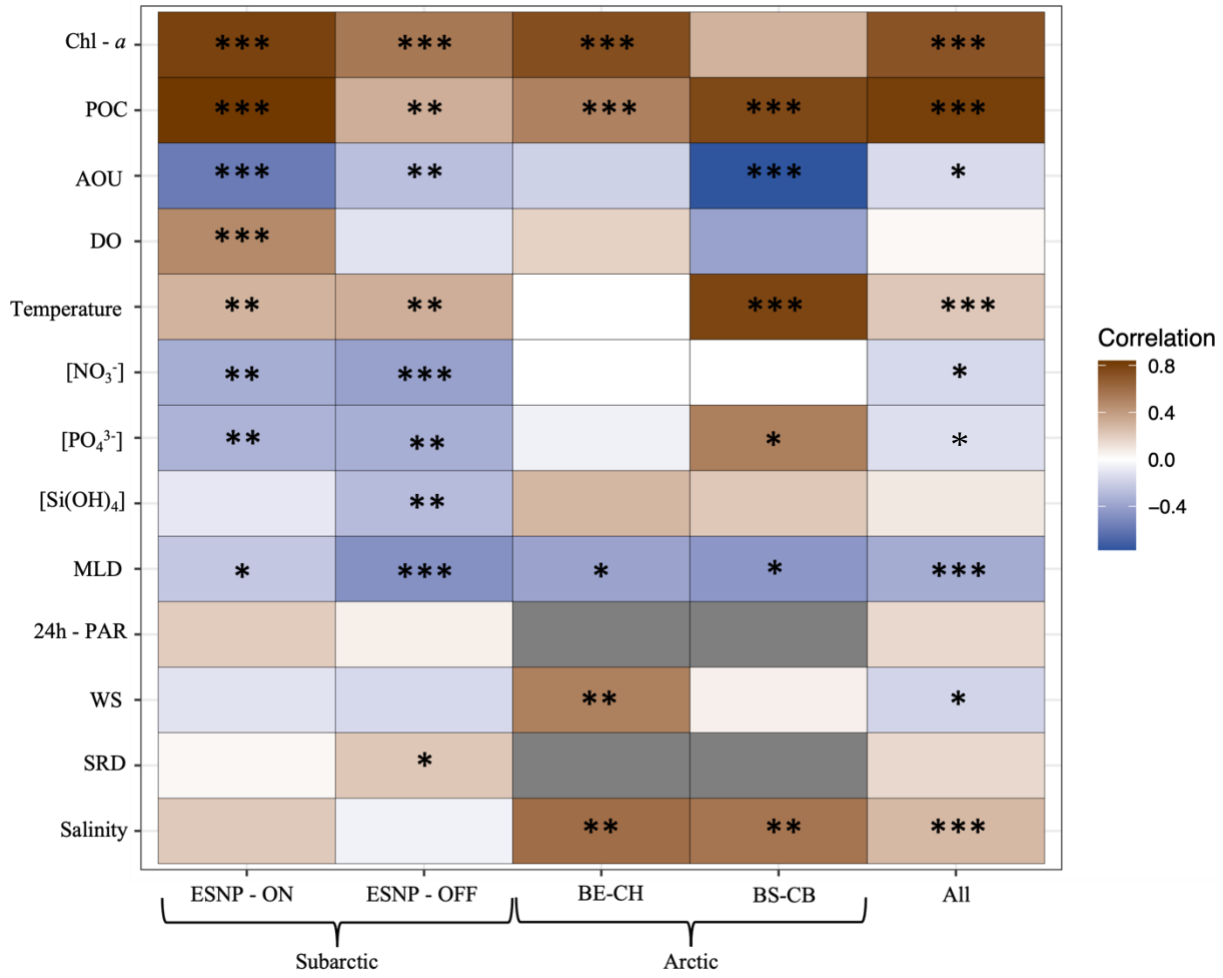


**Figure 2.3.** Linear correlation strengths and significance levels between TEP concentrations and predictor variables in the Subarctic Pacific (ESNP on-shelf (ON) and off-shelf (OFF)) and Arctic regions (Bering and Chukchi Seas (BE-CH) and Beaufort Sea/Canada Basin (BS-CB)) across all seasons and years sampled in this study. Predictor variables included chlorophyll a (chl - a; µg $L^{-1}$ ), particulate organic carbon (POC; µg $L^{-1}$), apparent oxygen utilization (AOU; ml $L^{-1}$), total dissolved oxygen (DO; ml $L^{-1}$) temperature (˚C), nitrate ([$NO_3^-$]; µM), phosphate ([$PO_4^{3-}$]; µM), silicic acid ([$Si(OH)_4^-$]; µM), mixed layer depth (MLD; m), 24h-average photosynthetically active radiation (24h-PAR; µE $m^2$ $d^{-1}$ ), wind speed (WS; m $s^{-1}$), solar radiation dose (SRD; W $m^{-2}$ ), and salinity (psu). Significance levels are denoted as $p < 0.05$ = *, $p < 0.01$ = **, $p < 0.001$ = ***, while boxes without asterisk represent non-significant correlations. The colour scheme represents the relative strength and direction of each correlation. Dark gray colours indicate absent values.

### 2.4.3 Identifying TEP Predictors Through Multiple Linear Regression Analyses

Multiple linear regressions (MLR) were derived from independent variables significantly correlated with TEP (Figure 2.3). In the Subarctic, this included chl-*a*, POC, AOU, temperature, MLD, [$PO_4^{3-}$], [$NO_3^-$], and WS (Figure 2.4A); in the Arctic regions, chl-*a*, POC, salinity, MLD, temperature and WS were evaluated as statistically significant (Figure 2.4B). 'Biological sources', as represented by chl-*a* and POC, were the largest influence on TEP concentrations across the Subarctic and Arctic regions as evidenced by the standardized coefficient estimates (Figure 2.4 A, B). Similar trends were evident for MLD and temperature, which were characterized by significantly negative and positive coefficients, respectively. There was also strong evidence for AOU and salinity as important TEP predictors in the Subarctic and Arctic regions, respectively (Figure 2.4 A, B).

The optimal predictive TEP model ($MLR_{Subarctic}$) within the ESNP was composed of: (i) chl-*a, (*ii) AOU, (iii) temperature, and (iv) MLD that explained 75% of the variance (Table 2.3). Note: POC was excluded as a model parameter due to multicollinearity with chl-*a* and a lack of available historical data along Line P in which to make predictions. The $MLR_{Subarctic}$ was cross validated upon new data inputs and yielded a MAE of ~10.8 µg XG eq $L^{-1}$ (Figure 2.5A). In contrast, the optimal model for the Arctic regions ($MLR_{Arctic}$) was composed of (i) chl-*a, (*ii) salinity, (iii) temperature, and (iv) MLD (Table 2.3), and explained 66% of variance in the dataset, with a MAE of 12.1 µg XG eq $L^{-1}$ when cross validated (Figure 2.5B).

**Table 2.3.** Multiple Linear Regression (MLR) models for estimating surface TEP concentrations in both the Subarctic (ESNP-ON and OFF) and Arctic (BE-CH + BS-CB) regions. MLRs were composed of significant predictor variables that did not violate any assumptions of linear modelling, as described in *2.3.9 Multiple Linear Regression Analyses*. The optimal models are described below as $MLR_{Subarctic}$ and $MLR_{Arctic}$ for both the Subarctic and Arctic regions, respectively. Coefficient strengths, direction, and significance values (p) are also shown. Significance levels are denoted as $p < 0.05$ = *, $p < 0.01$ = **, $p < 0.001$ = ***.

| $MLR_{Subarctic}$ | | | | |
|---|---|---|---|---|
| **Variables** | **Estimate** | **SE** | ***t* value** | **Probability, Pr (>\|*t*\|)** |
| Intercept | 32.00 | 5.51 | 5.81 | 3.93e-08 *** |
| Chl-a (log transformed) | 37.34 | 2.72 | 13.77 | < 2e-16 *** |
| AOU | -7.51 | 1.31 | 5.71 | 6.21e-08 *** |
| Temperature | 1.15 | 0.39 | 2.90 | 0.004** |
| Mixed layer depth | -0.15 | 0.06 | -2.40 | 0.01 * |

| $MLR_{Arctic}$ | | | | |
|---|---|---|---|---|
| **Variables** | **Estimate** | **SE** | ***t* value** | **Probability, Pr (>\|*t*\|)** |
| Intercept | -10.21 | 52.26 | -0.20 | 0.84 |
| Chl-a (log transformed) | 17.67 | 4.82 | 3.67 | 0.0006*** |
| Temperature | 0.19 | 0.92 | 0.20 | 0.85 |
| Salinity | 2.02 | 1.72 | 1.17 | 0.25 |
| Mixed layer depth | -1.00 | 0.49 | -2.01 | 0.04 * |

### 2.4.4 Identifying TEP Predictors Through Random Forest Regression Analyses

Random forest regressions (RFR) were also used to identify primary TEP predictors by estimating the relative importance of variables in predicting [TEP], expressed as percentage increase in mean squared error (% MSE Increase). Higher MSE values indicate a higher importance from a given variable, expressed as the % increase in mean squared error attributed to removing the variable from the model.

In the Subarctic Pacific, a RFR identified phytoplankton biomass (chl-*a* and POC) and AOU to be the most important predictors of surface [TEP], accounting for approximately 22%, 17%, and 10% of the model accuracy, respectively. Temperature and MLD were also identified as being important TEP predictors by the RFR, with each variable accounting for 12% and 8% of

the model accuracy, respectively. Nitrate and SRD were also responsible for ~8% and 6% of the model's accuracy, respectively (Figure 2.4C).

A RFR applied to the Arctic regions (BE-CH + BS-CB) identified similar trends in variable importance, with some notable differences (Figure2.4D). Chl-*a* and POC were still important predictors in the model (~8.4% and 6.3%, respectively), however, AOU only explained ~2.5% of the model's accuracy. In contrast, salinity and MLD were identified as contributing to the model's predictive accuracy in the Arctic with ~8% MSE increase if removed. The final RFR models for each dataset were built with the five most explanatory variables, as outlined in Table 2.4 (note, the %MSE increase for each variable in Table 2.4 is different than the original RFRs as variables with low explanatory power have been removed).

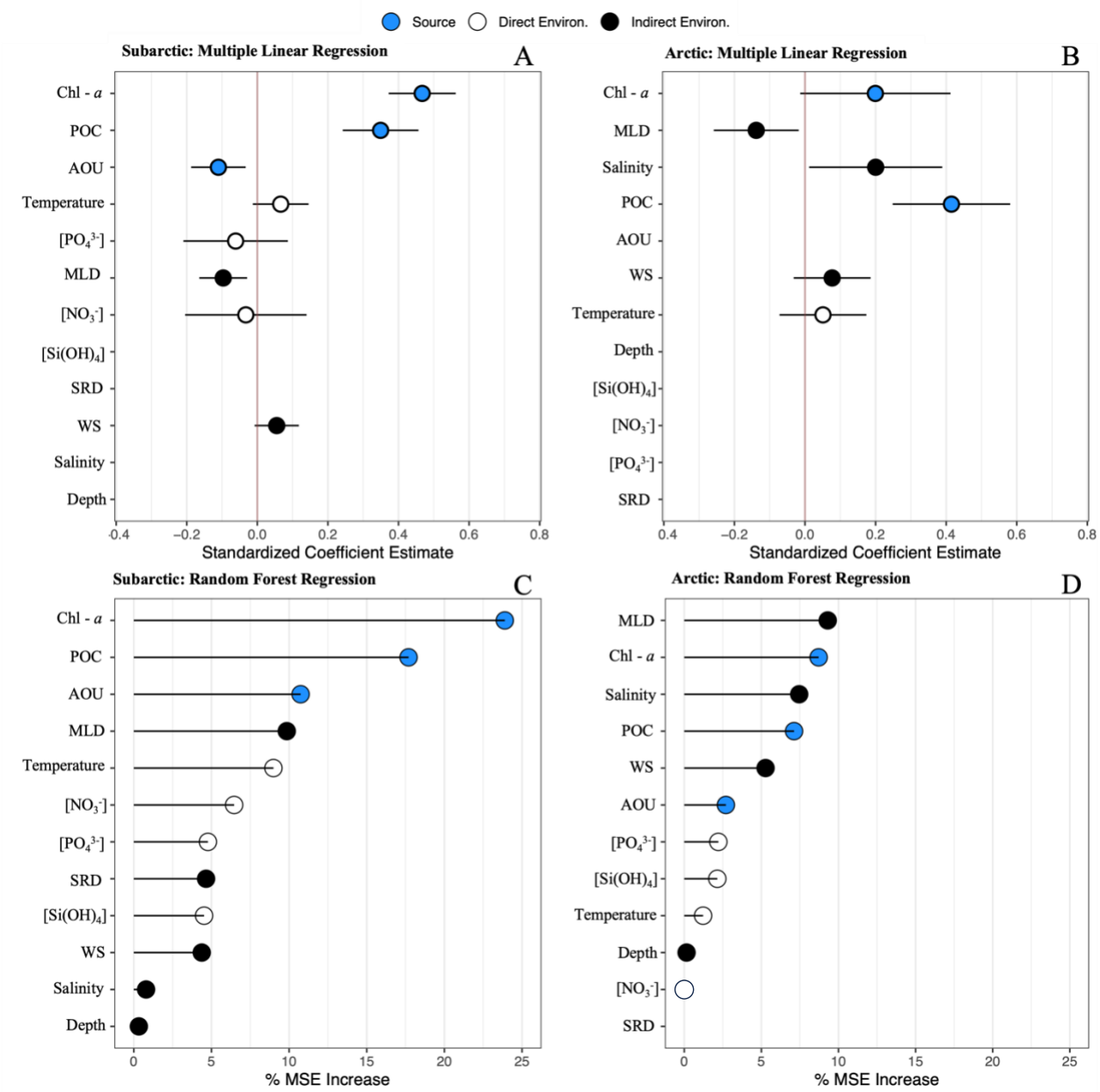


**Figure 2.4.** Model comparison and ranking of respective variable importance between RFRs and MLRs in estimating surface TEP concentrations across the Subarctic Pacific (ESNP on-shelf and off-shelf) and Arctic regions (BE-CH + BS-CB). In the MLR plots (**A** and **B**), predictor variables are plotted as a function of standardized coefficient estimates, representing the slope and standard error of each predictor on TEP concentrations. A vertical red line is plotted along the intercept; coefficient estimates closer to the red line have a lower influence on TEP concentrations. MLR plots are only composed of variables that were significantly correlated with TEP concentrations. In the RFR plots (**C** and **D**), explanatory variables are displayed as a function of percent Mean Square Error (MSE) increase, where higher values indicate a larger contribution to estimating TEP concentrations (percent MSE Increase corresponds to the increase in error when a given variable is removed from the model). Variables are ranked by descending

order of importance. The colour scheme presents a visual representation of major categories of commonly reported TEP predictors, including biological inputs (blue circles), direct (open circles), and indirect (black circles) environmental influences on TEP production or retention in the surface ocean. A lack of symbols corresponds to row variables that were not included in the analysis due to the absence of a significant correlation (MLR) or lack of available data (RFR).

**Table 2.4**. Explanatory variables included in RFR models for the Subarctic (ESNP-ON and OFF) and Arctic (BE-CH and BS-CB) regions and used for predicting historical patterns in surface TEP concentrations in the Subarctic. The top 5 significant predictor variables were selected for application in the model(s); the optimal models are described below as $RFR_{Subarctic}$ for the Subarctic, and $RFR_{Arctic}$ for the Arctic regions. POC was excluded from variable selection in these models due to a lack of data historical availability along Line P in the ESNP. Explanatory variables are displayed as a function of percent Mean Square Error (MSE) increase, where higher values indicate a larger contribution to estimating TEP concentrations (percent MSE Increase corresponds to the increase in error when a given variable is removed from the model).

| $RFR_{Subarctic}$ | |
|---|---|
| **Variable** | **% MSE Increase** |
| Chl-a | 39.14 |
| AOU | 12.83 |
| MLD | 10.65 |
| Temperature | 8.79 |
| Nitrate | 8.45 |
| **$RFR_{Arctic}$** | |
| Chl-a | 14.24 |
| Salinity | 15.22 |
| MLD | 13.88 |
| Temperature | 11.35 |
| AOU | 10.79 |

### 2.4.5 Variable Importance Comparison: RFR and MLR

Both MLR and RFR models converge on similar results for ranking of variable importance in predicting TEP. Proxies of phytoplankton biomass (chl-*a*, and POC) were consistently weighed as the most important explanatory variables across all regions and model types. AOU was also identified as a significant predictor of TEP, with the exception of $MLR_{Arctic}$. Temperature, [$NO_3^-$], and MLD were also important explanatory variables in both models. These results are also demonstrated in the refined model outputs for each regional model

type (Table 2.4). The refined models were derived from the most significant predictor variables for each model type, and avoid excess noise from redundant variables or, in the case of MLRs, violations of linear modelling assumptions. In the Subarctic, depth, salinity, SRD, and [$Si(OH)_4$] were not favoured by AIC selection criteria in MLR, and in addition to WS, were also not responsible for substantial %MSE increase in RFR; therefore, they were dropped from the refined models described in (Table 2.4) to avoid overfitting. Additionally, POC and [$PO_4^{3-}$] were removed from $MLR_{Subarctic}$ and $RFR_{Subarctic}$ due to concerns of multicollinearity with chl-*a* and [$NO_3^-$], respectively. In the Arctic, depth, nutrient concentrations, and SRD were removed from $MLR_{Arctic}$ and $RFR_{Arctic}$ due to lack of significant correlation with [TEP] and to avoid overfitting; AOU was also removed from $MLR_{Arctic}$ for the same rationale. Wind speed (WS) was also removed from both model types as including it as a model parameter violated the assumptions of normality required for linear modelling. Similarly, POC was removed from both models due to concerns of multicollinearity with chl-*a*. The refined models are presented in Tables 2.3 and 2.4. The $RFR_{Subarctic}$ was used for predicting spatiotemporal trends in surface [TEP] across Line P.

### 2.4.6 Evaluation of Model Performances

Overall, both model types were accurate in predicting [TEP] in both the Subarctic and Arctic hold out data sets (Figure 2.5A-D). The RFR was superior in terms of predictive accuracies, with a MAE of 8.44 µg XG eq $L^{-1}$ in the Subarctic and 14.4 µg XG eq $L^{-1}$ in the Arctic when tested upon hold out data (Figure 2.5C, D), corresponding to MAE percentages of 26% and 65%, respectively. In comparison, the optimal MLR for each dataset yielded MAEs of 10.7 µg XG eq $L^{-1}$ in the Subarctic and 16.2 µg XG eq $L^{-1}$ in the Arctic, corresponding to MAE

percentages of 41% and 45%, respectively (Figure 2.5A, B). However, it should be noted that low values bias MAE percentages towards higher error percentages.

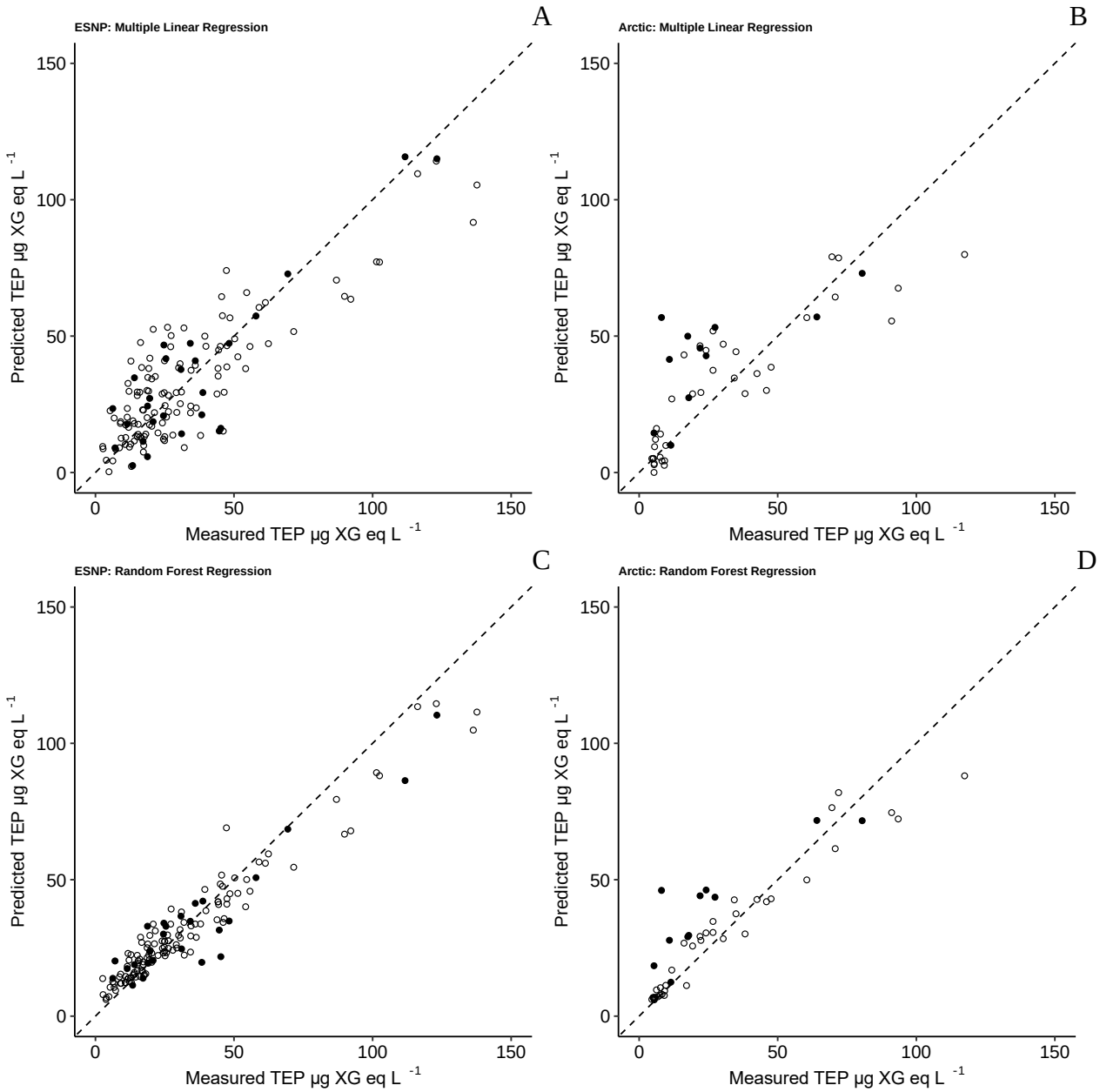


**Figure 2.5.** Comparison between observed and predicted values by both Multiple Linear Regression (MLR) (**A** and **B**) and Random Forest Regression (RFR) (**C** and **D**) models in the Subarctic and Arctic regions. The models were trained on 80% of the data (open circles) and tested on the "hold-out" 20% (filled circles). Dashed lines indicate a 1:1 slope between measured and predicted values.

### 2.4.7 Predicting Surface TEP-C from Historical Datasets in the Subarctic from 1998-2018

Estimations of past surface [TEP-C] were derived using $MLR_{Subarctic}$ and $RFR_{Subarctic}$ models, with input parameters for chl-*a*, temperature, AOU (derived from [DO], temperature and salinity), MLD, and [$NO_3^-$] obtained from the historical database collected by DFO along the Line P transect in the Subarctic from 1998-2018. Notably, the application of these models to the Line P database is within the same geographic range (including the exact sampling locations) from where data presented in this study were collected and from where the models ($MLR_{Subarctic}$ and $RFR_{Subarctic}$) were derived.

There was significant spatiotemporal variation in predicted historical [TEP-C] across the entire Line P transect at 5m depth (Figure 2.6). In the case of $MLR_{Subarctic}$ predictions, summer (mean = 16.5 $\pm$ 10.9, range = 0 – 72.0), spring (mean = 14.9 $\pm$ 9.3, range = 0 – 59.2), and winter (mean = 7.8 $\pm$ 5.1, range = 0 – 28.2), estimations of TEP-C (µg C $L^{-1}$) were significantly different from each other. Predictions made by $RFR_{Subarctic}$ displayed a similar trend, with summer (mean = 17.1 $\pm$ 8.3, range = 10.0 – 58.5), spring (mean = 15.9 $\pm$ 8.5, range = 4.9 – 58.5), and winter (mean = 7.2 $\pm$ 2.9, range = 3.9 – 18.2) seasons displaying significant variation from one another ($p < 0.05$), demonstrating the seasonality of TEP-C in the Subarctic. However, spatial variability was more pronounced in the predicted data, with higher and more variable [TEP-C] closer to shore, and a lower range in oceanic regions for both model types (Figure 2.6). After station P8 [TEP-C] was notably constant, and averaged 11.9 $\pm$ 4.5, 12.6 $\pm$ 5.3, and 5.8 $\pm$ 3.3 µg C $L^{-1}$ in spring, summer, and winter seasons respectively for $MLR_{Subarctic}$; for $RFR_{Subarctic}$, [TEP-C] predictions averaged 12.8 $\pm$ 3.9, 14.1 $\pm$ 2.4, and 6.2 $\pm$ 1.9 µg C $L^{-1}$ in spring, summer, and winter seasons respectively. In contrast, the average and standard deviations of measured [TEP-C] ranged from 10.5 $\pm$ 6.8, 12.4 $\pm$ 5.1, and 3.4 $\pm$ 2.3 µg C $L^{-1}$ in spring, summer, and

winter seasons respectively. Stations closer to shore (P1-P4) were characterized by higher mean [TEP-C], and a much larger upper range (Figure 2.6).

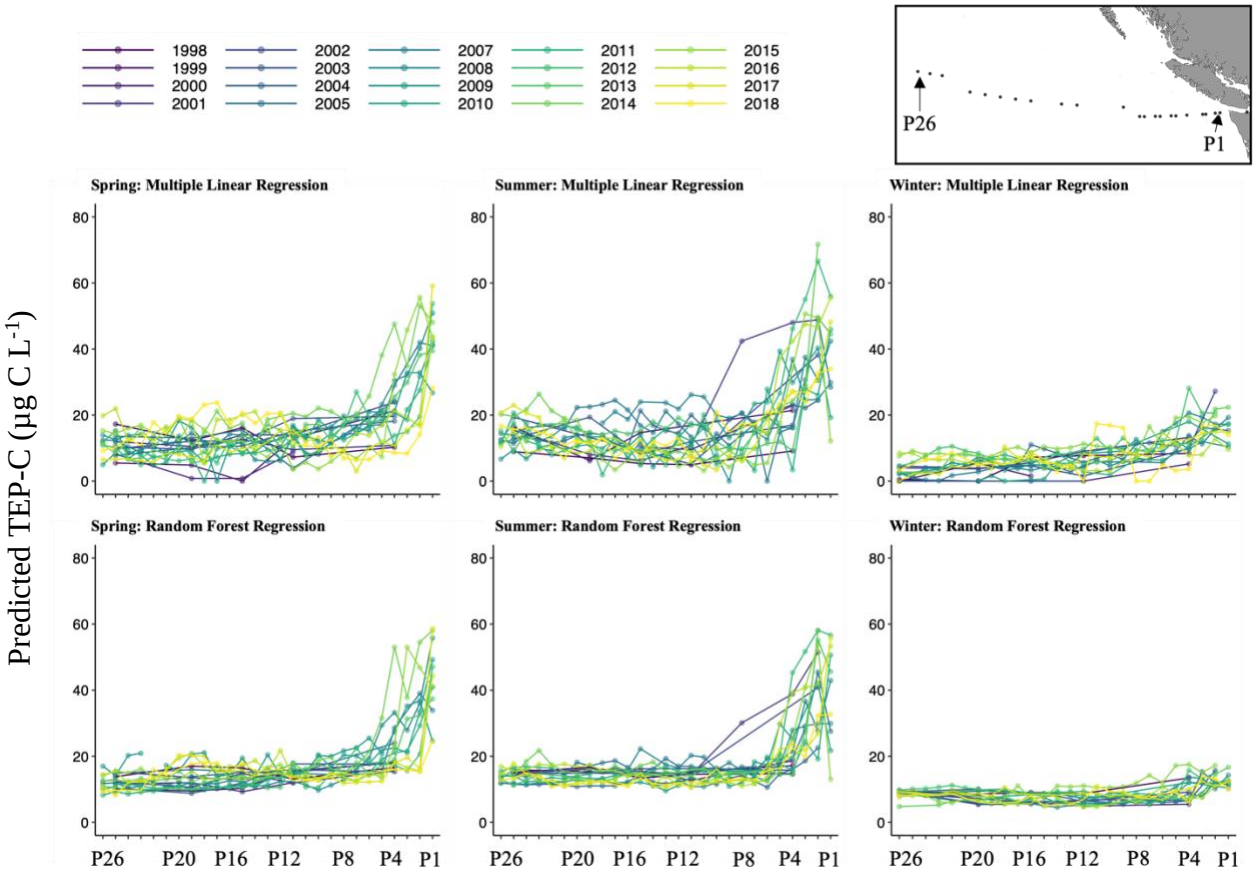


**Figure 2.6.** Predicted spatiotemporal variation in surface (~5 m) TEP-C concentrations along the Line P transect in the Subarctic (includes both ESNP - ON and ESNP - OFF). TEP-C concentrations, expressed in µg C $L^{-1}$, were derived from predicted TEP concentrations (µg XG eq $L^{-1}$) by using the conservative conversion factor of 0.51 from Engel and Passow, (2001). Predicted TEP-C concentrations were derived from both $MLR_{Subarctic}$ and $RFR_{Subarctic}$, consisting of chl-a, AOU, temperature, MLD, and nitrate concentrations as explanatory variables. Seasonal cruises (spring, summer, winter) from the years 1998-2018 are displayed and represented by the discrete colour scheme. Individual lines represent independent cruises for a given season and year, while the points indicate stations. Station locations relative to the west coast of Vancouver Island is displayed in the upper right-hand corner.

## 2.5. Discussion

While the production and dynamics of TEP formation in the ocean are complex and the result of a multitude of processes, there are consistent trends throughout the literature that identify major TEP predictors in both *in situ* and experimental settings (summarized in Table 2.2). This study identified and grouped these explanatory variables into 3 distinct categories: (i) biological sources as the underpinning of all marine TEP, (ii) direct environmental influences that stimulate the production of TEP relative to biological source material, and (iii) indirect environmental influences that act to increase the formation, retention, or degradation of surface TEP. Variables representative of each category were measured alongside [TEP] across large gradients in space and time to derive a representative dataset for the Subarctic and Arctic regions. Two distinct modelling approaches (MLR and RFR) were then used to (i) identify major predictors of TEP across large spatiotemporal scales, and (ii) predict spatiotemporal patterns in [TEP-C] and estimate [TEP-C] in oceanic regions of the Subarctic.

### 2.5.1 Multivariate modelling of surface TEP

The models used in this study, MLRs and RFRs, converged upon the importance of biological influences as key TEP predictors. Chl-*a* and total POC concentrations were consistently ranked as having the highest importance, while AOU was also identified as a potentially significant TEP predictor. It was necessary to exclude POC from the final models ($MLR_{subarctic}$ and $RFR_{Subarctic}$) due to a violation of linear modelling assumptions (excess multicollinearity with chl-*a*, in the case of MLR), and because of a lack of available data in which to apply the model (in the case of MLR and RFR). When assessed alone, chl-*a* and AOU resulted in accurate MLR predictions of [TEP] (at the horizontal, surface scale), with a $R^2$ of

68% and MAE of ~12 µg XG eq $L^{-1}$ when tested upon new data inputs for the Subarctic. This result is supported by recent evidence from Ortega-Retuerta et al., (2017), who observed a strong coupling between [TEP] and chl-*a* across horizontal scales, and with [DO] and bacterial production at the vertical scale. These results support the hypothesis formulated by Ortega-Retuerta et al., (2017), who suggest that remote sensing chl-*a* and DO can be used as a predictors of TEP (Ortega-Retuerta et al., 2017). In RFR analyses, chl-*a* and AOU accounted for ~38% of total predictive accuracy across the Subarctic, which while notable, also highlights the need for additional parameters to better capture variance in marine [TEP]. This result is not entirely surprising, and sufficient evidence exists in the literature of temporal decoupling of TEP and chl-*a* during periods of warmer temperatures and nutrient limitation (Mari et al., 2017; Ortega-Retuerta et al., 2017, 2018; Thornton, 2014).

Both model types identified temperature, MLD, and $NO_3^-$, or salinity as key environmental influences, which in combination account for an additional ~ 15-30% of mean error accuracy in RFRs (Figure 2.4). The addition of temperature, MLD, and $NO_3^-$ also reduced MAEs to ~10.7 µg XG eq $L^{-1}$ in the Subarctic, while the addition of MLD and salinity reduced MAE to ~11.9 µg XG eq $L^{-1}$ in Arctic regions. This provides support for the use of multivariate approaches to estimating marine [TEP], and in particular, the inclusion of environmental predictors in conjunction with proxies of phytoplankton biomass and productivity. Furthermore, each of these parameters is supported by both experimental and *in situ* evidence of having an important influence on [TEP], as discussed below.

### 2.5.2 Biological Sources as Predictors of Surface TEP

My results indicate that phytoplankton biomass and productivity are key predictors of

marine TEP. The relationship between TEP, phytoplankton biomass, and activity is also well demonstrated in a study by Zamanillo et al. (2019), who observed a strong correlation between chl-*a* and TEP at 4 m depth over a transect across the Atlantic Ocean, from Cartagena, Spain, to Punta Arenas, Chile (Zamanillo, Ortega-Retuerta, Nunes, Rodríguez-Ros, et al., 2019). Similarly to my study, these results are compelling due to the large gradients in space and time over which TEP and associated biological relationships were observed. However, the lower density of TEP than seawater (Azetsu-Scott & Passow, 2004) and the tendency of TEP to accumulate above the deep chlorophyll maxima may result in a vertical decoupling of TEP and chl-*a* (Ortega-Retuerta et al., 2017). Chl-*a* and TEP may be further decoupled during late summer periods, which is often attributed to conditions of low nutrient availability, higher temperatures, and stronger stratification (Engel, 2002a; Mari et al., 2017; Ortega-Retuerta et al., 2018), all of which are known to promote TEP production or retention in the ocean's surface. Therefore, while there is strong support for chl-*a* as an important predictor of surface TEP, chl-*a* alone is unlikely to explain significant variance in surface [TEP] during periods when environmental conditions promote increases in TEP production and accumulation relative to chl-*a* or total biomass. The inclusion of other environmental variables that are linked to the decoupling between chl-*a* and TEP are therefore necessary to derive accurate TEP predictions.

Ortega-Retuerta et al. (2019, 2017) and Kodama et al. (2014) observed strong correlations between [DO] and [TEP] in the field, implying that community productivity may be a major predictor of TEP. Phytoplankton release large amounts of photosynthetic products in the form of polysaccharides during photosynthesis, and TEP may represent 5-10% of total primary production (Mari et al., 2017). Bacterial respiration has also been correlated with [TEP]; however, trends in the literature attribute bacterial production as both a potential source

(Ramaiah & Furuya, 2002) or sink of TEP via respiration (Bar-Zeev et al., 2009; Mühlenbruch et al., 2018). Bacteria are known to actively colonize TEP, as it provides an ideal substrate for bacterial growth (Ortega-Retuerta, Reche, et al., 2009; Ramaiah & Furuya, 2002). As such, it is likely that bacteria both simultaneously produce and consume TEP. This duality implies that bacterial respiration, production, or abundance are not ideal predictors for TEP which is more likely to be a product of phytoplankton exudation (Zamanillo, Ortega-Retuerta, Nunes, Estrada, et al., 2019). In this study, I did not directly measure bacterial production or respiration. However, my analysis did include estimates of AOU, which can represent a broad proxy for either net community production ($[DO_{measured}] > [DO_{equilibrium}]$) or net community respiration ($[DO_{measured}] < [DO_{equilibrium}]$), which would capture the influence of bacterial respiration on total community productivity. A linear regression between TEP and AOU ($R^2 = 0.21$, $p < 0.001$) was much more significant, and explained more variance, than a regression between TEP and DO ($R^2 = 0.07$, $p < 0.05$). This implies that AOU is a better predictor of [TEP] than total [DO] as AOU is a better indication of new community production.

### 2.5.3 Direct Environmental TEP Predictors

*Temperature*

The results from this work suggest that temperature represents an important predictor of [TEP], and there is also a large body of research documenting the causative effect of temperature on EPS release by phytoplankton in laboratory settings (Table 2.2). Furthermore, several field studies have also observed a strong correlation between the two variables, or a significant accumulation of TEP in late summer months when temperatures are typically elevated. Therefore, I hypothesize that the observed trends between TEP and temperature in this study are

due to a combination of three factors: i) direct stimulation of phytoplankton enzymatic activity and EPS release (Claquin et al., 2008; Engel et al., 2011; Fukao et al., 2012; Guo et al., 2022; MorÁn et al., 2006), ii) enhanced C over consumption under higher temperatures (Taucher et al., 2012), and iii) a correlation with nutrient limitation and stratification during higher temperature regimes.

*Dissolved nutrients*

The excretion of EPS by phytoplankton is thought to be largely a result of cellular C overflow, where phytoplankton C fixation exceeds growth and an excess amount of C is produced (Mari et al., 2017; Thornton, 2014). This physiological process is enhanced under conditions of nutrient limitation. Accumulation of TEP has been frequently observed during the onset of nutrient depletion across experimental and observational studies (Mari et al., 2005; Pedrotti et al., 2010; Thornton, 2014) (Table 2.2). The decoupling between phytoplankton biomass and TEP is commonly observed during late summer periods associated with heavily stratified, warm, and nutrient-depleted waters (Mari et al., 2017; Ortega-Retuerta et al., 2018). This suggests that TEP predictions, derived from proxies of phytoplankton biomass, can be improved with the inclusion of proxies of nutrient limitation (i.e., low nutrient concentrations, season, MLD). The models derived in this study support this hypothesis, as the addition of nutrient concentrations, temperature and MLD improved the predictive performance of both MLR and RFR models.

TEP concentrations were significantly negatively correlated with $NO_3^-$ and $PO_4^{3-}$ (but not $Si(OH)_4$) concentrations in the Subarctic. These relationships may be due to phytoplankton growth in the Subarctic being more frequently limited by $NO_3^-$ than $Si(OH)_4$, particularly in

coastal regions and in the summer (Varela & Harrison, 1999). Previous studies have demonstrated the stimulatory effects of N or P limitation to TEP production in phytoplankton assemblages (Corzo et al., 2005; Li et al., 2023). Furthermore, Staats et al. (2000) found that exopolysaccharide accumulation was stimulated under conditions of N and P limitation, but not of $Si(OH)_4$ or Fe limitation, on a batch culture of an epipelic diatom, suggesting that N and P metabolism in phytoplankton is important for TEP production relative to other macro or micronutrients. This is further supported by evidence in my study, where TEP:chl *a* increased with decreasing [$NO_3^-$] and [$PO_4^-$], but not with decreasing [$Si(OH)_4$] (data not shown).

### 2.5.4 Indirect Environmental TEP Predictors

Indirect TEP predictors, which were classified in this study as environmental influences that affect [TEP] independent of biological sources, varied widely in importance for predicting [TEP]. In particular, the depth of the mixed layer (MLD) represented an important TEP predictor and was significantly negatively correlated with [TEP] across the entire study scope. The accumulation of TEP in stratified summer seasons has been well documented (Mari et al., 2001; Mari & Burd, 1998; Ortega-Retuerta et al., 2018), as stratified conditions create strong density gradients at the bottom of the mixed layer that may trap buoyant TEP gels in the upper layers of the water column. High [TEP] and shallow, warmer summer mixed layers likely coincide with nutrient limitation (Ortega-Retuerta et al., 2018). My results confirmed these findings as the MLD was responsible for 8% of the mean decrease accuracy in RFRs and had a negative coefficient with TEP in MLRs. As such, including MLD as a model parameter is important for capturing seasonal variation in [TEP] relative to chl-*a*, and allowing for the prediction of TEP across temporal scales. It is reasonable to postulate that the inclusion of MLD, temperature and

nutrient concentrations is potentially redundant, and may induce multicollinearity (and thus excess noise in the model) in the case of MLRs. However, all three of these parameters capture unique influences on surface ocean TEP (i.e., nutrient limitation, increased EPS exudation, and density 'trapping'), and no excessive multicollinearity was detected in the models.

The influence of other indirect environmental predictors was less notable, apart from salinity in the BE-CH and BS-CB. Salinity was identified as being an important model parameter in both MLR and RFRs for the Arctic regions, a result that is supported in part through similar field correlations presented in the literature (Islam et al., 2021; Zamanillo, Ortega-Retuerta, Nunes, Estrada, et al., 2019). Higher salinity levels may stimulate TEP aggregation due to increasing cation availability (Wetz et al., 2009), which may act to increase TEP stickiness and aggregation potential through the formation of cation bridges; lower salinities levels due to ice melt may have the opposite effect (Sun et al., 2012). However, no significant relationship was observed between TEP and salinity across the ESNP in this study.

Wind speed (WS) was correlated with [TEP] in the ESNP and BE-CH regions, however the direction of the slope of the regression were opposite for each (Figure 2.3). As such, there was not enough statistical significance for WS to explain variance in TEP or to be favoured in either model. Wind driven mixing has been shown to be an important predictor of TEP aggregation rates (Beauvais et al., 2006; Burns et al., 2019; Passow, 2000; Zamanillo, Ortega-Retuerta, Nunes, Estrada, et al., 2019). It is likely that turbulence in the upper mixed layer can act to promote TEP aggregation, but also to reduce its concentrations through deep mixing or aerosolization (Wurl et al., 2011). TEP concentrations have also been shown to be influenced by light and UV radiation, but a variety of studies have arrived at differing conclusions. It has been experimentally observed that UV radiation can increase photodegradation of TEP particles

(Ortega-Retuerta, Passow, et al., 2009b), and significant inverse correlations between SRD (W $m^{-2}$) and TEP have also been observed in the field (Zamanillo, Ortega-Retuerta, Nunes, Estrada, et al., 2019). In contrast, other studies have suggested that a coupling between total photosynthetic activity and TEP production is stimulated under high light conditions, promoting photosynthesis and downstream production of TEP precursors (Claquin et al., 2008) or that microorganisms produce TEP in reaction to solar radiation stress (Iuculano et al., 2017). In this thesis, I observed slightly positive correlations between TEP, SRD, and 24h averaged PAR in the ESNP (data was not available for the Arctic regions), however, neither variable was significant in explaining [TEP] for either MLRs or RFRs. Therefore, the dynamic relationships among wind speed, turbulence, and TEP aggregation/export is difficult to parametrize, especially in linear models.

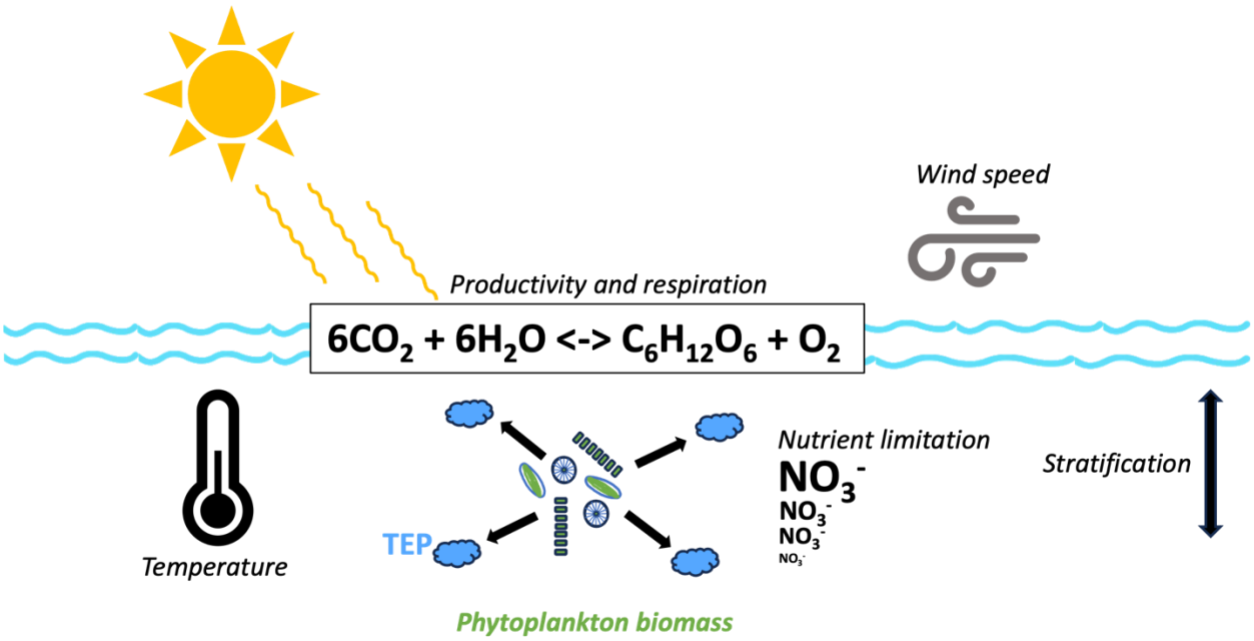


**Figure 2.7** Major predictors of marine TEP in the surface of the Subarctic and Arctic regions. Temperature, phytoplankton biomass, productivity and respiration (as proxied by AOU), stratification, nutrient limitation, and wind speed were identified as important TEP predictors by both random forest regression and multiple linear regression approaches.

### 2.5.5 Spatiotemporal Trends in Marine TEP-C Across the ESNP

Historical predictions of TEP based C (TEP-C) along Line P were derived using $MLR_{Subarctic}$ and $RFR_{Subarctic}$. Overall, the RFR model yielded slightly more accurate predictions of TEP when cross validated upon new data inputs (Figure 2.5C, D). This is likely due to the ability of RFR to capture non-linear relationships in the data. However, RFRs are limited in their predictive ability as they are constrained by the range in the training dataset, are therefore not well suited for predicting outside of the range in values of training data. In contrast, MLR are not limited by the range of their training sets, and therefore more suited for extrapolating [TEP-C] predictions from historical data outside the range of the training data. There was noticeable seasonality in [TEP-C] predictions across Line P from 1998-2018, with summers characterized by significantly higher [TEP-C], and winter observations significantly lower than both spring and summer seasons (Fig 2.6). These predictions are consistent with observed summer TEP maxima in the literature (Mari et al., 2001; Mari & Burd, 1998; Ortega-Retuerta et al., 2018). This trend is also paralleled in the measured [TEP-C] from this study (which constitutes the training data set), with summer periods characterized by having the highest observed [TEP-C], although not significantly higher than spring.

Along Line P, there is also significant spatial variation in estimated [TEP-C], with elevated and variable concentrations closer to shore, and more consistent, lower values offshore towards high nutrient low chlorophyll (HNLC) conditions. These results can be attributed to the spatial gradient in phytoplankton biomass, with consistently low chl-*a* values offshore (Varela & Harrison, 1999) due to Fe limitation (Boyd et al., 1996). The uniformity in chl-*a* across the offshore regions of Line P (i.e., beyond station P8), coupled with the modelled relationships

between TEP and AOU, temperature, nutrients, and stratification shown in this study suggest that it may be possible to estimate [TEP-C] in the open-ocean regions of the ESNP using these models. My predictions suggest a yearly average of 12.6 µg C $L^{-1}$ along the oceanic regions of the Line P transect (or 24.7 µg XG eq $L^{-1}$) (Figure 2.6). These results and predictions are in agreement with several other studies that have measured TEP in HNLC or low chl-*a* regions of the Pacific Ocean to be between 20 – 50 µg XG eq $L^{-1}$ (Boyd et al., 2005; Guo et al., 2022; Iuculano et al., 2017; Kodama et al., 2014; Yamada et al., 2017).

The results from this study demonstrate that [TEP-C] can be predicted from proxies of phytoplankton biomass (i.e., chl-*a*) and productivity (i.e., AOU), in addition to direct and indirect environmental predictors of TEP (i.e., temperature, MLD, nutrient concentrations). However, Ortega-Retuerta et al., (2017) also suggests that remote sensing of chl-*a* (i.e., as a satellite derived product) can be used to predict horizontal gradients in surface TEP. Therefore, I attempted to derive large-scale surface estimations of [TEP-C] concentrations across the ESNP from satellite derived chl-*a* and temperature (as the inclusion of temperature as a model parameter improves predictive ability and is available from remote sensing). The methodology and results from this extension of the research are shown in *Appendix C: Remote-sensing derived TEP predictions using chlorophyll-a and temperature as predictors*.

### 2.5.6 Model Assumptions and Limitations

Certain limitations exist within the context of this study. Firstly, the modelled relationships derived were only obtained from the upper layers of the water column (i.e., the upper mixed layer), and therefore a potential decoupling of chl-*a* and TEP (Ortega-Retuerta et al., 2017) with depth may limit the application of these models to the upper ocean alone.

Secondly, all empirical relationships were derived from Subarctic (ESNP-ON + OFF) and Arctic (BE-CH and BS-CB) regions and may not be representative in other marine regions with distinct oceanographic differences. For example, the model(s) will likely not accurately predict TEP in regions with strong anthropogenic or terrestrial POC inputs such as coastal sources, kelp forests, sewage runoff, etc.). These inputs may represent sources of TEP that have not been considered as parameters in the models. In contrast, areas such as the unproductive offshore regions of the Subarctic are characterized by relatively consistent TEP predictors, and [TEP] is more likely to be driven and constrained by the model parameters. Thirdly, the maximum [TEP] used in the model (measured in this study) was ~ 150 µg XG eq $L^{-1}$, and therefore any predicted TEP values from RFR models will be limited by this threshold. Lastly, MLR and RFR models were derived from measurements that are commonly reported in the literature and from remote sensors (i.e., Argo floats, satellites). While this approach is beneficial to deriving large scale estimates of marine TEP, it does not include less commonly reported variables that may be important in predicting TEP, such as phytoplankton functional group abundances and zooplankton grazing.

### 2.5.7 TEP-C: An Important Standing Stock of C with Broad Implications for C Export

Estimating [TEP-C] alongside [POC] and estimates of primary production can provide a valuable insight into the surface ocean C cycle and efficiency of the BCP. As discussed above, the results from this chapter show that C in the form of TEP can be estimated to be ~5-15 µg C $L^{-1}$ throughout the open ocean, low-chl-*a* regions of the Subarctic year-round. Mari et al. (2017) modelled the effects of the relative concentrations of TEP-C and non-TEP-C on POC retention and export, and demonstrated that a theoretical aggregate, composed of POC and diatoms, would only sink if less than 5% of its total C content was composed of TEP-C (%TEP-C = 5%).

Furthermore, their model suggests that if a given POC aggregate was composed of 20% TEP-C, it would take ~3 days to degrade to 5% TEP-C and be exported (Mari et al., 2017). While this model assumed 100% diatom-based aggregates, the insights can nonetheless be directly compared with the measured and predicted [TEP-C] in low chl-*a* regions of the ESNP presented in this thesis. Average seasonal measured [TEP-C] and [POC] in low chl-*a* regions of the ESNP show a %TEP-C ratio of 5-15% (Table 2.5). Mari et al., (2017) suggests that this ratio drives the temporal decoupling of primary production and C export in the upper layers of the water column, which has been frequently observed in field studies (Boyd et al., 2000, p. 19; Kiørboe et al., 1998; Pitcher et al., 1991; Rinaldi et al., 1995).

This study provides measured [TEP-C] and %TEP-C values from 2019-2021 and predicted [TEP-C] from 1998-2018 along Line P in the Subarctic. To extrapolate %TEP-C from 1998-2018, measured [POC] are required for the same timeframe. However, historical [POC] in the region is only available through satellite remote sensing. Table 2.5 combines predicted [TEP-C] and %TEP-C values in low chl-*a* regions of the Subarctic using 8-day satellite derived POC estimates from 2015-2021. Historical 8-day average 5 m POC concentrations were obtained for the same 8-day period as the respective Line P cruise and combined with the respective [TEP-C] predictions. Historical remote sensing-based estimates of POC and predicted (5m) TEP-C in the region suggest that the %TEP-C ratio ranged from 13.3-21.8% in the region from 2015-2018 (Table 2.5). A similar trend is observed for 2019-2021, where predicted %TEP-C ranged from 9.5-23.5%. Measured %TEP-C values collected in this study over the same period (2019-2021) were slightly lower (5.2-14.1%), owing to differences between measured and satellite derived POC concentrations. Nonetheless, these results demonstrate that TEP-C is a major fraction of the total POC pool in low-chlorophyll regions of the subarctic year-round, and likely consists of 5-

20% total POC. Comparing these results with the models derived in Mari et al., (2017) suggests that POC export in low-chlorophyll regions of Subarctic is a relatively inefficient process and standing POC concentrations may undergo delays in being exported from surface waters of up to 3 days. While these predictions and insights are limited by the assumptions of the models, my approach is the first of its kind to apply multivariate modelling techniques to identify major TEP predictors and to predict [TEP-C] across large spatiotemporal scales. Furthermore, by providing assessments of measured and predicted %TEP-C across large gradients in space and time, this work also provides new insights into C export efficiency in the Subarctic.

**Table 2.5.** Average predicted and measured TEP-C and %TEP-C along Line P in low chl-a regions of the Subarctic Pacific (includes stations P8 - P26) in spring and summer seasons from 2015 - 2021. Predicted %TEP-C was derived by dividing predicted historical TEP-C by satellite (Sat.) derived 8-day average POC. Average predicted TEP-C was obtained from a Random Forest Regression Model (with chlorophyll *a*, apparent oxygen utilization, temperature, and mixed layer depth as model inputs) applied to the historical Line P database. Average predicted and measured %TEP-C values are also displayed and highlighted in bold text. 8-day POC averages were taken between 48˚N and 50˚N, and 129˚W and 145˚W, approximating the distance between P8 – P26 along Line P. Empty rows indicate cruises where no measurements were taken.

| Year & Season | Sat. 8-day POC avg. (µg C $L^{-1}$) | Predicted TEP-C (µg C $L^{-1}$) | Predicted %TEP-C | Measured POC (µg C $L^{-1}$) | Measured TEP-C (µg C $L^{-1}$) | Measured %TEP-C |
|---|---|---|---|---|---|---|
| June 2015 | 69.49 $\pm$ 19.94 | 11.68 | **16.8%** | | | |
| August 2015 | 58.03 $\pm$ 12.52 | 9.10 | **15.6%** | | | |
| June 2016 | 69.48 $\pm$ 19.95 | 15.56 | **21.8%** | | | |
| August 2016 | 63.83 $\pm$ 14.63 | 10.40 | **16.3%** | | | |
| June 2017 | 69.62 $\pm$ 11.51 | 9.29 | **13.3%** | | | |
| August 2017 | 61.82 $\pm$ 11.79 | 10.95 | **17.7%** | | | |
| June 2018 | 85.50 $\pm$ 16.61 | 15.47 | **18.1%** | | | |
| August 2018 | 68.16 $\pm$ 18.54 | 12.75 | **18.7%** | | | |
| June 2019 | 102.04 $\pm$ 33.13 | 23.93 | **23.5%** | 130.52 | 18.41 | **14.1%** |

| | | | | | | |
|---|---|---|---|---|---|---|
| August 2019 | 79.80 ± 17.52 | 15.90 | **19.9%** | 120.31 | 16.20 | **13.5%** |
| May 2021 | 71.77 ± 22.25 | 6.81 | **9.5%** | 145.90 | 7.55 | **5.2%** |
| August 2021 | 94.95 ± 26.61 | 11.86 | **12.4%** | 169.60 | 11.72 | **6.9%** |

### 2.5.8 TEP in Future Ocean Scenarios

Based on the results of this study and modeling approaches, I hypothesize that the amount of TEP across the future ocean's surface will ultimately depend on the amount of phytoplankton biomass. If levels of phytoplankton decline over the next century, a subsequent decrease in [TEP] would also occur, particularly in open ocean environments. However, the amount of TEP relative to total biomass or POC (%TEP-C) may be subject to environmental change. It is possible that %TEP-C may increase in the ocean due to predicted increases in atmospheric and surface ocean temperatures (Collins et al., 2013), an induced decrease in the depth of the mixed layer (Bijma et al., 2013; Rost et al., 2008), and increased nutrient limitation (Rost et al., 2008; Steinacher et al., 2010). This is supported by the multivariate modelling approaches in this study. A similar hypothesis is presented by Mari et al., (2017), who synthesized large bodies of evidence (Table 2.2) to suggest that increasing ocean temperatures will promote increases in [TEP] and accumulation in surface waters, and that an overall reduction in the ratio of organic carbon export to primary production may occur (Mari et al., 2017).

# Chapter 3: Spatiotemporal trends in carbon export potential in the Eastern Subarctic North Pacific estimated from transparent exopolymer particles, carbon uptake and new production

## 3.1 Abstract

Transparent exopolymer particles (TEP) are gelatinous carbon-rich organic polymers that can moderate the efficiency of particulate organic carbon (POC) export from surface to deep waters in the ocean. When present in high concentrations relative to other forms of POC, positively buoyant TEP gels can reduce POC sinking rates and increase the exposure time of POC to remineralization in the surface ocean. This acts to potentially decouple primary production from carbon (C) export, and thus reduces the efficiency of the biological C pump (BCP). Despite the biogeochemical significance of TEP, little work has focused on quantifying TEP concentrations relative to C uptake (ρC) or downward export estimates in the field. In this study, I quantified TEP (and TEP based C, TEP-C) in comparison to ρC, nitrate uptake ($\rho NO_3^-$), and new production C rates (NP-C) over 4 years (7 research cruises) during multiple seasons and along a ~1400 km spatial gradient in environmental conditions in the Eastern Subarctic North Pacific (ESNP). I found that TEP was significantly positively correlated with ρC ($R^2 = 0.36$, $p < 0.01$), and to a lesser degree with $\rho NO_3^-$ ($R^2 = 0.28$, $p < 0.01$), across the entire study range. Despite the strong correlation between ρC and TEP-C, higher ratios of TEP-C concentrations ([TEP-C]) to ρC were observed across oceanic regions of the ESNP compared to productive coastal regions, suggesting that TEP-C represents a dominant C source in oceanic regions of the ESNP. Furthermore, a similar trend was observed between daily TEP-C turnover rates (derived from TEP-C residence time estimates), and ρC, where oceanic regions were characterized by significantly higher TEP-C turnover rates relative to ρC when compared to productive coastal regions. Elevated [TEP-C] and TEP-C turnover rates relative to ρC suggests that oceanic regions in the ESNP may undergo less efficient C export from surface waters due to the inherent buoyant nature of TEP. This chapter provides the first field-based observations of a significant

relationship between excess C consumption (relative to nitrate uptake) and TEP-C concentrations ($R^2$ = 0.23-0.34, $p$ <0.01). It further provides a new perspective on the role of TEP based C in surface ocean C cycling and demonstrates spatial variability in TEP-C relative to other C fluxes.

## 3.2 Introduction

The biological carbon pump (BCP) sequesters large amounts of C in deep waters via the gravitational settling of particulate organic carbon (POC) to depth. While phytoplankton fix approximately 50 Pg of C per year (Field et al., 1998), only 1 – 25% of this carbon escapes bacterial remineralization in the euphotic zone and is exported to the deep ocean (Buesseler, 1998; Martin et al., 1987). Variability in the efficiency of the BCP is predominantly a result of biological processes in the euphotic zone (Legendre & Rivkin, 2002), including the magnitude of microbial remineralization of POC, the aggregation and specific gravity of POC aggregates, grazing and fecal pellet production by zooplankton, and other factors such as mineral ballasting (De La Rocha & Passow, 2007, and references therin).

Transparent exopolymer particles (TEP) have received considerable attention in recent decades, owing to their influence in affecting the efficiency of the BCP (Mari et al., 2017). Traditionally, TEP is defined as particles greater than 0.4 μm, gelatinous in nature, and stainable with Alcian Blue dye (Passow & Alldredge, 1995a). TEP is produced from the coagulation of dissolved organic precursors, which are originally derived from the metabolic activities and exudations of phytoplankton and bacteria (commonly referred to as exopolymeric substances; EPS). A major pathway for TEP production is thought to be through the excess consumption of C beyond what is expected from Redfield stoichiometry (i.e., the uptake of excess dissolved inorganic C (DIC) than predicted from nitrate ($NO_3^-$) uptake) (Engel et al., 2002a). This process

has been defined as C overconsumption (Toggweiler, 1993; Sambrotto 1993), and results in the production and exudation of an excess amount of dissolved organic C (DOC) and EPS from phytoplankton cells. Current estimates have shown that ~10% of the ocean's DOC of ~70 Pg C are composed of TEP precursors. Therefore, TEP may exert a critical influence on C cycling and sequestration on a global ocean scale.

There are several important characteristics of TEP that play a role in influencing the magnitude and efficiency of the BCP. Firstly, it is a major facilitator of organic matter aggregation in the ocean (Engel, 2004; Passow & Alldredge, 1995b). This characteristic was thought to increase the efficiency of the BCP by promoting the aggregation of larger, faster sinking POC aggregates (Engel, 2004). However, TEP is less dense than seawater (Azetsu-Scott & Passow, 2004). As a result, when there is a large fraction of C in the form of TEP (TEP-C) relative to other forms of POC (i.e., the TEP:POC ratio, or %TEP-C), POC will become 'entrapped' within a buoyant TEP matrix, delaying export rates and increasing the exposure time of POC to bacterial remineralization in the surface ocean (Mari et al., 2017). Several recent studies have shown that TEP-C matrices play an important role in delaying C export due to its positive buoyancy(Bar-Zeev et al., 2009; Mari et al., 2017; Mühlenbruch et al., 2018; Romanelli et al., 2023). As such, TEP plays a critical role in mediating the relative rates of POC export and remineralization at the ocean surface, and ultimately affects the efficiency of the BCP (Mari et al., 2017).

Much of the ocean is characterized by inefficient C export from surface to deep waters (Buesseler, 1998; Martin et al., 1987), and C export is frequently decoupled from primary production in a variety of oceanographic settings (Boyd et al., 2000; Kiørboe et al., 1998; Pitcher et al., 1991; Rinaldi et al., 1995). However, no large-scale spatiotemporal studies between TEP-

C and C uptake or export currently exist. While some studies have measured TEP-C alongside primary production, they are mainly limited to experimental studies or single season/location sampling, resulting in a lack of spatiotemporal coverage. This gap in the literature is even more pronounced as Mari at al., (2017) recently demonstrated the significance of TEP-C: primary production ratios as a key influence on determining the fraction of primary production that can be exported from the euphotic zone, and therefore the efficiency of the BCP.

While most studies measure TEP-C, it is also valuable to be able to estimate its production and turnover rate in the ocean, to directly compare with daily estimates of primary productivity and export (Mari & Burd, 1998). The production of TEP is highly variable depending on the amount of primary productivity occurring, and may range from <5% to >50% of gross primary production (Alonso-Sáez et al., 2007; Karl et al., 1998; López-Sandoval et al., 2011; Marañón et al., 2004; Nagata, 2000). Currently, only three studies exist that have measured TEP residence times/turnover rates in the ocean. Wurl et al., (2011) measured TEP residence times in the Eastern Subarctic North Pacific (ESNP), along the oceanographic transect Line P, and obtained average TEP residence times of 4.6 days. This work provides the foundation for future studies, much like my own, to estimate TEP-C turnover rates in the region by dividing measured [TEP-C] by its residence time estimations. Turnover rates of TEP have been measured to estimate TEP-C fluxes relative to total seasonal primary production in order to understand its role in C fluxes in the upper ocean (Mari & Burd, 1998). These studies defined TEP turnover rates as the rate of formation and degradation/export of TEP from dissolved precursor materials (Mari & Burd, 1998; Wurl et al., 2011). This approach allows for the development of a new perspective on C fluxes in surface waters, as no studies currently exist that have attempted to compare [TEP-C] or TEP-C turnover rates with estimates of new and primary

production. As outlined above, TEP is a highly important substance in influencing C export efficiency. Therefore, by comparing [TEP-C] and TEP-C turnover rates with primary and new production, factors that influence the efficiency of the BCP can be better understood.

In this study, I measured TEP (and derived TEP-C) and estimated TEP-C turnover rates using residence times provided by Wurl et al., (2011) (using a coagulation theory model). I compared these values with ρC, $\rho NO_3^-$, silica uptake (ρSi), and estimates of C export potential (proxied by new production C; NP-C) across large gradients in space and time in the Eastern Subarctic Northeast Pacific (ESNP). I also estimated C overconsumption rates (defined as excess $\rho NO_3^-$ relative to ρC) and compared to [TEP-C]. Together, these analyses provide a unique perspective on upper ocean C fluxes and the efficiency of the BCP in the ESNP.

## 3.3 Methods

### 3.3.1 Sampling Locations and Seawater Collection

Seawater samples were taken on seven research expeditions throughout the ESNP on the Line P and La Perouse programs run by the Department of Fisheries and Oceans Canada (DFO) onboard the *CCGS John P. Tully*. The cruises were conducted over a four-year period, spanning three sampling 'seasons' (spring, summer, winter) (Table 3.1). Sampling at two depths was performed at each station, typically at 5 m and at the chlorophyll maximum for a total of 149 discrete samples and 48 stations (Table 3.1). Seawater for the measurement of TEP, POC, chlorophyll *a*, nutrients, ρC, and $\rho NO_3^-$ was collected using a rosette equipped with 24 10-L Niskin bottles, with a Sea-Bird (SBE-911plus) conductivity-temperature-depth (CTD) sensor attached to the rosette, with additional sensors for dissolved oxygen (DO) and *in situ* fluorescence.

**Table 3.1:** Information for each research cruise event in the Eastern Subarctic North Pacific (ESNP) regarding date ranges, reference seasons, and number and stations per cruise where uptake rate experiments were conducted. At every uptake experiment station, a total of 2 incubations were performed, at 5 m and the chlorophyll max, except for pSi in Spring Line P 2021 where only 5 m incubations were performed. Cruise ID refers to the Fisheries and Oceans Canada (DFO) cruise number.

| Program | Year -Cruise ID | Date range | Season | Total samples | Stations (uptake experiments) |
|---|---|---|---|---|---|
| La Perouse | 2019 -005 | May 18 – June 2 | Spring | 12 | B7, LBP3, LG02, CS02, LC11, LD09 |
| Line P | 2019 -006 | June 3 – 16 | Spring | 10 | P4, P12, P16, P20, P26 |
| La Perouse | 2019 -009 | Aug 29 – Sept 10 | Summer | 12 | LBP3, LC06, CS02, LB15, LG09 |
| Line P | 2019 -008 | Aug 15 – 29 | Summer | 10 | P4, P12, P16, P20, P26 |
| Line P | 2020 -001 | Feb 9 – 23 | Winter | 10 | P12, P16, P20, P26 |
| Line P | 2021 – 006 | May 4 – 18 | Spring | 39 | P4, P12, P16, P20, P26 |
| Line P | 2021 – 008 | Aug 24 – Sept 7 | Summer | 24 | P1, P4, P12, P16, P20, P26 |
| La Perouse | 2022 – 009 | August 28 – September 7 | Summer | 17 | CS06, LB08, LG02, CS02, SS5 |

Sampling locations were grouped into 4 oceanographic regions (Figure 3.1). High nitrate low chlorophyll ('HNLC') and 'Transition' regions are characterized by low year-round chlorophyll *a* (chl-a) (Harris et al., 2009; Whitney & Freeland, 1999) but high and intermediate iron (Fe) limitation, respectively, as described in LaRoche et al., (1996).'Shelf-break' and 'Coastal' regions are both characterized by episodic nutrient depletion and frequent phytoplankton blooms. Shelf-break stations have bottom depths >300 m, can experience topographically controlled upwelling along the continental shelf, and are effected by the southward flowing Shelf Break Current (Freeland et al., 1984). Coastal stations were defined as being shallower than 300 m and affected by the northward flowing Vancouver Island Coastal

Current, which brings low density and salinity water from the Juan De Fuca Strait onto the continental shelf (Freeland et al., 1984).

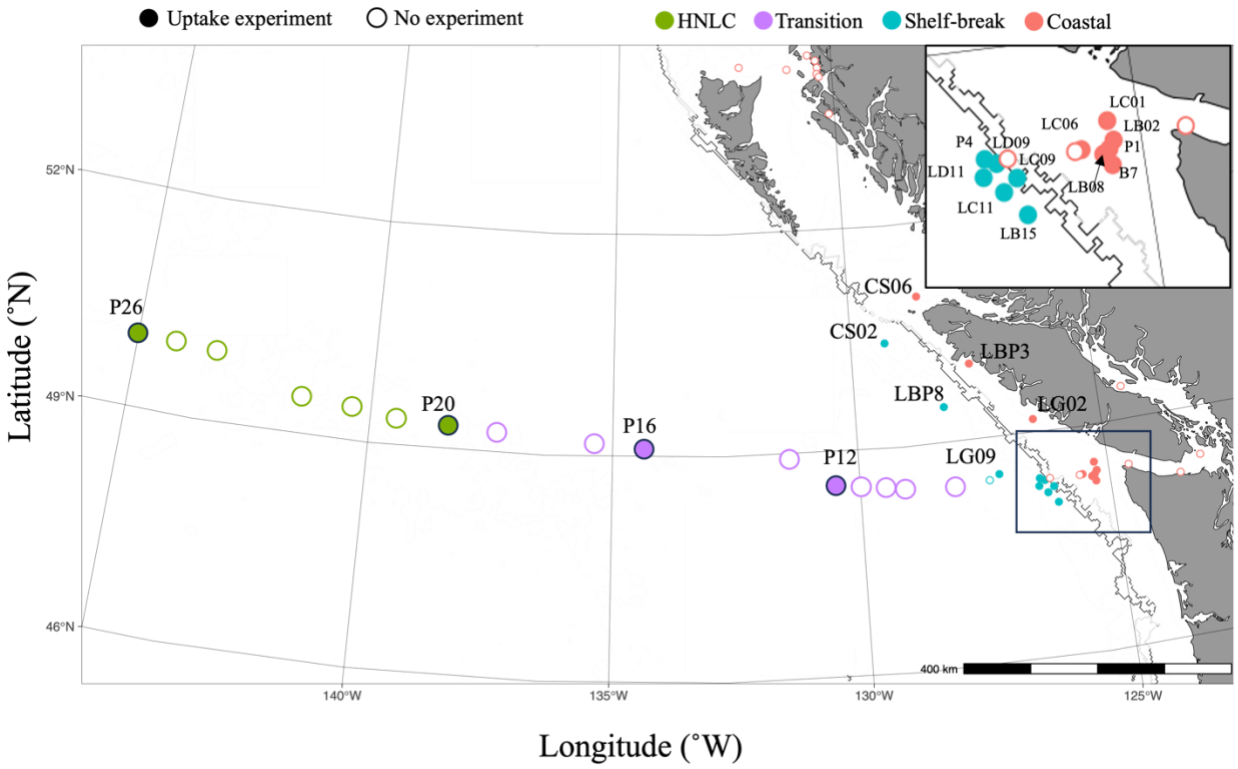


**Figure 3.1**. Station locations where surface seawater was sampled during winter (Feb – March), spring (May – June) and summer (August – September) over a four-year period from 2019 – 2022 over 7 cruises in the Eastern Subarctic North Pacific (ESNP). Sampling for TEP, POC, chl-a, and dissolved nutrients ($[NO_3^-]$, $[Si(OH)_4]$) was conducted at all stations, while experiments for ρC, $\rho NO_3^-$, and ρSi were performed at a subset of the total number of stations (filled symbols). Due to variations in stations sampled among cruises, not all stations shown in the map were sampled during every cruise; Table 3.1 specifies specific stations sampled for each cruise. Samples were taken at both 5 m and the chlorophyll max. Stations were spatially categorized into HNLC, transition, shelf-break, and coastal (<300 m, on-shelf) subregions. The shelf-break is illustrated by contour lines indicating 1500 m.

### 3.3.2 Transparent Exopolymer Particles (TEP) and Particulate Organic Carbon (POC)

Concentrations of TEP ([TEP]) were determined according to original (Passow & Alldredge, 1995a) and updated quantification methods (Bittar et al., 2018). Briefly, 100-500 ml

of seawater were filtered onto a 0.4 µm polycarbonate filter with a constant vacuum pressure of <150 mm Hg. The filter was stained with 500 µl of Alcian Blue (AB) solution (0.02%, pH 2.5) for 5 s, and was immediately stored at -20˚C. Clean filters stained with Alcian Blue solution were used as blanks. On shore, sample and blank filters were extracted with a 5 ml solution of 80% sulphuric for 2 h with intermittent agitation. The sample solution was then measured spectrophotometrically at 787 nm on a Beckman DU 530 UV/Vis spectrophotometer. All samples were analyzed within 1 month of collection. Filter blanks did not vary significantly throughout the cruises. Calibration curves for the AB dye were made with the use of Xanthan gum as a standard, and calibration factors were obtained as described in Passow and Alldredge (1995a) and Bittar et al., (2018). The calibration factors fell within the range of the calibration factors in the above studies (88-139) but varied slightly for each new batch of AB dye. The detection limit for calibration standards was determined to be 4-5 µg (XGeq.) $L^{-1}$, similar to values described by Bittar et al. (2018).

Samples for POC were taken by filtering 500 – 1000 ml of seawater through a pre-combusted (6 h at 450°C) glass fibre filter and immediately stored at -20˚C. Back onshore, filters were dried at 60°C for 48 h, and subsequently acidified (to remove inorganic carbon) in a desiccator saturated with HCl fumes for 12 h. After acidification, the filters were dried again and analyzed on an MICRO cube Elementar elemental analyzer at the University of British Columbia.

The C content in TEP (TEP-C) was calculated by multiplying [TEP] by a conservative conversion factor of 0.51 (Engel & Passow, 2001). The fraction of total POC composed of TEP-C (%TEP-C) was then calculated using equation 2, in accordance with Engel and Passow (2001):

$$TEP - C = [TEP] * 0.51 \quad [1]$$

$$\%TEP - C = \frac{TEP-C}{Total\ POC} * 100 \quad [2]$$

### 3.3.3 Turnover Rates of Transparent Exopolymer Particles

Turnover rates of TEP-C were estimated by using the [TEP] measured in this study and TEP residence times calculated by Wurl et al., (2011) along Line P in the ESNP. However, residence times reported in Wurl et al., (2011) ranged from 0.3 to 34 d with a mean = 4.6 d. To account for this variation, I calculated minimum, maximum, and average turnover rates of TEP-C (TEP-$C_{turnover}$) values based on the minimum, maximum, and average residence times reported by Wurl et al., (2011). TEP-$C_{turnover}$ rates were calculated by dividing the measured [TEP-C] by the residence time of TEP along Line P. The daily estimated average and ranges of TEP-$C_{turnover}$ in the surface layers were calculated as follows:

$$Average\ TEP{-}C_{turnover} = \frac{TEP-C\ L^{-1}}{4.6\ d} \quad (\mu g\ C\ L^{-1}d^{-1}) \quad [3]$$

$$Minimum\ TEP{-}C_{turnover} = \frac{TEP-C\ L^{-1}}{34\ d} \quad (\mu g\ C\ L^{-1}d^{-1}) \quad [4]$$

$$Maximum\ TEP{-}C_{turnover} = \frac{TEP-C\ L^{-1}}{0.3\ d} \quad (\mu g\ C\ L^{-1}d^{-1}) \quad [5]$$

### 3.3.4 Production Rates of Transparent Exopolymer Particles

Production rates of TEP were estimated via 3 incubation experiments at stations P4, P12, and P26 during the spring 2021 Line P cruise. Seawater was collected from 5 m depth and placed into clear, 4-L polycarbonate bottles. Bottles were immediately sampled for initial TEP, POC, chl-*a*, and dissolved nutrients measurements, before being placed into acrylic tubes covered with blue-coloured photographic film to simulate ambient light quality and quantity at 5m (~50%). Samples were incubated within the acrylic tubes in a flow-through temperature-controlled acrylic incubator using seawater pumped from 5m. Bottles were incubated in this fashion for 4 days, with samples for TEP, POC, chl-*a*, and nutrients collected every 24 h over the incubation period. Net daily TEP-C production ($TEPC_{PR}$) was calculated as described in (Iuculano et al., 2017):

$$TEP - C_{PR} = \frac{(TEP_{tf} - TEP_{t0}) * 0.51}{(tf - t0)} \quad (\mu g\ C\ L^{-1} d^{-1}) \qquad [6]$$

where $TEP_{tf}$ is the final [TEP], $TEP_{t0}$ is the initial [TEP], and 0.51 is the TEP to TEP-C conversion factor (Engel & Passow, 2001).

### 3.3.5 Carbon and Nitrate Uptake Rates

Carbon (C) and nitrate ($NO_3^-$) uptake rates were determined using the stable natural isotopes $^{13}C$ (99 atom% $C^{13}$, Cambridge Isotope Laboratories) and $^{15}N$ (98 atom% $N^{15}$, Cambridge Isotope Laboratories ) according to a dual tracer method (Dugdale & Goering, 1967; Dugdale & Wilkerson, 1986; Hama et al., 1983). Seawater collected from Niskin bottles from both 5m and the chlorophyll max, and put into 2.3-L acid washed polycarbonate bottles were

spiked with $^{13}$C-labelled $NaHCO_3$ and $^{15}$N-labelled $NaNO_3$ isotopic solutions and placed into acrylic tubes covered with neutral density and blue-coloured photographic film to simulate ambient light quantity and quality at 5m (~50%) and at the chlorophyll max (1-15%) within the acrylic incubator, as described above. Irradiance levels within the acrylic tubes were pre-calibrated using a Biophysical Instruments Inc. light meter, model QSL 100. Ambient dissolved inorganic carbon (DIC) concentrations were assumed to be 2000 µM. Samples were incubated for 24 h before being filtered onto a pre-combusted (at 450˚C for 6 h) glass fiber filters (0.7µm nominal porosity) and immediately frozen at -20˚C. Upon return to shore, filters were dried at 60˚C for a minimum of 48 h, packaged into tin vials, and analyzed using an elemental analyzer (Elementar Vario EL Cube) interfaced to a PDZ Europa 20-20 isotope ratio mass spectrometer at the Stable Isotope Facility at the University of California Davis.

Rates of C (ρC) and $NO_3^-$ ($\rho NO_3^-$) uptake were calculated according to Hama et al., (1983) and of Dugdale and Wilkerson (1986) (equations #6 and #3), respectively. The detection limit for ambient [$NO_3^-$] is 0.1µmol $L^{-1}$, therefore, when ambient [$NO_3^-$] were below detection limit, 0.1µmol $L^{-1}$ was used to calculate $\rho NO_3^-$.

### 3.3.6 New production rates

New production rates in C units (NP-C) were determined from $NO_3^-$ uptake rates ($\rho NO_3^-$). $NO_3^-$ uptake rates were converted into ρC by multiplying $\rho NO_3^-$ by the elemental POC: particulate nitrogen (PN) ratio observed for each sample (equation 7).

$$NP - C = \rho NO_3^- * POC{:}PN \qquad [7]$$

This calculation produces the approximate amount of C uptake fuelled by $NO_3^-$, as a proxy of new production (Eppley & Peterson, 1979). The fraction of new production to total production (*f*-ratio) was calculated as follows:

$$f - ratio = \frac{NP-C}{\rho C} \quad [8]$$

This method does have limitations; primarily, the calculation of the f ratio based solely on NP-C derived from $\rho NO_3^-$. The exclusion of other nitrogenous forms, such as ammonia and urea, which may result in an overestimation of the *f*-ratio (Varela & Harrison, 1999).

### 3.3.7 Carbon Overconsumption Estimates

Carbon overconsumption (COC) estimates were derived from ρC, $\rho NO_3^-$, and measured POC:PN ratios. To calculate COC, new production in C units, calculated from $\rho NO_3^-$ and POC:PN ratios, is subtracted from measured ρC. This produces the excess amount of ρC that is not accounted for by ρN (as a positive value). This approach was limited by the fact that only $\rho NO_3^-$ was directly measured and other N forms utilized by phytoplankton, notably ammonia and urea, were not. Negative C overconsumption values (when ρC measured < ρC predicted) were replaced as 0 values.

To estimate the maximum amount of COC possible ($C_{OC\ max}$), an *f*-ratio of 1 was used. An *f*-ratio of 1 is assumes 100% of N utilization to be fuelled by $NO_3^-$. While this value is likely an overestimate for the Transition and HNLC regions along Line P (Peña & Varela, 2007b; Varela & Harrison, 1999), it serves the purpose of capping the upper possible ranges of $C_{oc}$, and may account for productive coastal regions where *f*-ratios may be high and primary production

fueled more by $NO_3^-$ than by ammonia or urea. Furthermore, *f*-ratios of 1 have been occasionally observed along Line P (Meyer et al., 2022). Maximum COC was therefore defined as measured ρC minus predicted ρC, with ρC derived from $\rho NO_3^-$ multiplied by measured POC:PN and divided by an *f*-ratio of 1, as in equation 9:

$$C_{OC\ max} = \rho C_{measured} - \frac{(\rho NO_3^- * POC{:}PN)}{1} \quad [9]$$

Equation 10 provides a lower estimate of COC by using conservative f-ratios for the ESNP from the literature. This was based on a study by Varela and Harrison (1999), who determined that $NO_3^-$ uptake by phytoplankton along Line P to be 21% of total N uptake on average (Varela & Harrison, 1999). Similarly, Peña and Varela (2007) found the *f*-ratio along Line P to be ~ 0.27, which is within the range of f-ratios used in my calculations (Peña & Varela, 2007b). This lower limit was used to better constrain COC, and to provide a reasonable lower limit in which to compare with [TEP-C].

$$C_{OC\ lit} = \rho C_{obs} - \frac{(\rho NO_3^- * POC{:}PN)}{0.21} \quad [10]$$

### 3.3.8 Silicon Uptake Rates

Silicic acid uptake rates (ρSi) were measured through the use of the radioisotope $^{32}Si$, in accordance with the procedure of Brezinski and Phillips (1997). Seawater (250-500 ml) was collected in 500 ml polycarbonate incubation bottles and spiked with 100-187 µl of a 0.1 µCi/ml $^{32}Si(OH)_4$ solution of high specific activity immediately after collection. The incubation bottles were then placed within the flow-through on-deck incubator at *in situ* light levels (as described

above in section 2.3) for 24 h. Following the incubation period, the samples were filtered onto a 0.6 µm, 25 mm polycarbonate filter. The filtration funnels and incubation bottles were thoroughly rinsed with 0.6 µm filtered seawater to remove any residual $^{32}Si$ adhering to the materials and to rinse off excess $^{32}Si$ not incorporated into particles. The filters were subsequently mounted onto plastic planchettes and left to dry for 12-24 h, after which they were covered and wrapped with a thin mylar film. Samples were stored for >120 days to reach secular equilibrium with its daughter isotope $^{32}P$. Sample activity of $^{32}Si$ was determined using a Risø 25-5 low-level beta GM multicounter. Biogenic silica production rates were calculated using equations 16-22 in Brezinski and Phillips (1997).

### 3.3.9 Chlorophyll *a*

Chlorophyll *a* (chl *a*) analysis was conducted as outlined by Parsons et al., (1984). Seawater samples (500 ml) were filtered onto an glass fiber filter (0.7 µm nominal porosity) and frozen while onboard the vessel at -20˚C. Chlorophyll *a* concentrations were measured onshore using an acetone extraction (90% v:v) in the dark at -20˚C for 24 h, followed by fluorometric measurements on a Turner Designs Fluorometer.

### 3.3.10 Dissolved Nutrients

Samples for dissolved inorganic nutrients ($Si(OH)_4$, $NO_3^-$) were taken directly from the Niskin bottles and filtered through a 0.4 µm syringe filter into 15 ml centrifuge tubes. All filters were frozen immediately at -20˚C. Triplicate samples (~3 times / cruise) were collected to estimate variance in the procedure. Samples were analyzed on an Astoria Nutrient Analyzer,

following the protocol of Barwell-Clark and Whitney, (1996). Measurements of [$Si(OH)_4$] and [$NO_3^-$] were used to calculate ρSi and ρ$NO_3^-$, respectively.

### 3.3.11 Physical and environmental variables

Water temperature, salinity, *in vivo* fluorescence, DO, and density were measured throughout the water column from sensors on the Seabird CTD package at every station. At several stations, DO was measured via discrete water sampling according to Carpenter (1965). Mixed layer depth (MLD) was defined as the depth in the water column at which the density increased by more than 0.03 kg/$m^3$ from the average surface density (1-5 m) (de Boyer Montégut et al., 2004). Average 24-h photosynthetically active radiation PAR (μmol photons $m^{-2}$ $s^{-1}$) data were collected via continuous logging on a LI-COR LI-190 Quantum Light Sensor, positioned close to the on-deck incubator and away from shading.

### 3.3.12 Statistical analyses

The statistical programming language *R* and *dplyr* package were used to derive linear regressions between [TEP], nutrient uptake rates (C, $NO_3^-$, Si), and biological/environmental variables. One and two-way analysis of variance (ANOVA), Tukey HSD tests, and t-tests assuming unequal variance were performed to identify any significant differences in [TEP-C], uptake rates, TEP-C relative to C uptake and NP-C over regions and seasons. A multiple linear regression (MLR) was also used to determine if the relative amount of TEP-C to ρC varied significantly with distance from shore, using both distance from shore (Km) and a term for the sampling depth (either surface or chlorophyll max sample) as independent variables, and ρC:TEP-C as the dependent variable. This test was done in addition to the spatial ANOVA, as

the spatial ANOVA may have spatial autocorrelation because of stations occurring close together in space and not being statistically independent. All statistical tests were carried out using the statistical programming language R (v1.3.1093) in addition to the *dplyr* and *tidyverse* packages.

## 3.4 Results

### 3.4.1 Spatiotemporal trends in nutrient uptakes rates, new production and TEP

Uptake rates of C, $NO_3^-$ and Si, and NP generally followed similar spatial trends, with significantly higher ($p < 0.05$) and more variable rates closer to shore, and lower values in the other 3 regions (Figure 3.2A-D). The one exception to this rule was ρSi in HNLC vs coastal regions, where elevated ρSi was observed in coastal regions but it was not deemed significant ($p = 0.08$). No significant seasonal variation was observed for any of the uptake rates measurements, which is likely due to the small number of winter samples. For the entire region and for all seasons, ρC and $\rho NO_3^-$ ranged from 0.06 – 879.0 µg C $L^{-1}$ $d^{-1}$ and <0.01 – 5.1 µmol $NO_3$ $L^{-1}d^{-1}$, respectively, with NP ranging from 0.06 – 276.2 µg C $L^{-1}$ $d^{-1}$. Uptake rates of Si ranged from < 0.001 – 12.6 µmol Si taken up per $L^{-1}$ $d^{-1}$.

Concentrations of TEP paralleled trends in phytoplankton ρC and $\rho NO_3^-$, with high concentrations throughout coastal regions and significantly lower concentrations offshore towards HNLC regions ($p < 0.01$, Figure 3.2 E). For the entire region and all seasons, [TEP] ranged from ~ 4 – 138 µg XG eq $L^{-1}$. Values of %TEP-C exhibited significant spatial variation, with coastal regions having lower %TEP-C values on average when compared to all oceanic regions (i.e., shelf-break, transition, and HNLC) ($p < 0.05$). Measured [TEP] were significantly higher in spring and summer seasons when compared to winter ($p < 0.05$). Seasonal variation was also observed in the %TEP-C, with winter %TEP-C values (5.1 $\pm$ 2.6%) being significantly

lower than both spring (7.6 ± 4.1%) and summer ($p < 0.01$). For all regions and seasons, values of %TEP-C ranged from 2.4 - 33.5%, with an average of 7.8 ± 4.5%.

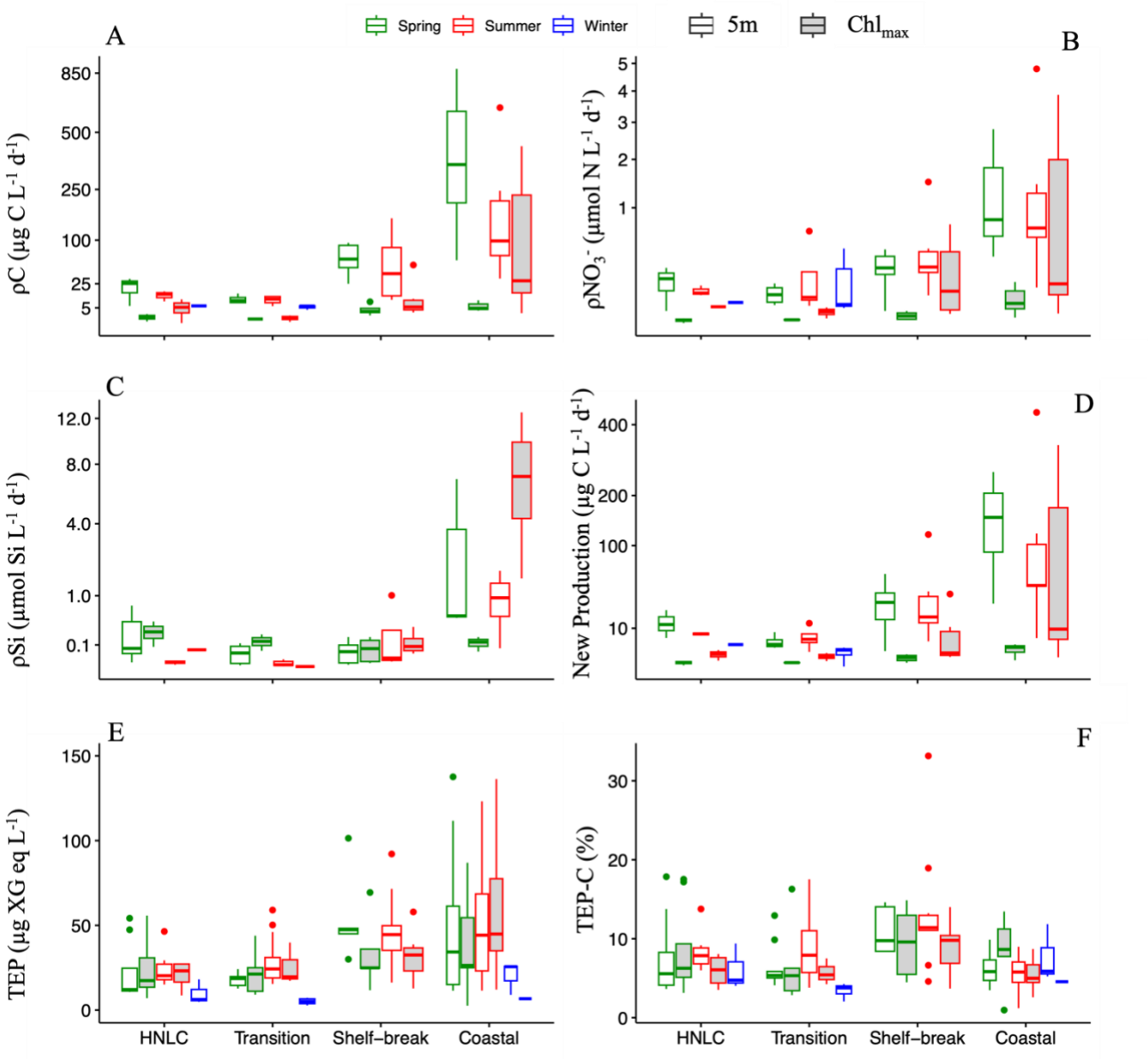


**Figure 3.2.** Boxplots displaying median and ranges in (A) carbon uptake (ρC), (B) nitrate uptake ($\rho NO_3^-$), (C) silicic acid uptake (ρSi), (D) new production, (E) TEP concentrations, and (F) %TEP-C, in the upper mixed layer in different seasons and subregions of the ESNP from 2019-2022. Colours of boxes correspond to different seasons as in legend. All values (n = 72 for ρC, $\rho NO_3^-$ uptake rate experiments and new production, n = 46 for ρSi uptake rate experiments, n = 149 for samples for TEP) represent spatial and seasonal averages from 2019-2022. Note the

variable scaling on the y axes. Boxes represent the 50% interquartile range, including the median values as a horizontal line, the vertical lines indicate the range in values outside the interquartile range, and dots indicating outliers.

### 3.4.2 Correlational analysis between nutrient uptake rates and TEP

The concentration of TEP was significantly positively correlated with ρC ($R^2$ = 0.36, $p$ <0.001), and $\rho NO_3^-$ ($R^2$ = 0.28, $p$ <0.001), but not with ρSi (Figure 3.3 A-C). TEP concentrations were also significantly linearly related to NP rates ($R^2$ = 0.24, $p$ <0.001; data not shown). There were no apparent seasonal patterns observed with these relationships, apart from very low [TEP] and uptake rates in the winter months (Figure 3.3 A-C). The %TEP-C was not correlated with uptake rates or with any other biological metrics (Table 3.2); however, significant relationships ($p < 0.05$) were observed for a number of environmental parameters, including positive correlations with temperature, salinity and 24-h PAR, and negative correlations with [$NO_3^-$], [$Si(OH)_4$], and MLD (Table 3.2).

**Table 3.2.** Linear regression statistics between dependant variables (Dep. Var.; TEP, %TEP-C) and independent biological or environmental variables (Ind. Var.) in the Eastern Subarctic North Pacific from 2019-2022. Bold font denotes statistical significance ($p < 0.05$). Explained variance ($R^2$) and coefficient of the regression slope are also shown.

| Ind. Var. | Dep. Var. | $R^2$ | $p$ | Coefficient | Dep. Var. | $R^2$ | $p$ | Coefficient |
|---|---|---|---|---|---|---|---|---|
| Chl-*a* | TEP | **0.60** | **<<0.01** | **6.50** | %TEP-C | 0.00 | 0.65 | |
| POC | | **0.66** | **<<0.01** | **0.11** | | 0.00 | 0.79 | |
| DO | | **0.08** | **<<0.01** | **11.09** | | 0.00 | 0.55 | |
| *In vivo* Fluorescence | | **0.62** | **<<0.01** | **7.34** | | 0.00 | 0.85 | |
| ρC | | **0.36** | **<<0.01** | **0.11** | | 0.00 | 0.31 | |
| $\rho NO_3^-$ | | **0.28** | **<<0.01** | **0.60** | | 0.00 | 0.56 | |
| New production | | **0.24** | **<<0.01** | **0.16** | | 0.00 | 0.34 | |
| ρSi | | 0.00 | 0.78 | | | 0.01 | 0.22 | |
| [$NO_3^-$] | | **0.09** | **<<0.01** | **-1.34** | | **0.08** | **<<0.01** | **-0.22** |
| [$Si(OH)_4$] | | 0.01 | 0.47 | | | **0.04** | **<<0.01** | **-0.10** |
| [$PO_4^{3-}$] | | **0.02** | **0.02** | **-9.75** | | **0.02** | **0.04** | **-1.92** |
| Temperature | | **0.08** | **<<0.01** | **2.10** | | **0.06** | **<<0.01** | **0.35** |
| MLD | | **0.16** | **<<0.01** | **-0.52** | | **0.02** | **0.04** | **-0.04** |
| Density | | 0.02 | 0.05 | -5.23 | | 0.00 | 0.15 | 0.34 |
| Salinity | | 0.00 | 0.66 | | | **0.03** | **0.04** | **0.85** |
| 24h-PAR | | 0.01 | 0.07 | | | **0.03** | **0.01** | **0.005** |

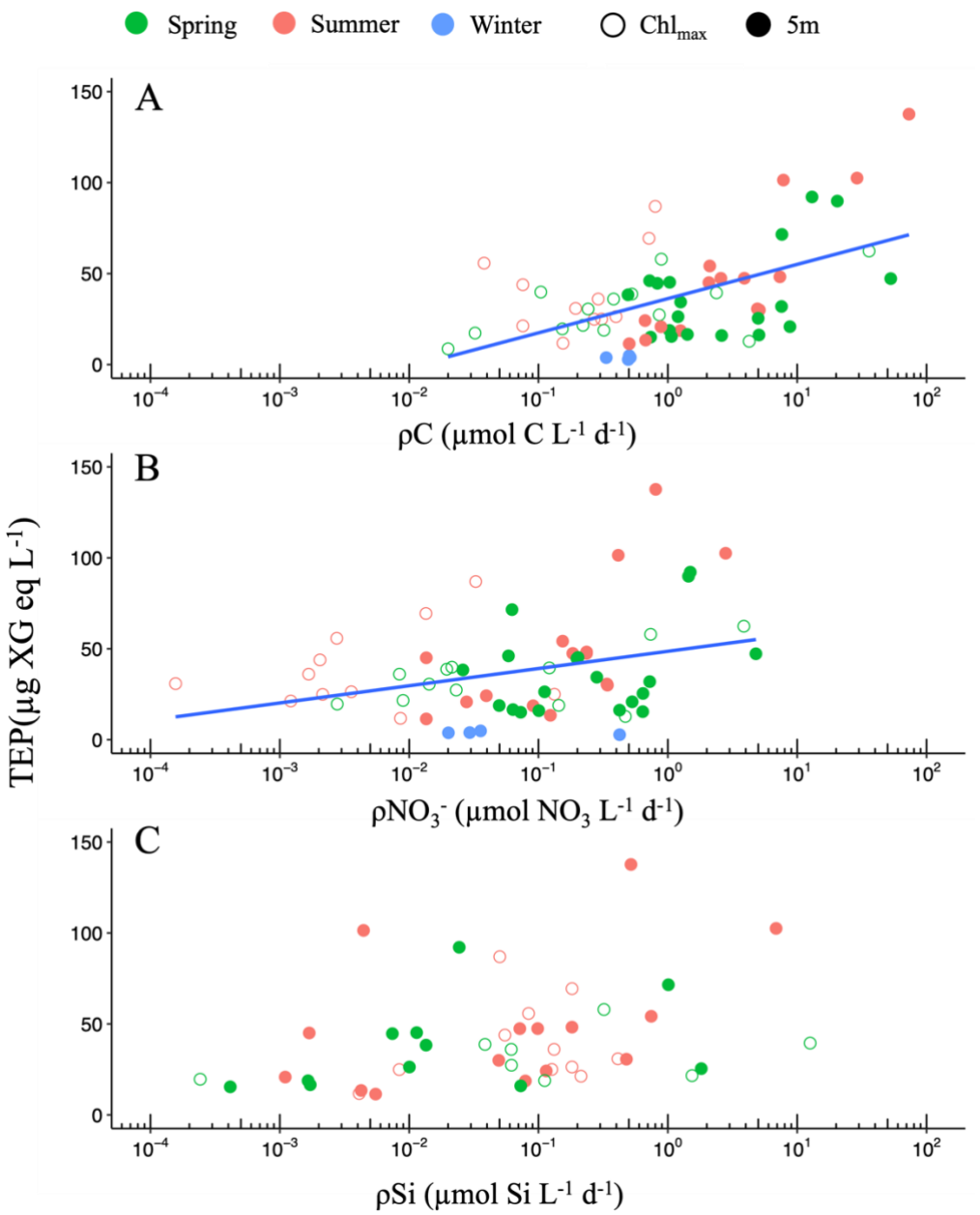


**Figure 3.3.** Relationships between total TEP concentrations and carbon (ρC), nitrate ($\rho NO_3^-$), and silicic acid (ρSi) uptake rates over a four-year period from 2019 – 2022 in the Eastern Subarctic North Pacific (ESNP). Samples were taken within the upper mixed layer, from 5m (filled symbols) and the chlorophyll maximum (open symbols). The solid blue line represents a significant linear regression line. TEP concentrations were significantly correlated with ρC ($R^2$ = 0.36, $p < 0.001$) and $\rho NO_3^-$ ($R^2$ = 0.28, p = < 0.001) rates, but not ρSi ($R^2$ = 0.0, p = 0.47). Note the logarithmic x axis scale.

### 3.4.3 Carbon overconsumption estimates relative to TEP-C

Carbon overconsumption estimates (COC) were significantly correlated with [TEP-C], including $C_{OC\ max}$ ($R^2 = 0.34$, $p < 0.001$) and $C_{OC\ lit}$ ($R^2 = 0.23$, $p < 0.001$), when assessed across the entire study range (Table 3.3). However, correlations between all $C_{OC}$ estimates and [TEP-C] were only significant within coastal and transition regions, while no significant relationship was observed in shelf-break or HNLC regions (Table 3.3).

**Table 3.3.** Linear regression equations and statistics describing the relationship between estimates of carbon overconsumption (COC) and TEP based carbon (TEP-C) across samples from the upper mixed layer in the Eastern Subarctic North Pacific from 2019-2022. COC was estimated in three ways: i) Maximum estimates assuming 100% of C uptake is fuelled by nitrate ($COC_{max}$; i.e. f ratio = 1), ii) using literature estimates of a mean *f*-ratio along Line P of 0.21 ($COC_{lit}$).

| Subregion | Independent var. | $R^2$ | p | Coefficient | # samples (*n*) |
|---|---|---|---|---|---|
| Coastal | $COC_{max}$ | **0.59** | **0.002** | **0.08** | **11** |
| | $COC_{lit}$ | **0.37** | **0.02** | **0.30** | **11** |
| Shelf-break | $COC_{max}$ | 0.04 | 0.16 | 0.19 | 25 |
| | $COC_{lit}$ | 0.03 | 0.20 | 0.22 | 25 |
| Transition | $COC_{max}$ | **0.33** | **0.02** | **0.96** | **13** |
| | $COC_{lit}$ | **0.60** | **<0.001** | **3.35** | **13** |
| HNLC | $COC_{max}$ | 0.01 | 0.31 | 0.74 | 10 |
| | $COC_{lit}$ | 0.00 | 0.80 | 1.10 | 10 |
| Entire study | $COC_{max}$ | **0.08** | **<0.001** | **0.74** | **62** |
| | $COC_{lit}$ | **0.32** | **<0.001** | **1.10** | **62** |

### 3.4.4 TEP production rates and estimates of TEP-$C_{turnover}$

Experimentally determined TEP-C production rates ranged from 0.83 µg C $L^{-1}$ $d^{-1}$ at P4, 1.2 µg C $L^{-1}$ $d^{-1}$ at P12, and 5.0 at P26 µg C $L^{-1}$ $d^{-1}$, with an average of 2.34 µg C $L^{-1}$ $d^{-1}$ across

all 3 stations. In comparison to TEP-C production rates, TEP-$C_{turnover}$ rates, estimated using an average residence time of 4.6 days, averaged 5.30 µg C $L^{-1}$ $d^{-1}$ in coastal regions to 2.36 µg C $L^{-1}$ $d^{-1}$ in HNLC regions.

### 3.4.5 Carbon uptake, new production, and TEP-C

The simultaneous measurement of TEP-C (µg C $L^{-1}$), ρC (µg C $L^{-1}$ $d^{-1}$), and NP-C estimates (µg C $L^{-1}$ $d^{-1}$) across the entire study area allowed for comparisons between total standing C concentrations, in the form of TEP-C, with daily uptake and export potential of C. The calculation of TEP-C turnover rates (calculated from ranges in TEP residence times along Line P), allowed for the comparison of total C fluxes from primary production with C turnover present in the form of TEP on daily time scales and in the same units (µg C $L^{-1}$ $d^{-1}$).

Significantly higher ratios of ρC relative to standing [TEP-C] were observed in coastal and shelf-break regions (Figure 3.4 A, B) when compared to transition and HNLC regions (Figure 3.4 C, D) ($p < 0.01$). In other words, the amount of C taken up per day was higher relative to standing [TEP-C] in coastal and shelf-break regions. Median (and average) values of [TEP-C] relative to C uptake, expressed as a % TEP-C of daily ρC, were 21% (115%), 116% (190%), 153% (538%), and 93% (696%) for coastal, shelf-break, transition, and HNLC regions, respectively. At higher ρC (> 50 µg C $L^{-1}$ $d^{-1}$) in coastal and shelf-break regions, ρC were higher than standing [TEP-C] by up to an order of magnitude, and t-test results demonstrate a significantly lower fraction of TEP-C relative to ρC during these events ($p < 0.01$). Additionally, a MLR demonstrated that TEP-C relative to ρC decreased significantly ($p = 0.01$) with distance from shore at both surface and chlorophyll max.

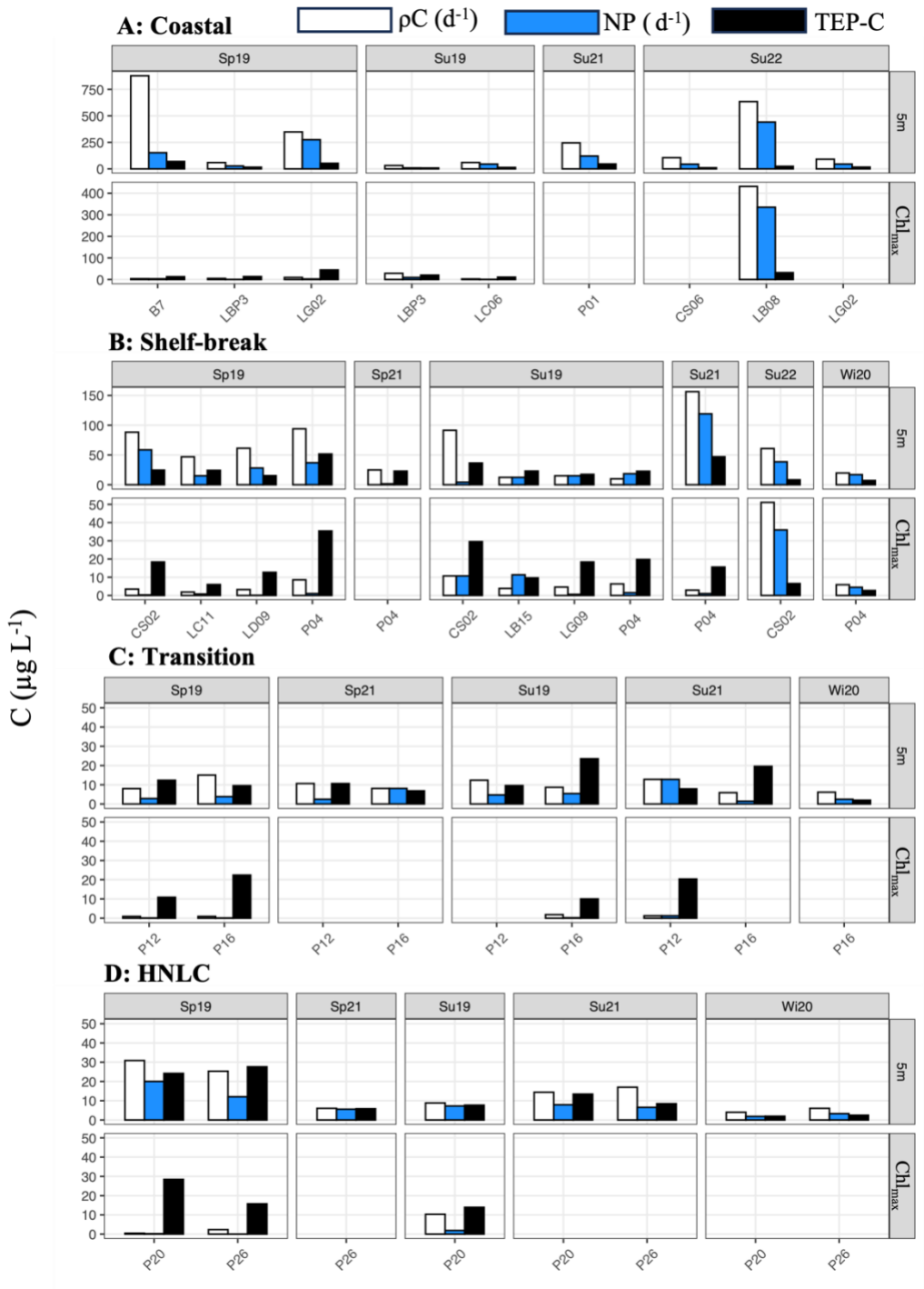


**Figure 3.4.** Carbon (C) uptake rates (ρC), new production (NP) (µg C $L^{-1}d^{-1}$), and TEP-C concentrations (µg C $L^{-1}$) for each station across the coastal (A), shelf break (B), transition (C) and HNLC (D) subregions of the ESNP at 5 m and chlorophyll max ($Chl_{max}$). Bars are further categorized into sampling season, including spring (Sp), summer (Su), and winter (Wi), over each sampling year (2019-22). Note the variation in y-axes scales.

Fluxes of C from measured ρC and estimated TEP-$C_{turnover}$ were also compared over daily scales (Figure 3.5). Daily ρC and average TEP-$C_{turnover}$ rates were highest closer to shore and decreased along the Line P transect towards the HNLC region, with higher values observed at 5m compared to the chlorophyll max depth (Figure 3.5). Significantly higher values of TEP-$C_{turnover}$ relative to ρC were observed in coastal and shelf-break regions compared to transition or HNLC regions ($p < 0.01$). Median (and average) values of TEP-$C_{turnover}$ relative to ρC, expressed as a percentage, were 5% (25%), 26% (41%), 33% (117%), and 21% (151%) for coastal, shelf-break, transition, and HNLC regions respectively (Figure 3.5). In other words, median ρC was 20x higher than TEP-$C_{turnover}$ in coastal regions, and ~5x higher in HNLC regions. During highly productive events at coastal/shelf-break stations LG02, LB08, CS06, P01, B7, CS02, and P04, the amount of ρC greatly exceeded the amount of TEP-$C_{turnover}$. In comparison, other low productivity stations (i.e., in transition and HNLC regions) were characterized by comparable values of ρC to TEP-$C_{turnover}$ (Figure 3.5).

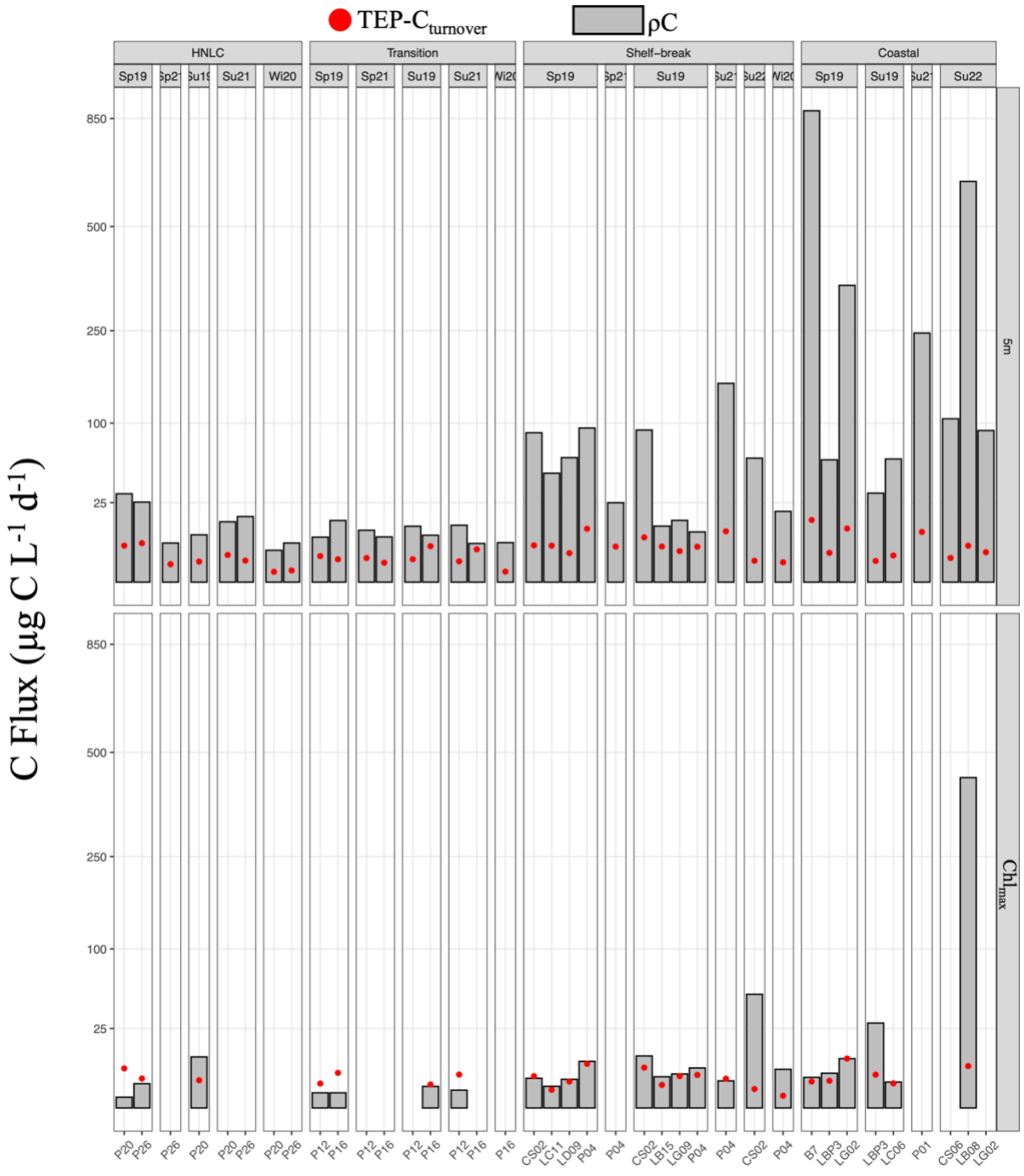


**Figure 3.5.** Carbon (C) uptake rates (ρC) and estimated average TEP-$C_{turnover}$ (µg C $L^{-1}d^{-1}$) for all stations across the HNLC, transition, shelf break, and coastal subregions of the ESNP at 5m and chlorophyll *a* max ($Chl_{max}$). TEP-$C_{turnover}$ rates are derived by using Wurl et al's (2011) average TEP residence time along Line P. The plot is further categorized into sampling season, including spring (Sp), summer (Su), and winter (Wi), over each sampling year (2019-22). Note the non-linear y axis scale.

## 3.5. Discussion

### 3.5.1 Comparing carbon and nitrate uptakes with TEP

Concentrations of TEP have occasionally been measured alongside C uptakes rates in the field, with a strong correlation between the two variables observed in the Baltic Sea (Engel, 2002b) and in the Southern Ocean (large-scale spatial study by Zamanillo et al., 2019), and temporal decoupling between them observed in Jaran Bay, Korea (Lee et al., 2020). The above studies do however lack significant spatiotemporal coverage, including measurements in low chl-*a* environments (i.e., HNLC and oligotrophic regimes) that are known to dominate most of the global oceans and are responsible for a significant portion (~23%) of global C uptake (Field et al., 1998). Indeed, to date there are no large-scale spatiotemporal studies that have compared these variables. *In situ* comparisons between TEP (or TEP-C) and other nutrient uptake rates (i.e., $NO_3^-$ or Si) do not exist. Furthermore, no research has investigated potential C export, using NP-C, and TEP-C concentrations.

In this study, I provide the first evidence of an *in-situ* relationship between C uptake and [TEP] over large spatial and temporal gradients at the ocean's surface. I show that ρC uptake and [TEP] are highly correlated across large spatial and seasonal gradients in the ESNP (Figure 3.3A). As phytoplankton are considered the primary sources of marine TEP, this relationship is both theoretically sound and supported by the literature (Passow and Alldredge, 1995). TEP precursors are primarily produced via extracellular release or cellular C overflow (Claquin et al., 2008; Engel et al., 2011); as a result, higher levels of ρC would be associated with higher levels of TEP.

It is reasonable to expect that [TEP] would also strongly correlate with $\rho NO_3^-$, or ρSi, given that diatoms have been shown to be major TEP producers (Passow, 2002b). Interestingly, [TEP] was more strongly correlated with ρC compared to $\rho NO_3^-$ and was not correlated with ρSi (Figure 3.3 C). These results show that ρC explain much more variance in [TEP] in the ESNP compared to $\rho NO_3^-$, while ρSi does not explain [TEP]. This result may be due to the inherent nature of TEP production being linked to phytoplankton cellular C overflow, and not necessarily dependant on the total ρN or source of N that is fuelling the process (i.e., ammonia or urea versus $NO_3^-$). This is supported by Engel et al., (2002), who found significant C:N decoupling during a mesocosm experiment, where DIC was taken up in excess to that inferred from $NO_3^-$ supply and Redfield stoichiometry, and it was associated with increased [TEP]. Furthermore, TEP production has been linked to C and N limitation in phytoplankton, but not to Fe or Si limitation (Staats et al., 2000) which may explain the lack of correlation between [TEP] and ρSi observed in my study. I provide further evidence of C overconsumption, on a broad geographic scale from two lines of evidence i) the higher degree of correlation strength between [TEP] and ρC vs TEP and $\rho NO_3^-$ or ρSi (Figure 3.3), and ii) the significant linear relationship between [TEP-C] and C overconsumption, as discussed below and shown in Table 3.3.

### 3.5.2 Carbon overconsumption estimates and TEP-C

According to (Sambrotto, 1993), C overconsumption can be determined as a higher drawdown of DIC relative to $NO_3^-$, exceeding what is predicted from Redfield stoichiometry (Sambrotto, 1993). This has further been observed to be correlated with [TEP] in experimental studies (Engel, 2002a). I estimated C overconsumption as excessive ρC relative to ρC predicted from $\rho NO_3^-$. One limitation of this approach is that $NO_3^-$ is not the only N source for

phytoplankton in the ESNP. Varela and Harrison (1999) found that $NO_3^-$ uptake consisted of ~21% of total N uptake along Line P. With that in mind, I derived two distinct estimates of C overconsumption (as discussed in section 3.3.7) using both maximum and minimum estimates of $NO_3^-$ utilization by phytoplankton. All approaches yielded significant linear correlations with TEP-C concentrations over the entire range of the study; however, there was no significant correlation observed in shelf-break and HNLC regions if assessed individually (Table 3.3). It should be noted that I observed several instances of relatively high TEP-C concentrations and a value of 0 for carbon overconsumption in coastal and shelf-break regions (data not shown). This could be explained by: i) estimates being too low, or ii) high TEP concentrations not being linked to phytoplankton C overconsumption.

Subsequent studies have linked C overconsumption to the accumulation of large amounts of buoyant organic matter in the field, particularly in summer or nutrient depleted conditions (Mari et al., 2001, 2017; Mari & Burd, 1998). Data in Table 3.3 support previous evidence and suggest that TEP accumulation is correlated with C overconsumption, as higher amounts of TEP-C were generally associated with elevated $\rho C$ relative to $\rho NO_3^-$. I provide the first large scale field evidence of a link between estimates of C overconsumption and TEP-C (although this evidence is limited by a lack of alternative N sources, as described above), which helps to better understand marine C cycling at the ocean's surface. I further hypothesize that an increase in the frequency or intensity of $NO_3^-$ limitation in future ocean scenarios could lead to increasing instances of C overconsumption by phytoplankton, and subsequently, increases in [TEP-C] relative to phytoplankton biomass.

### 3.5.3 TEP-C: Implications for Decoupling of Production and Export

Despite the strong correlation between ρC and [TEP] (Figure 3.3 A), there was significant spatial variation in the amount of [TEP-C] relative to ρC (Figure 3.4). Nearshore regions (i.e., coastal and shelf-break), characterized by higher levels of ρC, showed a considerably higher total ratio of ρC relative to [TEP-C]. In contrast, in off-shelf and oceanic regions (i.e., transition and HNLC subregions), standing [TEP-C] to daily ρC ratios were generally lower (Figure 3.4). The same trend is observed for [TEP-C] and NP-C (Figure 3.4). This result suggests that there is higher amount of C in the form of TEP relative to ρC and NP-C in low productivity regimes on daily time scales. However, since the above analysis compared concentrations of TEP-C to daily ρC rates, a direct comparison is challenging to interpret. If I divide [TEP-C] by its estimated turnover rates along Line P, I can obtain an estimate of daily TEP-C turnover, which in turn can be directly contrasted with daily ρC.

While I did not directly measure TEP turnover or TEP residence times, the work done by Wurl et al. (2011) (across the same spatial range as my study) allowed us to estimate average TEP-C turnover rates, and to further constrain minimum and maximum values based on the ranges in TEP residence times provided in their study. To account for this range in residence times, I calculated boundary limits for TEP turnover rates using both minimum and maximum TEP residence times from Wurl et al., (2011) (Section 3.3.4). I provide further support for the use of Wurl's TEP residence time estimations by comparing TEP-C production rates with estimates of TEP-C turnover (using a residence time of 4.6 d to estimate average TEP export). I measured TEP-C production rates of 2.34 µg C $L^{-1}$ $d^{-1}$ on average (from P4, P12, and P26), compared to estimated TEP-$C_{turnover}$ rates of 2.6 – 5.2 µg C $L^{-1}$ $d^{-1}$ along Line P. This implies that the rate of TEP-C turnover (either through export or disaggregation) is similar in magnitude to its

production rate. This result is supported by the relatively consistent year-round [TEP] I observed in open-ocean HNLC and Transition regions of the ESNP.

Using TEP-$C_{turnover}$ rates estimates obtained from Wurl et al (2011)'s residence times estimates, C fluxes derived from TEP-$C_{turnover}$ can be compared to total ρC (Figure 3.5). Highly productive stations, with elevated ρC, were characterized by higher ratios of ρC relative to TEP-$C_{turnover}$ (Figure 3.5). Coastal/shelf-break stations B7, LG02, P01, CS06, LB08, CS02 (Spring 2019), and P04 (Summer 2021) recorded the highest ρC rates in this study. These locations were also characterized as having the highest amount of TEP-$C_{turnover}$ relative to ρC, with values ranging from 1-8% relative to ρC if an average residence time for TEP-C is used. Furthermore, if the minimum estimated residence time for TEP-C is used (implying a high amount of TEP-$C_{turnover}$), the amount of C flux from ρC still exceeded the magnitude of C flux as TEP-$C_{turnover}$ (data not shown) in productive coastal stations. This demonstrates that at these locations, the high rates of ρC greatly exceeded [TEP-C] and TEP-$C_{turnover}$ rates. As TEP is a positively buoyant substance, it can be hypothesized that C export at these locations was likely more efficient than in lower productivity regimes because the total flux of C from ρC far exceeded the flux of C as TEP-$C_{turnover}$. In contrast, in low productivity regions, estimates of average TEP-$C_{turnover}$ relative to ρC were higher and of similar magnitude, which this implies that a higher fraction of the C derived from primary production is being turned over (i.e., recycled or exported) as TEP-C. This can have important implications for C export, as Mari et al. (2017) demonstrates that high fractions of TEP-C relative to total primary production will determine the efficiency of C export from surface waters.

My results provide support and additional context to a variety of field-based observations regarding the temporal decoupling between C uptake and export. Many studies have observed

the decoupling between the standing stock of POC in the euphotic zone (from primary production) and POC export across oceanographic regimes, as reviewed by Mari et al. (2017). This has been observed in upwelling (Kiørboe et al., 1998; Pitcher et al., 1991), coastal (Rinaldi et al., 1995), and HNLC (Boyd et al., 2000) regions. A hypothesis to explain this phenomenon is put forward by Mari et al., (2017), who suggests that a positively buoyant, gelatinous organic matrix (TEP) may help to explain the decoupling between ρC and POC export. High levels of TEP relative to available C export would result in a more buoyant POC matrix, delayed C export, and increased bacterial remineralization exposure in the upper ocean (Bar-Zeev et al., 2009; Mari et al., 2017; Mühlenbruch et al., 2018).

My results support the hypothesis of Mari et al., (2017), as I demonstrate that low chl-*a*, open ocean HNLC and transition regions have high concentrations of standing stock TEP-C relative to total ρC and export potential (i.e. NP-C), which suggests less efficient export of C. Interestingly, Buesseler (1998) demonstrated that much of the ocean is characterized by low efficiencies of C export (relative to ρC), apart from highly-efficient episodic pulses during phytoplankton blooms. In this study, I show that areas of elevated ρC and NP-C (i.e., phytoplankton blooms) were characterized by relatively lower levels of [TEP-C] and TEP-$C_{turnover}$. In contrast, I show that lower productivity regions experience TEP-$C_{turnover}$ levels as a much higher % of ρC.

While my estimates of TEP-$C_{turnover}$ are limited by the lack of directly measured TEP residence times, they are nonetheless comparable with a study by Guo et al., (2022), who used sediment traps to measure TEP fluxes in two oligotrophic regions. They recorded that TEP contributed an average of 61% and 46% to total C export in the South China Sea and Western Tropical North Pacific, respectively. Furthermore, a recent study performed at Ocean Station

Papa (the terminal station along Line P in the ESNP), demonstrated the importance of TEP as a key mediator of POC sinking efficiency as suspended aggregates had three times [TEP] compared to sinking aggregates (Romanelli et al., 2023). These studies, coupled with my results, demonstrate the high prevalence of TEP in the suspended C and C export pool throughout low chl-*a* regions.

### 3.5.4 Conclusions

This study provides a unique perspective on the relationship between [TEP] and nutrient uptake rates. I provide the first field evidence of the coupling of ρC, and [TEP-C] across large gradients in time and space in an oceanic region. I also demonstrate the importance TEP-C to C cycling in the ESNP, with implications for low chl-*a* oceanographic regions. These results indicate that perennially low chl-*a* regions are characterized by higher ratios of TEP-C relative to daily ρC and NP-C, and similarly relatively higher TEP-$C_{turnover}$ rates. In contrast, productive coastal regions can experience the opposite trend, with elevated values of ρC and NP-C relative to [TEP-C] and TEP-$C_{turnover}$ rates. As TEP is a positively buoyant substance, this suggests that C export may be more efficient during highly productive phytoplankton blooms as the total amount of productivity and export can greatly exceed the amount of C in the form of TEP. Furthermore, this is the first study to assess the magnitudes of ρC and export potential relative to [TEP-C] and estimated TEP-$C_{turnover}$ in the upper ocean. As TEP is a key mediator of the balance between POC aggregation, export, and remineralization in the surface oceans, this study presents new insights into the driving factors behind a major component of the biological C pump.

# Chapter 4: Spatiotemporal trends in the contributions of small-cell phytoplankton to biogeochemical cycles in the Northeast Pacific Ocean

## 4.1 Abstract

Small celled phytoplankton (<5µm in size) are known to be competitively more dominant than larger cells under conditions of nutrient scarcity in marine environments. With a forecasted increase of 2-4˚C in world temperature, the ocean's water column will become more stratified and nutrient limited, favouring the proliferation of smaller cells over larger celled phytoplankton. A shift in the size composition of phytoplankton assemblages will have implications for the ocean biogeochemical cycling, the biological carbon pump (BCP), and the transfer of energy between trophic levels. To understand the implications of such a shift, it is necessary to i) quantify the magnitude of small-celled phytoplankton contributions to nutrient uptake in the ocean, and ii) determine the environmental influences that affect the relative contributions of small cells to these cycles. Carbon (C), nitrate ($NO_3^-$), and silicic acid ($Si(OH)_4$; Si) uptake rates, as well as new production estimates (NP), were measured for both total phytoplankton assemblage and small cell fractions (<5µm) over a four-year, multi-seasonal study across a 1400 km transect that expanded from coastal to open ocean waters in the Eastern Subarctic North Pacific (ESNP). The production rates of transparent exopolymer particles (TEP-C) were also calculated for each size fraction during one research cruise. Small cell contributions to nutrient uptake rates (ρC, $\rho NO_3^-$, and ρSi) were measured relative to the rates of the whole assemblage for each oceanographic region and season to estimate spatiotemporal variability. Small phytoplankton fractions (<5µm) dominated ρC (78%), and $\rho NO_3^-$ (76%) in perennially low chlorophyll *a* regions of the ESNP. Uptake and particulate ratios of C:N were similar between smaller and larger size fractions. In contrast, smaller cells contributed significantly less to ρSi, and were characterized by higher ratios of Si:C uptake and particulate Si:C ratios. The <5 µm size fraction was also responsible for most of the production of TEP-C. Small cell uptake rates

and percent contributions were not observed to be affected by any of the environmental variables measured, with only the depth of the mixed layer (MLD) and distance from shore (DFS) shown as significant controlling factors. This study is one of a small number of papers to investigate the role of small phytoplankton to nutrient uptake rates across large spatiotemporal ranges and is the first of its kind to measure size fractionated ρSi across such a scale. This study emphasizes the importance that small cells have on biogeochemical processes in oceanic regions of the ESNP and provides a quantification of their contributions to nutrient uptake rates, new production, and TEP production.

## 4.2 Introduction

Phytoplankton fix carbon dioxide ($CO_2$) from the atmosphere into organic matter, and are responsible for capturing approximately 50 Pg of carbon (C) per year (Field et al., 1998) and produce ~50% of Earth's oxygen. Small-celled phytoplankton (such as nano (2-20µm) and pico (<2µm) phytoplankton) currently comprise a major fraction of the total phytoplankton biomass and primary production in the world's oceans, and are particularly dominant across low productivity regimes, such as warm oligotrophic waters or high nitrate low chlorophyll (HNLC) regions (Agawin et al., 1998, 2000). There is a large and growing body of evidence that suggests that small-celled phytoplankton may hold a competitive advantage over their larger celled counterparts in future ocean scenarios. Small cells are characterized by a natural advantage in acquiring nutrients, as they have larger surface area to volume ratios and smaller diffusion boundary layers than larger cells (Raven, 1998). These traits confer a competitive advantage in regions that are nutrient limited, such as macronutrient limited oligotrophic regions or micronutrient limited high nutrient low chlorophyll (HNLC) regions (Booth et al., 1993).

Variation in the availability of iron (Fe) is a key control on phytoplankton productivity and the abundance of larger cells throughout the HNLC regions of the Eastern Subarctic North Pacific (ESNP). Ocean warming is expected to intensify the degree of thermal stratification in the water column and reduce nutrient mixing from deep waters to the euphotic zone (Boyce et al., 2010; Polovina et al., 2008). As such, small-cell phytoplankton may be able to outcompete larger celled phytoplankton in a future nutrient-limited ocean, as has been predicted in several studies (Beaugrand et al., 2010; Li et al., 2009; Morán et al., 2010; Pauly & Cheung, 2018) as well as directly observed in the Eastern Subarctic Northeast Pacific (ESNP) through 2014 -16 due to a greater degree of nutrient limitation and stratification (Peña et al., 2019).

Small celled phytoplankton are responsible for a large but variable portion of total C uptake in marine environments, and have been found to be periodically responsible for >30% of the total C uptake in the Barents Sea (Hodal & Kristiansen, 2008), Chukchi Sea (Lee et al., 2013), Western Arctic (Lee et al., 2012), Southern Oceans (Irion et al., 2021), and the Greenland Sea (Legendre et al., 1993). Recently, Meyer at al., (2022) found that small phytoplankton dominated C uptake (89%) at Ocean Station Papa (OSP) in the HNLC region of the ESNP, highlighting the importance of small cells to C production in the region. However, many studies only include a single sampling event or sampling location, and therefore do not necessarily estimate variations in C uptake by small phytoplankton in a large spatiotemporal setting. Similarly, the contributions of small cells to total nitrogen (N) and nitrate ($NO_3^-$) uptake rates have been measured in only a handful of studies, and often with limited spatiotemporal resolution. Estimates exist of ~38% of total $NO_3^-$ uptake owing to small cells in the Chukchi sea (Lee et al., 2013), 50-55% and 73% in the ESNP (Varela 1997; Meyer 2022).

It has been traditionally accepted that larger, Si-shelled phytoplankton - diatoms - are the predominant agents of Si uptake in the ocean (Monferrer et al., 2021; Tréguer, 2014). However, there is a growing body of evidence that suggests small phytoplankton may also contribute to Si uptake (Brzezinski et al., 2022; Franck et al., 2005; Krause et al., 2017; Wei, et al., 2021) and particulates (Baines et al., 2012; Krause et al., 2017). Krause et al. (2017) concluded that while small celled phytoplankton have a small, but consistent regional contribution to biogenic silica (bSi) production, small cell contributions to global Si uptake may be underestimated given their global distribution. While recent research highlights the potential importance of small cells to the Si cycle, the contributions of small cells to Si uptake remain poorly estimated in space and time. Additionally, it is unknown how variation in environmental stressors may affect their relative contributions to Si uptake.

The classical viewpoint suggests C export via small celled phytoplankton is proportionally reduced compared to their larger-celled counter parts , primarily as a result of reduced sinking velocity, increased remineralization in the euphotic zone, and the disproportionate contributions of larger cells to carbon uptake/export (Richardson, 2019). This view has received considerable criticism in recent years, as several studies have suggested that small cells may contribute to C export at rates proportional to their production rates (Richardson & Jackson, 2007), potentially due to the aggregation of small phytoplankton cells into large detrital aggregates (Albertano et al., 1997; Olli & Heiskanen, 1999) such as those formed by transparent exopolymer particles (TEP) (Passow, 2002a). In the ESNP, Varela (1997; thesis) found that picophytoplankton accounted for most of the new production (NP) at OSP, suggesting that small cells may play an important role in the export of C from the surface ocean in this

region. Despite this evidence, spatiotemporal estimations of small cells contribution to NP estimates remain poorly understood in the ESNP.

Given the current projections of an expansion of small cell phytoplankton in marine environments under climate-induced environmental change, it is important to first quantify the contributions of small phytoplankton to biogeochemical rates in the ocean. Here, I present small cell contributions to whole assemblage uptake rates of C, $NO_3^-$, $Si(OH)_4$, and new production over a 1400 km spatial gradient in environmental conditions, across multiple seasons over a 4-year period. I further quantified the production of transparent exopolymer particles (TEP) by small cells to further investigate their role in the upper ocean C cycle. The main goals of this study were to (i) quantify the contributions of small celled phytoplankton to biogeochemical cycling (C, $NO_3^-$, Si uptake rates, NP rates, and TEP production), (ii) estimate the contributions of small cells in low chlorophyll-*a* (chl-*a*) regions of the ESNP, and (iii) investigate the role of environmental variables in influencing the contribution of small cells to biogeochemical rates.

## 4.3 Methods

### 4.3.1 Sampling Regime

Sampling for size-fractionated nutrient (C, $NO_3^-$, $Si(OH)_4$) uptake rates, in addition to discrete water sampling for chlorophyll-*a* (chl-*a*), particulate carbon and nitrogen (PC/PN), biogenic silica (bSi), dissolved nutrients ($NO_3^-$, $Si(OH)_4$, and $PO_4^{3-}$), and environmental conditions (salinity, temperature, mixed layer depth) was taken during the Line P and La Perouse programs (operated by the Department of fisheries and Oceans Canada (DFO) and onboard the *CCGS John P. Tully*) in the ESNP. Sampling stations ranged from the productive coastal waters of Vancouver Island to the high nutrient low chlorophyll (HNLC) regions of the Subarctic

Alaskan Gyre, resulting in a spatial range of over 1400 km. The Line P transect represents much of this spatial range, originating from the west coast of Vancouver Island to a terminal station known as Ocean Station Papa (OSP/P26) located at 50˚N and 145˚W within the HNLC region of the NE Pacific (Figure 4.1). The La Perouse program consisted of a series of transects that ranged from coastal to deeper offshore waters and spans the south-north range of Vancouver Island. A total of nine research cruises were conducted over a four-year period, and spanned winter, spring, and summer seasons (Table 4.1). Seawater was collected using a sampling rosette (24 10-L Niskin bottles), with a conductivity-temperature-depth sensor (Seabird SBE-911 CTD) attached to the rosette. Samples were taken at both 5 m depth and at the chlorophyll maximum (CM) (as determined by depth of maximum *in vivo* fluorescence). Sampling times were variable and largely depended on cruise logistics; when possible, samples for nutrient uptake rate experiments were collected just prior to sunrise.

**Table 4.1**. Information on cruise programs and their corresponding date ranges, defined seasons, number of nutrient experiments performed, and station location of experiments (as detailed in Figure 4.1). At each station, a total of 2 uptake rate experiments for C (ρC), $NO_3^-$ ($\rho NO_3^-$), and $Si(OH)_4$ (ρSi), were performed (at both 5 m and the chlorophyll max depth); cruise 2021-006 was the exception where ρSi uptake experiments were only performed at 5m. Cruise ID corresponds to the Department of Fisheries and Oceans program name, year, and number.

| Program | Year - Cruise ID | Date range | Season | Total # of uptake experiments (n) | Stations for uptake experiments |
|---|---|---|---|---|---|
| La Perouse | 2019 -005 | May 18 – June 2 | Sp | 12 | B7, LBP3, LG02, CS02, LC11, LD09 |
| Line P | 2019 -006 | June 3 - 16 | Sp | 10 | P4, P12, P16, P20, P26 |
| La Perouse | 2019 -009 | Aug 29 – Sept 10 | Su | 12 | LBP3, LC06, CS02, LB15, LG09 |
| Line P | 2019 -008 | Aug 15 - 29 | Su | 10 | P4, P12, P16, P20, P26 |
| Line P | 2020 -001 | Feb 9 - 23 | Wi | 10 | P4, P12, P16, P20, P26 |
| Line P 2021 | 2021 – 006 | May 4 – 18 | Sp | 10 | P4, P12, P16, P20, P26 |
| Line P 2021 | 2021 – 008 | Aug 24 – Sept 7 | Su | 11 | P1, P4, P12, P16, P20, P26 |
| La Perouse 2022 | 2022 – 009 | September 4–11 | Su | 8 | CS06, LB08, LG02, CS02 |

### 4.3.2. Regional categorization

To investigate spatial variations in the dataset, I grouped the data into four oceanographic regions broadly characterized by variations in their physical characteristics, and macronutrient and trace metal concentrations. Variation in the availability of iron (Fe) is a key control on phytoplankton productivity throughout the HNLC regions of the ESNP. A such, regions were categorized according to high, intermediate, or low Fe limitation as determined in LaRoche et al., (1996) along Line P using Flavodoxin concentrations as a proxy for Fe limitation stress (La Roche et al., 1996). Stations characterized by high Fe limitation and Flavodoxin concentrations

were classified as ‘HNLC’ (P26, P20). In contrast, offshore regions that (i) have lower levels of Fe limitation, (ii) have relatively uniform water properties (salinity, mixed layer depth, nutrient concentrations) within a given season, and (iii) are not influenced by coastal currents (Shelf Break Current and Vancouver Island Current) or topographically driven upwelling along the shelf break, were classified as ‘Transition’ stations (P16, P12). The water properties and physical oceanographic data supporting this classification can be found in Whitney and Freeland (1999) and Harris et al., (2009), respectively. All other remaining stations are located much closer to Vancouver Island, and proximal to, or within the influence of the currents that dominate its west coast. Stations in these areas were classified as ‘Shelf-break’ or ‘Coastal’ regions and are characterized by episodic nutrient depletion and phytoplankton blooms. Shelf-break stations were classified as locations with a bottom depth >300 m, located along the continental shelf-break, and experience topographically controlled upwelling (Harris et al., 2009). Stations shallower than 300m and situated upon the continental shelf were classified as coastal stations in accordance with Harris et al. (2009).

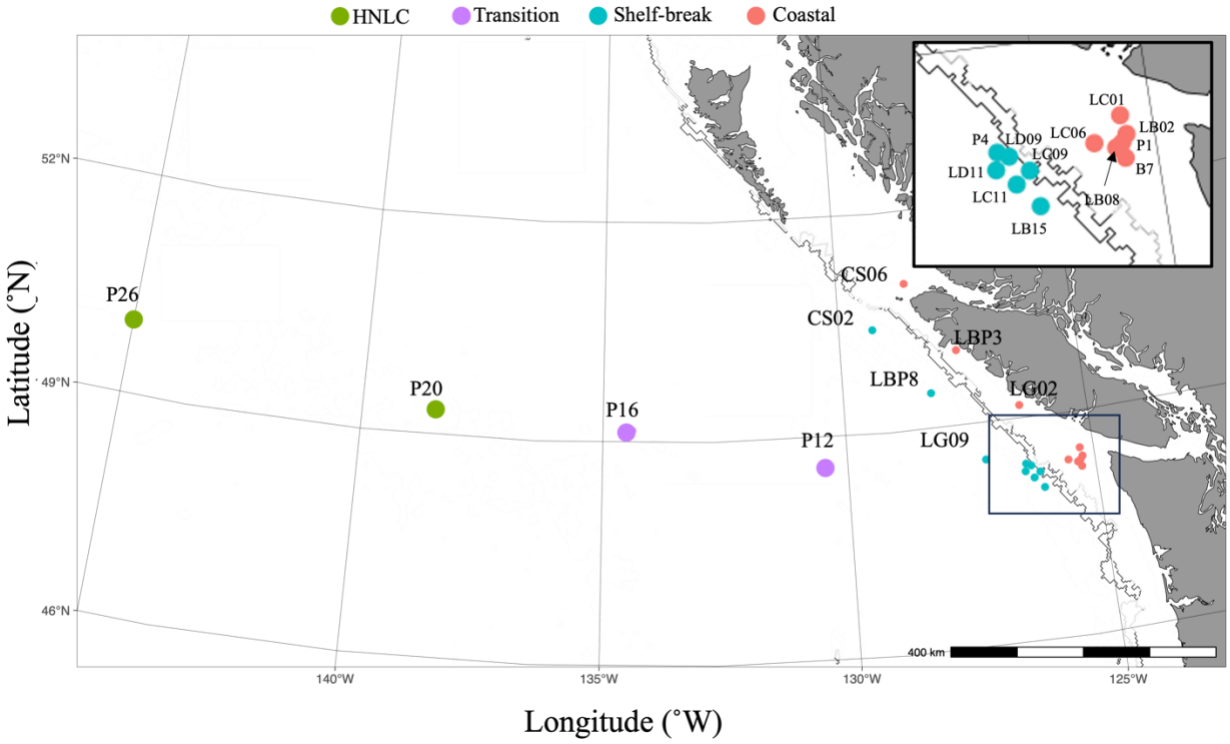


**Figure 4.1.** Sampling locations in the Eastern Subarctic North Pacific Ocean (ESNP) for all measurements taken over a four-year period from 2019 – 2022, from shallow coastal waters off the coast of Vancouver Island to the HNLC regions of the Southern Alaskan Gyre (-145˚W, 50˚N). Samples were collected and grouped within three distinct seasons: winter (Feb – March), spring (May – June) and summer (August – September). Stations were spatially categorized into HNLC, transition, shelf-break, and coastal subregions. The gray contour line indicates a 300 m shelf-break, and serves to define coastal stations (<300m, on-shelf). Several of the shown stations were sampled repeatedly over the temporal range of the study, while other stations were only sampled once. Table 4.1 provides more detail on sampling dates, cruises, and stations.

### 4.3.3 Nutrient uptake rate and particulate composition

Carbon (C) and nitrate ($NO_3^-$) uptake rates (ρC and ρ$NO_3^-$) were measured using a dual tracer $^{13}C$ - $^{15}NO_3$ method as described in Hama et al. (1983) and Dugdale and Goering (1967). Seawater was collected in 2.3-L acid washed polycarbonate bottles, from two depths (5 m and the CM), and $^{13}C$-labeled $NaHCO_3$ (99 atom % $^{13}C$, Cambridge Isotope Laboratories) and $^{15}N$-labeled $NaNO_3$ (98 atom % $^{15}N$, Cambridge Isotope Laboratories) were added immediately after sample collection. Isotopic enrichments were made at $\leq$ 10% ambient dissolved organic carbon

(DIC); DIC concentrations were assumed to be 2000µM. All additions of stable isotopes were done at <10% ambient concentrations; ambient dissolved inorganic carbon (DIC) concentrations were assumed to be 2000 µM, while ambient [$NO_3^-$] were estimated from previous years. After isotopic inoculation, sample bottles were incubated for 24 h by placing them in acrylic tubes wrapped in neutral density and blue-colored light films to mimic ambient light levels. Irradiance levels under the films were pre-calibrated using a Biophysical Instruments Inc. light meter, model QSL 100. Surface (5m) samples were placed within tubes that allowed 50% of incident irradiance to go though, while CM samples were placed in light tubes that most closely matched the ambient light levels at the respective CM depth, as calculated from irradiance data. Acrylic tubes were positioned in a temperature-controlled flow-through on-deck incubator, with temperature controlled via circulation of 5m seawater. To estimate variance in the procedure, two triplicate samples were taken per cruise at different stations and depths.

After 24 hours, incubations were terminated by filtering the water samples (vacuum pressure < 150 mm Hg) through 5µm polycarbonate filters, and the filtrates subsequently filtered through a pre-combusted 0.7µm glass-fibre filters to obtain $\rho C/\rho NO_3^-$ rates for the 0.7-5 µm small phytoplankton size class. Another incubation aliquot was filtered directly through a pre-combusted (6h, 450°C) 0.7 µm glass-fibre filter (to obtain 'total assemblage' rates). Filters were stored at -20˚C until analysis. Back onshore, samples were dried at 60˚C for at least 48 h, and the total particulate (PC/N) and elemental isotopic composition for each sample was measured using an elemental analyzer (Elementar Vario EL Cube) interfaced to a PDZ Europa 20-20 isotope ratio mass spectrometer at the Stable Isotope Facility at the University of California Davis. Total and size-fractionated $\rho C$ and $\rho NO_3^-$ were calculated as outlined in Hama et al., (1983) (equation #3), and Dugdale and Goering (1986) (equation #6), respectively. Size-fractionated uptake rates

for the larger size fraction (>5µm) were subsequently calculated as the difference between total uptake (>0.7 µm) and 07-5µm uptake rates.

New production (NP) rates, expressed in µg C $L^{-1}$ $d^{-1}$, were calculated by converting $\rho NO_3^-$ uptake rates to C units using the empirical particulate C:N ratio observed for each incubated sample (Eppley & Peterson, 1979). If the calculated NP rate exceeded the measured ρC, it was assumed that all ρC uptake was fuelled by NP. The fraction of new production to total primary production (*f-ratio*) for each size-fraction was calculated by dividing the NP by the total ρC. These calculations are described in more detail, and with the relevant equations, in *Chapter 2.3.4*.

Silicic acid ($Si(OH)_4$) uptake rates (ρSi) were measured using the radioisotope $^{32}Si$, following the procedure of Brezinski and Phillips (1997) (Brzezinski & Phillips, 1997). Seawater (250-500 ml) was collected and spiked with 0.02-0.06 µCi of high specific activity $^{32}Si(OH)_4$ immediately after collection. Incubations were performed in the same fashion as for $C/NO_3^-$ rate experiments. After 24h, the incubation was terminated by filtering separate water samples onto 5 µm and 0.6 µm polycarbonate filters. Samples filtered onto the 0.6 µm served to estimate total ρSi, while samples filtered onto the 5 µm filter served to estimate ρSi in both the >5 µm and <5 µm size classes; <5 µm ρSi rates were calculated as total ρSi minus >5 µm ρSi. The filtration apparatus and bottles were rinsed thoroughly onto the filter to remove any $^{32}Si$ adhering to the apparatus. The filters were then mounted onto 25mm diameter planchettes and left to dry for 24 h before wrapping the disk in Mylar film. Mounted filters were stored for at least 120 days to reach secular equilibrium with its daughter isotope $^{32}P$ (i.e. when the decay rate of $^{32}Si$ is equal to its production rate). Sample activity of $^{32}Si$ was determined using a Risø 25-5 low-level beta GM

multicounter. Biogenic silica production rates, expressed as ρSi (µmol $L^{-1}$ $d^{-1}$), was calculated as in Brezinski and Phillips (1997).

The contributions of small phytoplankton to whole assemblage nutrient uptake rates were quantified relative to the total uptake rates and expressed as a percentage (equation 1).

$$Small\ cell\ contribution\ (\%) = \left(\frac{<5\mu m\ uptake\ rate}{total\ uptake\ rate}\right) * 100$$

[1]

### 4.3.4 Dissolved nutrients

Samples for dissolved inorganic nutrients were taken directly from Niskin bottles, and syringe filtered (sterile, 0.2µm polycarbonate filters) into 15 ml centrifuge tubes. All samples were frozen immediately at -20˚C until analysis onshore on an Astoria Nutrient Analyzer (Barwell-clarke et al., 1996). Triplicate samples were occasionally taken to determine error coefficients.

### 4.3.5 Ambient Particulate Concentrations

Chlorophyll-*a* analysis was conducted as outlined by Parsons et al., (1984). Briefly, seawater samples (500 ml) were filtered onto a glass fiber filter (0.7 µm nominal porosity) and frozen onboard the vessel at -80˚C. Analysis for chl-*a* concentrations was done onshore through acetone extraction (90% v:v) in the dark at 4˚C for 24 h, followed by fluorometric measurements on a Turner Designs Fluorometer (Parsons, 2013).

Particulate organic carbon and nitrogen (PC/PON) samples were taken by filtering 500 – 1000 ml of seawater through a pre-combusted (6h, 450°C) glass fibre filter (GFF), and

immediately frozen. Additional samples were taken from the end of the C/$NO_3^-$ incubations, and therefore were already size fractionated as described above. The PC/PN content of these samples was corrected for 24h growth in the incubation. No significant differences were observed between ambient samples and corrected incubation samples, and therefore the incubation samples were used for size fractionated PC/PN particulate analysis. The filters were dried and analyzed using an elemental analyzer at the Stable Isotope Facility at the University of California Davis as described above.

Seawater (0.5-2.5 L) for biogenic silica (bSi) analysis was filtered onto 0.6 µm and 5µm; filters were immediately frozen (-20˚C) onboard the vessel before transportation to shore. On-shore, filters were dried for 48h at 60˚C and kept dry until analysis. Biogenic silica analysis was then performed as outlined in Brzezinski and Nelson (1995); briefly, a serial NaOH digestion procedure was performed (~1h) to digest biogenic silica, and subsequently [$Si(OH)_4$] from each digestion was then measured with a Beckman DU 530 UV/Vis spectrophotometer.

### 4.3.6 Size-fractionated TEP Production Rates

Size-fractionated rates of transparent exopolymer particle (TEP) production were experimentally measured at three distinct stations (P4, P12, P26) during the May 2021 Line P cruise. Seawater (4 L) was collected for each size fraction; <5µm size fraction bottles were first pre-filtered through a 5µm polycarbonate filter to remove any materials larger than 5µm. Total TEP production rates were measured as described in *Chapter 3.3.4 Transparent Exopolymer Production Rates*. Each bottle corresponding to (i) total rates or (ii) <5µm rates were incubated for 4 days in the same fashion as the ρC and $\rho NO_3^-$ nutrient uptake experiments, with discrete samples for TEP, PC, chl-*a*, and nutrients taken each day.

TEP concentrations were determined using the updated method for TEP quantification (Bittar et al., 2018), based on the original TEP quantification method (Passow & Alldredge, 1995a). Seawater subsamples (250 ml) were filtered through 0.4 µm polycarbonate filters under low filtration pressure (<150 mm Hg). Before removing the filters from the filtration unit, they were stained with 0.5 ml of Alcian blue (AB) dye (0.02%, pH 2.5) for <5 s, rinsed with deionized water to remove any excess dye, and frozen at -20 ˚C until laboratory analysis (within 1 month). Blank samples (clean/new filters stained with AB dye and measured as described above) were taken throughout the experiment. Onshore, filters were then placed in 6 ml of extraction solution (80% $H_2SO_4$) for 2.5 hours and the solutions were analyzed on a Beckman DU530 spectrophotometer at 787 nm. Values were expressed as µg Gum Xanthan equivalents (XG eq.) $L^{-1}$.

### 4.3.7 Physical and environmental variables

Physical and environmental parameters, including temperature, salinity, dissolved oxygen (DO), and mixed layer depth (MLD) were obtained from the CTD. Average 24h PAR (µm photon $m^{-2}$ $s^{-1}$) data was collected via continuous logging on a LI-COR LI-190 Quantum Sensor, positioned close to the on-deck flow-through incubator and away from shading. MLD values were calculated in accordance with de Boyer Montegut et al., (2004) (de Boyer Montégut et al., 2004), using density data obtained from the CTD.

### 4.3.8 Statistical analyses

Two-factor analysis of variance (ANOVA) and Tukey HSD tests were performed to identify any significant differences in both total and small cell rates (C, $NO_3^-$, $Si(OH)_4$), as well

as small cell contributions, across subregions, seasons, and years. Multiple linear regressions (MLR) were also used to determine if small cell contributions to nutrient uptake rates varied significantly with distance from shore (DFS) in addition to the spatial ANOVA (as spatial autocorrelation may occur due to grouping of stations close together in space). Multiple linear regression analyses were also performed to estimate the effects of DFS and season on *f-ratios* for each size fraction. A localized regression, or local polynomial regression ('loess') was also used to fit a moving average and to compute 95% confidence intervals for the fraction (%) of small cell contributions to ρC, $\rho NO_3^-$, and ρSi uptake rates as a function of DFS. All statistical tests were carried out using the statistical programming language R (v1.3.1093) using the *dplyr*, *aov*, and *tidyverse* packages.

## 4.4 Results

### 4.4.1 Size fractionated nutrient uptake rates and *f*-ratios

Over the entire spatiotemporal range of the study, total ρC, $\rho NO_3^-$, and ρSi ranged from <0.01-73.2 µmol C $L^{-1}d^{-1}$, <0.01-4.8 µmol N $L^{-1}d^{-1}$, and <0.01-12.6 µmol Si $L^{-1}d^{-1}$, respectively (Figure 4.2). Two-way ANOVA results indicate that coastal regions were characterized by significantly higher total C, $NO_3^-$, and Si uptake rates compared to all other regions ($p < 0.05$; Figure 4.2). There was no significant seasonal variation observed for any of the measurements (data not shown), which may be a product of the relatively small amount of winter data points. Uptake rates of C, $NO_3^-$, and Si also decreased significantly with DFS as determined through MLR analyses ($p<0.05$).

Small cell uptake rates followed a similar trend to total uptake rates, but with less overall variability. Uptake rates of C, $NO_3^-$, and Si for <5µm size fractions ranged from <0.01-24.7 µmol

C $L^{-1}d^{-1}$, <0.01-2.3 µmol N $L^{-1}d^{-1}$, and <0.01-0.53 µmol Si $L^{-1}d^{-1}$, respectively (Figure 4.2). Uptake rates of C and $NO_3^-$ displayed significant spatial variation in the smaller size fraction, with coastal regions having significantly higher values than transition and HNLC regions; slight yearly variation was also observed in small cell C uptake (Table 4.2). Uptake rates of Si did not vary significantly in space for the small cell fraction; however, the large cell fraction displayed significant higher values in coastal regions (Figure 4.2; Table 4.2).

**Table 4.2:** Results from a two-factor Analysis of Variance (ANOVA) on statistical variation in size fractionated carbon (ρC), nitrate ($\rho NO_3^-$), and silicic acid (ρSi) uptake rates in the ESNP throughout a multi-seasonal sampling program from 2019 – 2022. The three-factor ANOVA covers all seasons, region, and years in this study. Columns indicate whether significant variation was observed across seasons, regions, or years (with n.s. indicating a lack of significance).

| Uptake Rate (all season and regions) | Fraction | Season | Region | Year |
|---|---|---|---|---|
| ρC | Large (>5µm) | n.s | $p < 0.01$ | $p < 0.01$ |
| | Small (<5µm) | n.s | $p < 0.01$ | $p < 0.05$ |
| | % Small cell contribution | $p < 0.05$ | $p < 0.01$ | n.s |
| $\rho NO_3^-$ | Large (>5µm) | n.s | $p < 0.01$ | n.s |
| | Small (<5µm) | n.s | $p < 0.05$ | $p < 0.05$ |
| | % Small cell contribution | n.s | $p < 0.01$ | n.s |
| ρSi | Large (>5µm) | n.s | p < 0.01 | n.s |
| | Small (<5µm) | n.s | n.s | n.s |
| | % Small cell contribution | $p < 0.01$ | $p = 0.05$ | $p < 0.01$ |

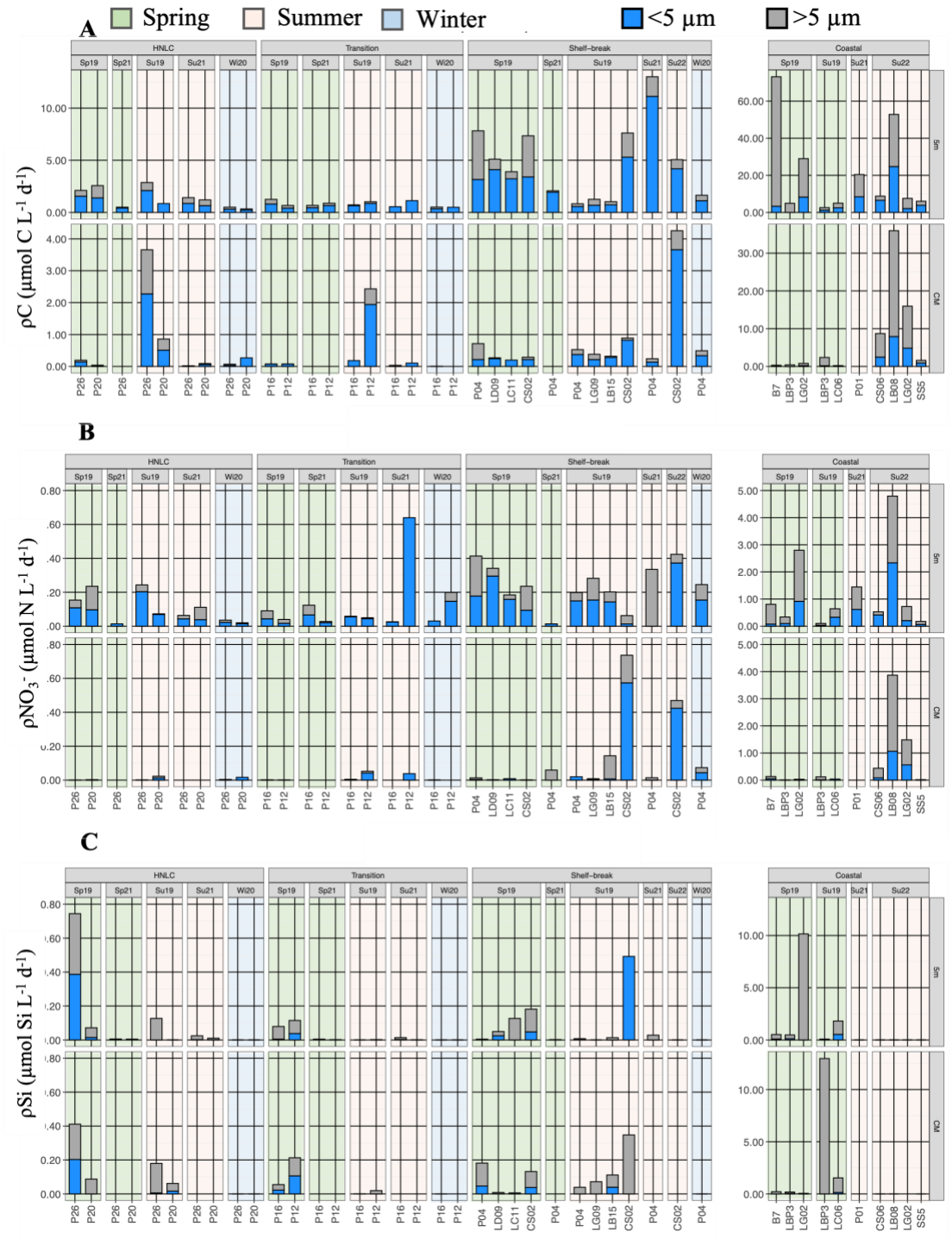


**Figure 4.2**: Size fractionated (>5µm and <5µm) nutrient uptake rates of (A) carbon (ρC), (B) nitrate ($\rho NO_3^-$), and (C) silicic acid (ρSi) in the Eastern Subarctic North Pacific for winter (Wi), spring (Sp) and summer (Su) for 2019 - 2022. Data is displayed for each subregion (HNLC, transition, shelf-break and coastal) at both 5m depth and the chlorophyll max (CM). Note the different y-axis scales for each panel.

There were no significant differences in *f*-ratios between size fractions, although there was notable spatial and temporal variation among the two size classes (Figure 4.3). For the smaller size fraction, no significant spatial variation between subregions was observed in *f*-ratios when analyzed via a two-way ANOVA; however, multiple linear regression analyses revealed a significant decline in *f*-ratios with distance from shore if season is also accounted for as a model parameter ($p < 0.05$) (Figure 4.3). Small cell f-ratios were significantly higher during winter months compared to spring and summer ($p < 0.01$). In contrast, no significant spatial or seasonal variation in large cell *f*-ratios was observed (either through ANOVA or linear regression techniques).

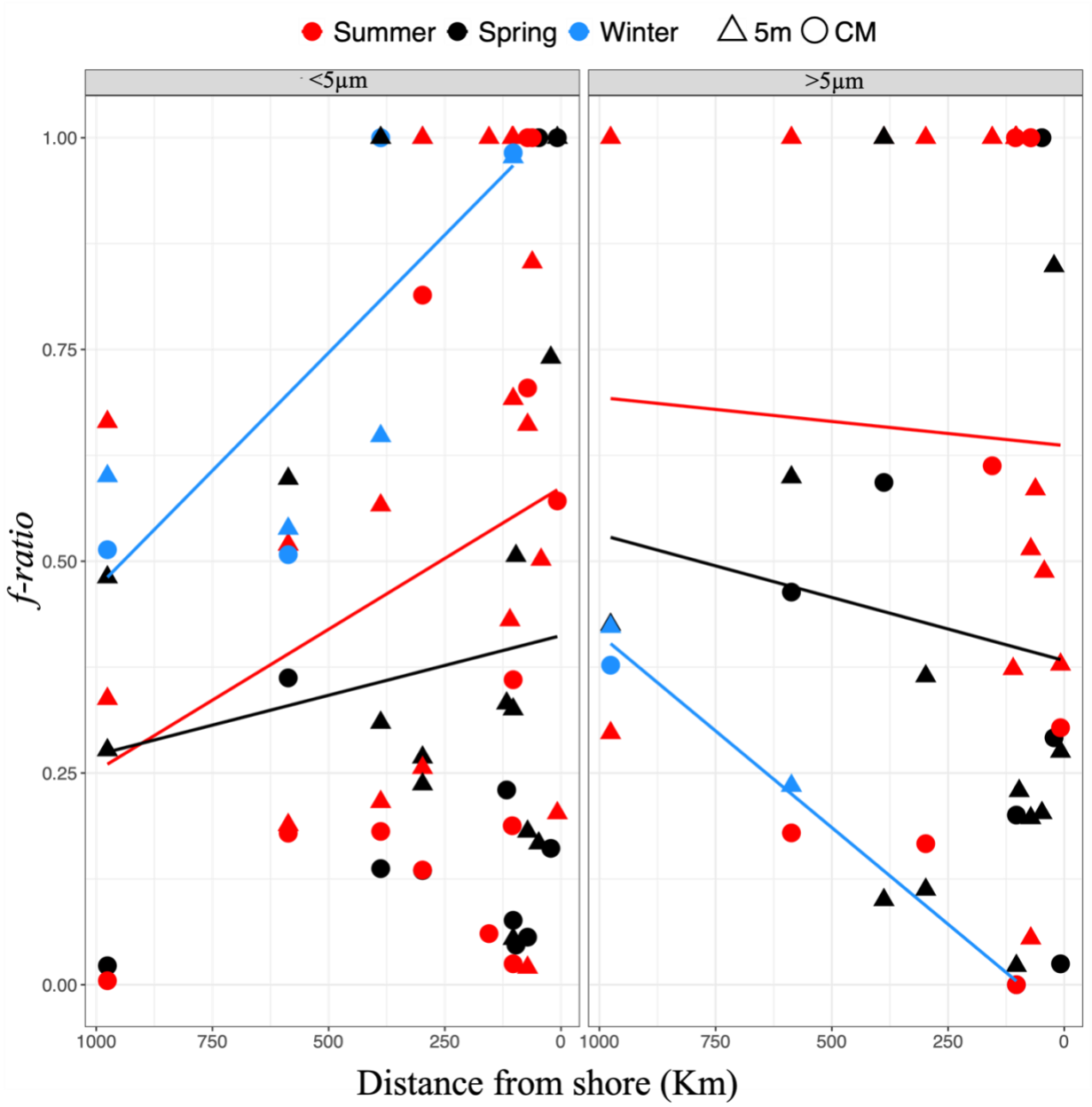


**Figure 4.3:** Size-fractionated (<5µm and >5µm) f-ratios plotted as a function of distance from shore in the Eastern Subarctic North Pacific, for spring, summer, and winter seasons from 2019-2022. Data points are colour coded according to sampling season. Filled circles indicate samples taken at 5m, while empty circles indicate samples taken at the chlorophyll max (CM). The solid lines represent a linear regression line for each size fraction and season. Significant linear relationships were only observed for the <5µm fraction for the winter and summer seasons.

### 4.4.2 Small-cell contributions to whole-assemblage nutrient uptake rates

The contribution of small cells to total ρC varied across regions and seasons. Two-way ANOVA results identified significant spatial differences in small-cell contributions to total ρC, with transition and HNLC regions characterized by higher contributions compared to coastal regions across all seasons ($p < 0.001$; Figure 4.4; Table 4.2). Similarly, small cell contributions to ρC and $\rho NO_3^-$ increased significantly with DFS as determined by MLR analyses ($p < 0.05$). Small cell contributions to ρC were also well conserved in perennially low chl-*a* regions (transition and HNLC regions), with an average and standard deviation of 78.5 $\pm$ 16.8% (Table 4.3). Significant seasonal variation existed in small cell contributions to total C uptake across the ESNP, with summer and winter months being 11.8 and 18.4% (data not shown) higher on average than spring months ($p < 0.05$; Table 4.3).

The fraction of small cell contributions to total $\rho NO_3^-$ were followed similar patterns to ρC within the HNLC and transition regions (Figure 4.4). Small cell contributions to total $\rho NO_3^-$ averaged 76.9 $\pm$ 22.5% throughout low chl-*a* regions of the ESNP (transition and HNLC) (Figure 4.4). In contrast, small cell contributions to $\rho NO_3^-$ in coastal regions averaged 42 $\pm$ 26% (Figure 4.4). Small cells contributed significantly more to $\rho NO_3^-$ in transition regions compared to coastal regions ($p < 0.001$; Figure 4.4). Small cell contributions to $\rho NO_3^-$ did not show any significant seasonal differences (Table 4.2).

Small cell contributions to total ρSi were significantly lower than their contributions to ρC and $\rho NO_3^-$ ($p < 0.01$, Figure 4.4). Small cells contributed approximately 20 $\pm$ 21% and 10 $\pm$ 13% in oceanic (transition + HNLC) and coastal regions, respectively. Small cells contributed significantly more to ρSi in transition and HNLC regions compared to coastal zones ($p < 0.05$)

(Figure 4.2). Summer seasons were also characterized by significantly higher small-cell contributions to total ρSi ($p < 0.05$; data not shown).

To assess temporal variation in small cell and large cell nutrient uptake in perennially low chl-*a* regions of the ESNP (Transition + HNLC regions) alone, a two-factor ANOVA was performed using season and year as factors (Table 4.3). The results from these ANOVA's indicate that neither small or large fraction nutrient uptake rates varied significantly across seasons or years within transition and HNLC regions, apart from large cell ρSi. Table 4.3 also highlights small cell contributions to nutrient uptake rates by providing averages and standard deviations for each rate measurement. These results demonstrate the consistent contributions of small celled phytoplankton to nutrient uptake rates in the oceanic regions of the ESNP, as demonstrated by the lack of significant variation across years or seasons.

**Table 4.3:** Size-fractionated nutrient uptake rates and small cell contributions to nutrient uptake in HNLC and transition regions only. A two-factor Analysis of Variance (ANOVA) was performed to determine statistical variation in size fractionated carbon (ρC), nitrate ($\rho NO_3^-$), and silicic acid (ρSi) uptake rates in perennially low chlorophyll-a regions (transition and HNLC subregions) of the ESNP, throughout a multi-seasonal sampling program from 2019 – 2022. Season and year columns indicate whether significant variation was observed, with n.s representing no statistical variation and bold font indicating statistical variation. The values column provides the mean ± standard deviation in either the uptake rate (μmol $L^{-1}$ $d^{-1}$) or the % contribution of small cells.

| Uptake rate (all seasons for transition/HNLC regions) | Fraction | Season | Year | Values |
|---|---|---|---|---|
| ρC | Large (>5μm) | n.s | n.s | 0.30 ± 0.36 |
| | Small (<5μm) | n.s | n.s | 0.60 ± 0.61 |
| | % Small fraction contribution | n.s | n.s | 78.5 ± 16.8 |
| $\rho NO_3^-$ | Large (>5μm) | n.s | n.s | 0.03 ± 0.03 |
| | Small (<5μm) | n.s | n.s | 0.06 ± 0.12 |
| | % Small fraction contribution | n.s | n.s | 76.9 ± 22.5 |
| ρSi | Large (>5μm) | n.s | **$p < 0.05$** | **0.06 ± 0.09** |
| | Small (<5μm) | n.s | n.s | 0.03 ± 0.09 |

| | | | |
|---|---|---|---|
| % Small fraction contribution | $p < 0.01$ | $p < 0.05$ | 30.2 ± 26.4 |

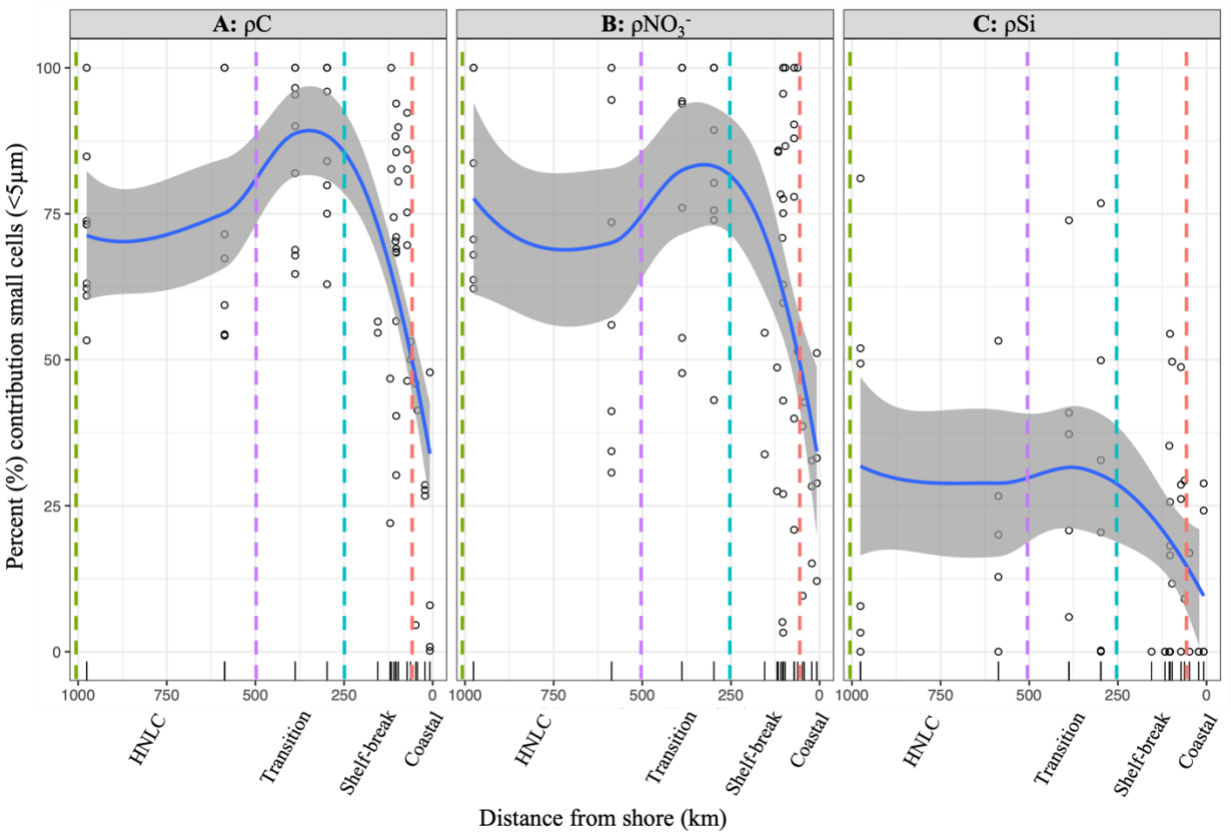


**Figure 4.4:** Small cell (<5µm) contributions (%) to (**A**) carbon (ρC), (**B**) nitrate ($\rho NO_3^-$), and (**C**) silicic acid (ρSi) uptake as a function of distance from shore in the Eastern Subarctic North Pacific, for spring, summer, and winter seasons. A smoothed localized regression line is plotted for each rate; the gray shaded area represents the 95% confidence interval of the mean. The subregions of the Eastern Subarctic North Pacific are shown by the dashed; each border is colour coded as in Figure 4.1 (coastal, red; shelf-break, turquoise; transition, purple; HNLC, green). The ticks on the x-axis indicate the location of sampling stations as a function of distance from shore.

### 4.4.3 Spatiotemporal trends in particulate ratios in small and large size fractions

Figure 4.5 illustrates the uptake (ρC, $\rho NO_3^-$, ρSi) and particulate (C, N, bSi) ratios of the two size fractions across subregions of the ESNP. Small and large size-fractionated ρC: $\rho NO_3^-$ were overall similar, with median values of 13.6 and 13.7 respectively, and did not vary significantly between size classes, seasons, or subregions (Figure 4.5A). Particulate C:N ratios

followed a similar pattern, with median values between small and large fractions of 5.81 and 5.23, respectively and did not vary significantly across size fractions, seasons, or subregions (Figure 4.5B).

Uptake and particulate ratios between C and Si were more variable across size fractions. Median ρSi: ρC were lower in smaller (ρSi: ρC = 0.002) than larger (ρSi: ρC = 0.15) size fractions and decreased with distance from shore, although no statistical significance was detected between size fractions (Figure 4.5C). A similar trend was observed in median particulate bSi:C ratios, with the smaller size class characterized by significantly lower bSi:C ratios ($p < 0.01$) than larger size fractions (0.04 and 0.23, respectively), with no significant spatial variation (Figure 4.5D).

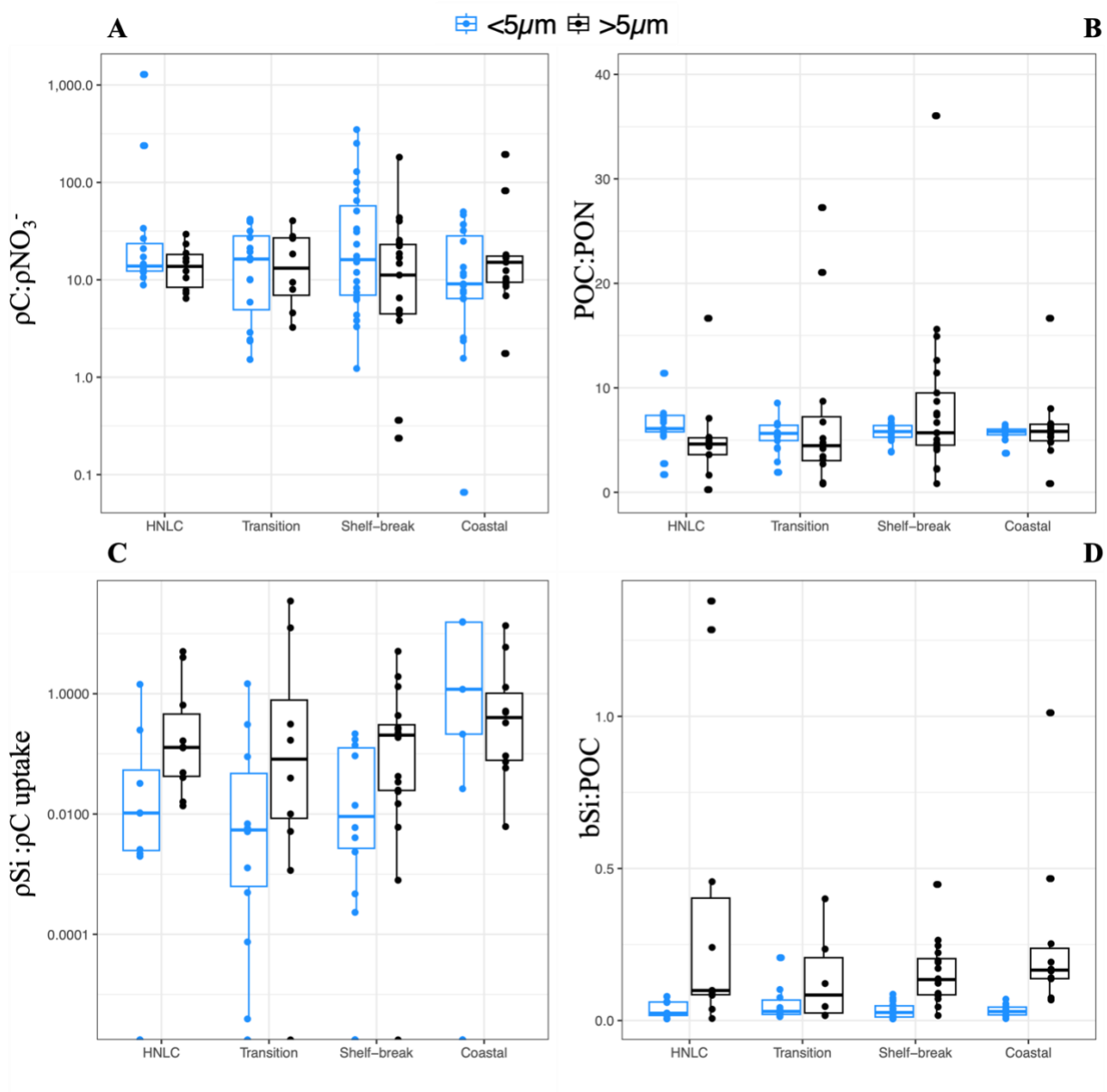


**Figure 4.5:** Size-fractionated uptake rate ratios of (**A**) carbon (ρC) to nitrate ($\rho NO_3^-$), particulate elemental ratios for (**B**) organic C to nitrogen (POC: PN), size fractionated uptake rate ratios of (**C**) silicic acid (ρSi) to carbon (ρSi: ρC), and (**D**) particulate organic C to biogenic silica (POC: bSi) in the Eastern Subarctic North Pacific (ESNP). Size fractions <5μm (blue) and >5μm (black) are shown. Data is grouped categorically by region in the ESNP. Note the logarithmic scaling of y axes for panels **A** and **C**.

### 4.4.4 Comparing rates of transparent exopolymer particle (TEP) production, C uptake, and new production in small and large phytoplankton

Size-fractionated TEP-C production rates were measured in conjunction with ρC uptake and NP during a single cruise along Line P in May 2021 (Figure 4.6); with the units of all measurements in μg C $L^{-1}$ $d^{-1}$. The amount of TEP-C produced at stations P4, P12, and P26 was primarily attributed to < 5 μm size fraction, with rates ranging from 1.01 – 7.7 μg C $L^{-1}$ $d^{-1}$. At stations P4 and P12, ρC of both size fractions exceeded TEP-C production and NP rates. However, at station P26, TEP-C production rates in smaller size fractions were comparable in magnitude to ρC. Small cell TEP-C production rates at stations P4 and P26 exceeded NP rate estimates and was of a similar magnitude at station P16 (Figure 4.6). TEP-C production rates ranged from 12.5-90.4% of ρC and 53.1-548% of NP in the smaller fraction, and 5.2-43% of ρC and 30.0-40.4% NP in the larger fraction (as indicated by their respective bars in Figure 4.6).

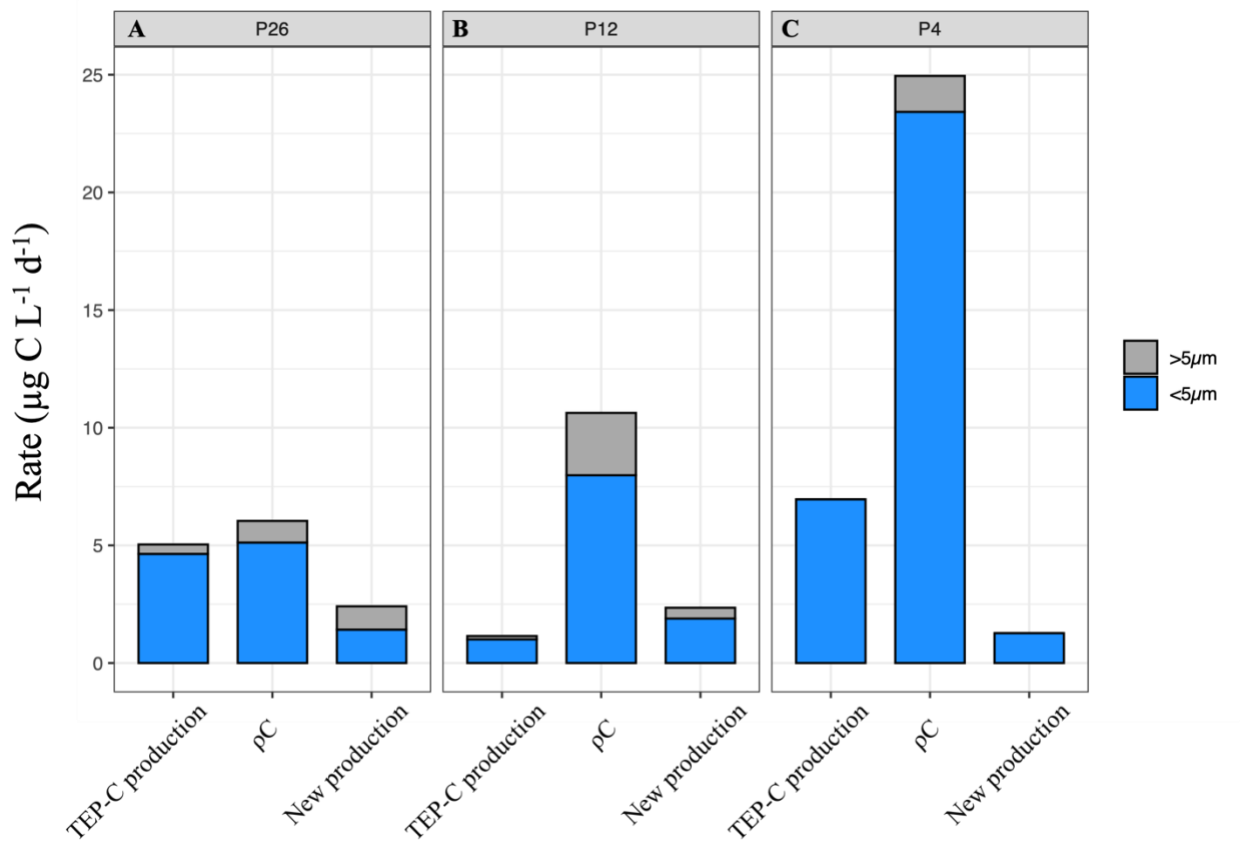


**Figure 4.6:** Size-fractionated uptake and production rates of C in terms of TEP-C production, total C uptake (ρC), and New-production C (µg C $L^{-1}$ $d^{-1}$) along Line P in the Eastern Subarctic North Pacific in May 2021. TEP-C production rate estimates were derived from a 4-day incubation, while ρC and new production rates were estimated from daily uptake rate incubations. Incubations were performed at stations P26 (**A**), P12 (**B**), and P4 (**C**) along the Line P transect. No TEP-C or new production was measured for the >5µm size fraction at P4.

### 4.4 5 Environmental influences on total and small cell contributions to biogeochemical rates

Total ρC, $\rho NO_3^-$, and ρSi were not significantly correlated with temperature, PAR, $[NO_3^-]$ or $[Si(OH)_4]$ over the entire study period and range. Total ρC was negatively correlated with both salinity and distance from shore (DFS), while positively correlated with DO concentrations. Total $\rho NO_3^-$ was not significantly correlated with any physical and environmental variables.

Total NP were negatively correlated with both DFS and MLD, while total ρSi were negatively correlated with DO concentrations (Table 4.4).

The environmental influences on small cell rates were distinct from total uptake rates. Small cell ρC was negatively correlated with MLD and DFS, while small cell ρSi were negatively correlated with salinity and positively correlated with $[Si(OH)_4]$ concentrations. There was no significant relationship between any environmental variable and small cell $\rho NO_3^-$ (Table 4.4).

Percent small cell contributions to total ρC were significantly correlated with several environmental variables, including a positive relationship with MLD and DFS, and a negative relationship with PAR, $[NO_3^-]$, and $[Si(OH)_4]$. Similarly, small cell contributions to total $\rho NO_3^-$ were positively correlated with both MLD and DFS. Percent small cell contributions to total pSi were positively and negatively correlated with MLD and temperature, respectively (Table 4.4).

There was little evidence for significant environmental effects on *f*-ratios in the small or large size fractions; this included salinity, irradiance, MLD, DFS, total ρC, $[Si(OH)_4]$, and $[PO_3^-]$ as environmental variables. However, temperature and $\rho NO_3^-$ were significantly positively correlated with large and small fraction *f*-ratios, respectively ($p < 0.05$, data not shown).

**Table 4.4:** Linear regression statistics for total and small cell uptake rates, as well as small cell contributions to nutrient uptake rates (dependent variables) for a series of independent environmental variables (temperature, salinity, photosynthetically active radiation (PAR), mixed layer depth (MLD), distance from shore (km), nitrate concentrations ($[NO_3^-]$), silicic acid concentration ($[Si(OH)_4]$), and dissolved oxygen (DO)). Explained variance ($R^2$), significance (p), and coefficients are shown. Significant correlations are indicated in bold.

| Ind. Var. | Dep. Var. | $R^2$ | *p* | Coefficient | Dep. Var. | $R^2$ | *p* | Coefficient | Dep. Var. | $R^2$ | *p* | Coefficient |
|---|---|---|---|---|---|---|---|---|---|---|---|---|
| Temperature | Total ρC | 0.00 | 0.64 | | Small cell ρC | 0.03 | 0.15 | | % Small cell C contribution to ρC | 0.02 | 0.30 | |
| Salinity | | **0.130** | **0.00** | **-183.6** | | 0.04 | 0.10 | | | 0.02 | 0.24 | |
| PAR | | 0.001 | 0.77 | | | 0.00 | 0.61 | | | **0.16** | **<0.01** | **-0.06** |
| MLD | | 0.05 | 0.08 | | | **0.09** | **0.02** | **-0.29** | | **0.09** | **0.01** | **0.29** |
| DFS | | **0.06** | **0.04** | **-0.10** | | **0.10** | **0.01** | **-0.02** | | **0.09** | **0.01** | **0.02** |
| $[NO_3^-]$ | | 0.014 | 0.34 | | | 0.01 | 0.28 | | | **0.07** | **0.03** | **-1.18** |
| $[Si(OH)_4]$ | | 0.00 | 0.83 | | | 0.00 | 0.48 | | | **0.06** | **0.05** | **-0.61** |
| DO | | **0.07** | **0.03** | **47.2** | | 0.00 | 0.59 | | | 0.03 | 0.18 | |

| Ind. Var. | Dep. Var. | $R^2$ | *p* | Coefficient | Dep. Var. | $R^2$ | *p* | Coefficient | Dep. Var. | $R^2$ | *p* | Coefficient |
|---|---|---|---|---|---|---|---|---|---|---|---|---|
| Temperature | Total $\rho NO_3^-$ | 0.00 | 0.87 | | Small cell $\rho NO_3^-$ | 0.03 | 0.62 | | % Small cell $NO_3^-$ contribution to ρN | 0.00 | 0.52 | |
| Salinity | | 0.02 | 0.27 | | | 0.04 | 0.35 | | | 0.02 | 0.28 | |
| PAR | | 0.00 | 0.62 | | | 0.00 | 0.99 | | | 0.06 | 0.06 | |
| MLD | | 0.03 | 0.14 | | | 0.09 | 0.18 | | | **0.07** | **0.03** | **0.28** |
| DFS | | 0.02 | 0.24 | | | 0.10 | 0.29 | | | **0.07** | **0.03** | **0.02** |
| $[NO_3^-]$ | | 0.00 | 0.58 | | | 0.01 | 0.50 | | | 0.00 | 0.88 | |
| $[Si(OH)_4]$ | | 0.00 | 0.73 | | | 0.00 | 0.89 | | | 0.00 | 0.91 | |
| DO | | 0.00 | 0.55 | | | 0.00 | 0.68 | | | 0.00 | 0.59 | |

| Ind. Var. | Dep. Var. | $R^2$ | *p* | Coefficient | Dep. Var. | $R^2$ | *p* | Coefficient | Dep. Var. | $R^2$ | *p* | Coefficient |
|---|---|---|---|---|---|---|---|---|---|---|---|---|
| Temperature | Total ρSi | 0.00 | 0.68 | | Small cell ρSi | 0.00 | 0.75 | | % Small cell Si contribution to ρSi | **0.14** | **0.006** | **-3.15** |
| Salinity | | 0.00 | 0.73 | | | **0.19** | **<0.01** | **-0.20** | | 0.00 | 0.84 | |
| PAR | | 0.02 | 0.36 | | | 0.01 | 0.47 | | | 0.03 | 0.67 | |
| MLD | | 0.07 | 0.06 | | | 0.03 | 0.19 | | | **0.28** | **0.00** | **1.00** |
| DFS | | 0.04 | 0.16 | | | 0.00 | 0.91 | | | 0.01 | 0.45 | |
| $[NO_3^-]$ | | 0.05 | 0.12 | | | 0.08 | 0.03 | | | 0.00 | 0.72 | |
| $[Si(OH)_4]$ | | 0.05 | 0.13 | | | **0.24** | **<0.01** | **0.006** | | 0.00 | 0.95 | |
| DO | | **0.10** | **0.03** | **-0.87** | | 0.01 | 0.39 | | | 0.08 | 0.04 | |

## 4.5 Discussion

This study is one of a small number to quantify small cell contributions to nutrient rates across large gradients in space and time; in particular, it is also the first of its kind to quantify the contributions of small cells to Si cycling across large spatiotemporal gradients. The results of this study highlight the importance of smaller cells to C, $NO_3^-$, and Si uptake in the ESNP,

particularly in low-productivity regions. I demonstrate the lack of significant seasonal or annual variation in small cell C and $NO_3^-$ uptake, and further quantify their contributions in low-productivity regions of the ESNP. These results also demonstrate that small cell contributions to nutrient uptake rates were generally not correlated with changes in environmental conditions (besides some evidence for higher percent contributions during low nutrient concentrations, deeper mixed layers). I observed significant TEP-C production by the small size fraction relative to new production, which highlights the importance of small phytoplankton in the production of TEP.

### 4.5.1 Spatiotemporal trends in size fractionated C and $NO_3^-$ uptake in the ESNP

Most of the variation in ρC and $\rho NO_3^-$ by both large and small size fractions was observed spatially in the ESNP. As expected, coastal regions were characterized by significantly higher rates in both size fractions than in the low productivity transition and HNLC regions. This result is almost certainly due to the increasing degree of iron limitation with distance from shore along Line P (La Roche et al., 1996), as is supported by the evident decline in uptake rates in transition and HNLC regions in Figure 4.2. Additionally, large episodic inputs of macronutrients closer to shore would favour the proliferation of large celled phytoplankton blooms. Phytoplankton ρC in HNLC, transition, and shelf-break regions were 96%, 98%, and 89% lower than in coastal regions for the large size fraction, and 83%, 87%, and 51% lower than in coastal regions for the small size fraction, on average. Unexpectedly, no significant seasonal variation was observed despite winter seasons in the ESNP typically characterised by lower overall productivity, which is likely due to the lower sample size of winter data set. I hypothesize that this result would be significant if greater sampling and winter coverage was obtained.

The relative dominance of smaller size fractions (i.e., their % contribution) to ρC and $\rho NO_3^-$ was also primarily a function of spatial variation and not temporal variation. Figure 4.4 highlights the dramatic change in % small cell contribution to nutrient uptake rates from productive coastal regions to the low productivity open ocean regions of the ESNP. Further offshore from the shelf-break, the relative contributions of small cells were consistent and increased from 33% and 37% in coastal regions to 78% and 76% in transition/HNLC regions for ρC and $\rho NO_3^-$, respectively. These results, together with evidence of no significant seasonal or annual variation in HNLC/transition regions (Table 4.3), suggests consistent, year-round contributions from small cells to primary production and $\rho NO_3^-$ in oceanic regions of the ESNP. Therefore, it is likely that the contributions of both ρC and $\rho NO_3^-$ by small cells can be estimated to be ~0.6 $\pm$ 0.6 µmol C $L^{-1}$ $d^{-1}$ and 0.06 $\pm$ 0.12 µmol N $L^{-1}$ $d^{-1}$, respectively, for HNLC and transition regions in the ESNP.

A small number of studies examined the spatial variability of small cell contributions to total ρC, and found that small cell contributions ranged from 24-53% to 20-63%, from coastal to oceanic regions, respectively (Harrison & Wood, 1988; Lee et al., 2012). An excellent comparison to my study exists in recent work performed at OSP, where Meyer et al., (2022) showed that small cells contributed ~89% to total ρC at OSP, closely matching the results of my own study in the same HNLC region (Figure 4.4) (Meyer et al., 2022). My results are also supported by Boyd and Harrison (1999), who observed that <5µm cells dominated primary production along Line P past P12, in which there was also little interannual variability observed (Boyd & Harrison, 1999). The contributions to $\rho NO_3^-$ by smaller cells (defined as <5µm or <2µm) have also been quantified on several instances in the literature, including coastal-oceanic estimates of 5-43% in the NW Atlantic (Harrison & Wood, 1988), 31-89% in the Arctic (Bhavya

et al., 2018), and 10-27% in the Benguela upwelling system (Probyn, 1985). In the ESNP, Peña and Varela (2007), Varela (2013), and Meyer et al., (2022) found that smaller cells contributed ~50, 83, and 73% of total $NO_3^-$ uptake, respectively. These results emphasize the dominance and consistent contributions of the smaller fraction of phytoplankton to biogeochemical cycling in low-productivity regions of the ESNP.

Throughout the spatiotemporal range of this study, I did not observe any significant evidence of short-term variation in environmental conditions (which included temperature, salinity, PAR, nutrient concentrations, or dissolved oxygen concentrations) significantly affecting the magnitudes of small cell ρC or $\rho NO_3^-$ (Table 4.4). Small cell ρC was significantly negatively correlated with both DFS and MLD; however, these results are likely due to the overall low productivity observed in oceanic regions (i.e., further from shore, with deeper MLD) induced by Fe limitation. In contrast, the relative contributions of the smaller size fraction (i.e., percent small cell contributions) to whole-assemblage nutrient uptake were correlated with several environmental variables, especially for ρC (Table 4.4). The fraction of total ρC attributed to small cells was significantly negatively correlated with nutrient concentrations ($[NO_3^-]$, $[Si(OH)_4]$) and 24h-avg PAR. The negative association with nutrient concentrations could be attributed to the competitive advantage of smaller cells in lower nutrient regimes. However, I did not observe any significant correlation of large cell ρC with nutrient concentrations, which may be attributed to the fact that larger cells are simply less dominant in low nutrient conditions, skewing the ratio towards the smaller size fraction.

Considering two distinct lines of evidence, I can draw conclusions as to how changes in the size structure of phytoplankton assemblages may impact biogeochemical cycling in the future. Firstly, ρC and $\rho NO_3^-$ in offshore ESNP regions are dominated by smaller cells, with

~75% of whole-assemblage ρC and $\rho NO_3^-$ attributed to cells <5µm in size. Secondly, over short timescales, no direct evidence of perturbations in temperature, nutrients, salinity, or PAR affected the magnitude of small cell ρC or $\rho NO_3^-$. I can then hypothesize that a changing oceanic environment, including shoaling of the mixed layer and increases in temperature, will likely not drastically affect the total magnitude of ρC or $\rho NO_3^-$ in low-productivity regions of the ESNP.

### 4.5.2 Variation in *f*-ratios between large and small phytoplankton fractions

I observed no significant variation in *f*-ratios in either small or large size fractions across the range of this study, with a high degree of variability within each size fraction. Overall, I observed an average ($\pm$ standard deviation) *f*-ratio of 0.48 $\pm$ 0.34; slightly higher f-ratios were observed for the larger cells than smaller cells (0.51 and 0.46, respectively). This is similar to the results found by Peña and Varela (2007) along Line P, who recorded an average *f*-ratio of 0.32 $\pm$ 0.15. My recorded *f*-ratios are notably higher and more variable, which is due to the larger coverage of coastal stations in this study. However, it is also likely that the *f*-ratios recorded in this study are overestimated due to the exclusion of urea and ammonia uptake rates (Peña & Varela, 2007b; Varela & Harrison, 1999).

There is some evidence of spatiotemporal trends in *f*-ratios for small phytoplankton. For example, while the *f*-ratios of the larger fraction did not vary significantly in space or time, small cells were characterized by having significantly lower *f*-ratios with increasing distance from shore (if accounting for season as a linear model parameter) and during spring/summer months compared to winter (Figure 4.3). Peña and Varela (2007) similarly found that small cells (<5µm) contributed less to new production during the summer compared to winter along Line P,

suggesting that they may be utilizing more regenerated forms of N during these periods (Peña & Varela, 2007b).

### 4.5.3 Spatiotemporal trends in size fractionated Si uptake in the ESNP

This study is among the first of its kind to measure small cell Si uptake rates over large spatiotemporal gradients. Other studies, including by Brzezinski et al., (2022), Wei et al., (2021), and Krause et al., (2017) have also measured small cell ρSi (<5µm, <2µm, and <2µm small cell definitions, respectively) in oligotrophic and HNLC regions. These studies found that 19%, 43%, and 55% of total ρSi was attributed to the smaller fraction (Brzezinski et al., 2022; Krause et al., 2017; Wei et al., 2021), respectively. In comparison, my study shows that phytoplankton <5 µm in size were responsible for ~27.8%, 32.6%, 18.5%, and 10.8% of total ρSi in HNLC, transition, shelf-break, and coastal regions of the ESNP, respectively. These results, in conjunction with similar studies, suggest that small phytoplankton are important contributors to global ρSi given the ubiquity of oligotrophic and HNLC regions across the world's oceans.

While this study (and the studies discussed above) are among the first to address the contributions of small phytoplankton to Si uptake, there have been several works showing notable bSi biomass in small size fractions, including pico– and nanoplanktonic cells (Baines et al., 2012; Krause et al., 2017; Ohnemus et al., 2016; Tang et al., 2014). A possible explanation for these observations is proposed by Krause et al., (2017), who demonstrated that the majority of the observed bSi in smaller size fractions could be attributed to detrital bSi; this suggests that Si accumulation in smaller fractions is a result of the breakdown of larger detrital bSi derived from diatoms (Krause et al., 2017). However, a recent study by Wei at al., (2021), (and supported by evidence from this study) refutes this theory, as they demonstrate Si uptake directly

by smaller phytoplankton and thus reveal the importance of small cells to Si uptake. In my study, only in cases of relatively low total ρSi (<1 µmol Si $L^{-1}$ $d^{-1}$) did smaller cells represent a large fraction of total Si uptake (Figure 4.2). Total ρSi in coastal regions was orders of magnitude larger than oceanic regions and was dominated by the larger size fraction (Figure 4.2). Therefore, while my results identify consistent contributions of small cells to ρSi, they also emphasize the importance of the large size classes (which overwhelmingly contributed to the majority (~77%) of ρSi at across all regions).

### 4.5.4 Size-fractionated uptake and particulate ratios

There was little observed variation in ρC: $\rho NO_3^-$ or particulate PC:PN ratios between smaller and larger size fractions, despite large variability within each group. There was also no significant spatial or temporal variation observed, as demonstrated in Figure 4.5. In contrast, there were notable differences observed in the uptake and particulate ratios of Si:C between size fractions. While no significant differences were observed between size fractions for ρSi: ρC uptake, smaller fractions were, on average, generally characterized by lower uptake ratios (ρSi: ρC = 0.003) compared to larger fractions (ρSi: ρC = 0.15) and declined with distance from shore. These results are in close agreement with similar size fractionated ρSi: ρC ratios reported by Franck et al., (2005), with average ratios for <5µm and > 5µm of approximately <0.01 and 0.25 for the Humboldt current, and <0.01 and 0.23 for Peru current locations in the Eastern Tropical Pacific, respectively (Franck et al., 2005). This observation is likely due to the presence of larger celled diatoms in the >5µm fraction, whose requirement for Si would increase ρSi: ρC ratios when present in the larger size fraction. Higher ρSi: ρC ratios may also be the product of Fe limitation, as Fe limitation will depress ρC and $\rho NO_3^-$ to a greater extent than ρSi (Firme et al.,

2003; Franck et al., 2003; Franck et al., 2000), and much of the study region is characterized by Fe limited waters (i.e., HNLC and transition regions). However, I observed elevated ρSi: ρC ratios across all regions (with no significant differences between regions) including coastal regions not limited by Fe; this implies that Fe limitation is likely not the only explanation for elevated ρSi: ρC in measured in the larger size fraction.

Larger cells were characterized as having significantly higher particulate Si:C ratios (Si:C = 0.23) compared to the smaller fraction (Si:C = 0.04) in my study (Figure 4.5). These results are notably lower than analyses of Si:C ratios performed by Wei et al. (2021), who estimated an average Si:C for phytoplankton <2µm of 0.14 in the oligotrophic western Pacific, and by Brzezinski (1985) who determined an averaged Si:C ratio of 0.13 for 18 species of diatoms (Brzezinski, 1985). Higher particulate Si:C ratios in larger size fractions emphasize the importance of larger, heavily silicified cells (i.e., diatoms) to C export, as aggregates composed of higher Si:C ratios will generally sink more efficiently due to the increase in ballasting (Armstrong et al., 2001). Recent studies have postulated that with changing ocean conditions and a potential favouring of small sized phytoplankton, a reduction in the Si:C of phytoplankton assemblages may reduce overall C export due to a reduction in Si ballasting (Tréguer et al., 2018). My results support the above model, as I demonstrate that both Si:C uptake and particulate ratios are demonstrably lower in smaller size fractions.

### 4.5.5 Implications of this study to the understanding of carbon cycling in the surface ocean

This study is the first of its kind to simultaneously measure TEP-C production rates alongside ρC and NP in different size fractions of phytoplankton in a natural setting. My results demonstrate that smaller phytoplankton fractions were responsible for most of the TEP-C

production along Line P (Figure 4.6). Similarly, other studies have reported TEP-C production in experimental conditions by small phytoplankton and cyanobacteria, including Prochlorococcus (Iuculano et al., 2017) and Synechococcus (Callieri et al., 2019; Thornton & Chen, 2017). I further quantify the rates of TEP-C production in each size fraction relative to total ρC and export potential (as proxied by NP) to provide further insights into the role of small cells in the surface C cycle. Of note is the magnitude of TEP-C production rates relative to total ρC and NP. It is immediately obvious that daily TEP-C production can exceed NP along Line P but is of a lower magnitude to ρC in my experiments. This suggests that TEP-C is an active and dominant C source in the ESNP (and driven largely by small cells at the stations I measured). This is important because high concentrations of TEP-C relative to primary production will impact C export efficiency due to the inherent positive buoyancy of TEP (Mari et al., 2017). Specifically, TEP-C production rates in the smaller size fraction represented 12.5-90.4% of ρC and 53.1-548% of NP, while in the larger fraction TEP-C production rates were lower relative to C uptake (5.2-43%) and NP (30-40.4%); these statistics ignore P4 for the larger fraction, where no TEP-C production or NP was observed (likely due to $NO_3^-$ depletion, as I observed $NO_3^-$ below the detection limit – data not shown). This suggests that TEP-C represents a larger amount of C relative to ρC and NP in small size fractions, which would further imply that assemblages dominated by small cells may experience relatively more inefficient C export due to the increased dominance of buoyant TEP particles. However, it should be noted that there are limitations to my study which include both low experimental sample size ($n = 3$ incubations) and the fact that I could not account for TEP production vs aggregation of dissolved precursors already present in the seawater; therefore, the observed TEP production rates should be assessed in this context.

These findings have important implications for C cycling and export, due to the differences in TEP-C production between small and larger size classes of phytoplankton. While smaller cells are responsible for most of the C fixation, new production, and TEP-C production in the oceanic regions of the ESNP, traditional research suggests that smaller cells are inefficient at removing fixed C from the upper ocean compared to their larger-celled counterparts (Michaels & Silver, 1988). This paradigm has recently been challenged by works demonstrating that the contributions of a small cells to total primary production are proportional to their contributions to C export, if both direct and indirect export mechanisms are accounted for (Richardson, 2019; Richardson & Jackson, 2007). My results challenge this idea by demonstrating higher TEP-C production in smaller size fractions relative to ρC and NP, suggesting that small cell dominance in low productivity regions of the ESNP may result in more inefficient C export from surface waters.

### 4.5.6 Conclusions

The results of this study emphasize the importance of small celled phytoplankton to biogeochemical cycling in the surface ocean of the ESNP. I demonstrate that cells smaller than 5 µm dominate ~75% of ρC and $\rho NO_3^-$ year-round in oceanic regions of the ESNP, and do not appear to be correlated with short-term variations in environmental conditions. Furthermore, while I provide evidence that small cells can contribute to total ρSi (but to a lesser degree than ρC and $\rho NO_3^-$), total ρSi is primarily driven by the larger fractions of phytoplankton. The production of organic gel substances, known as TEP-C and a key mediator of C export, is also dominated by small cells along Line P. I also provide some evidence that suggests that small cell phytoplankton assemblages are characterized by relatively higher rates of TEP-C production

relative to total ρC and export potential (i.e., NP), which may indicate more inefficient C export from surface waters in regions dominated by small celled phytoplankton.

# Chapter 5: General Conclusions

## 5.1 Novelty and Significance

This thesis provides new perspectives on the understanding of the cycling of marine C and the efficiency of surface C export by examining a suite of previously understudies biological elements in addition to primary productivity and nutrient uptake. To my knowledge, this study is the largest of its kind to measure TEP concentrations across large gradients in space and time. As such, it provides a unique assessment of spatiotemporal variability in TEP concentrations across high variation in environmental conditions. It is also the first of its kind to develop statistical models (MLRs and RFRs) to quantitively predict TEP concentrations from predictor variables and to predict variability in these C gels over a multi-decadal dataset. While this idea has been proposed in a few studies, no attempts have currently been made to estimate TEP from environmental predictors. As TEP is a biogeochemically important substance and is ubiquitously distributed throughout the surface of the ocean, these models (and predictions) provide the first insights into how TEP based C (TEP-C) may be quantified on large scales. Furthermore, this study also measured TEP-C relative to estimates of C uptake (ρC) and C export potential (new production; NP), providing a new perspective on the amount of available C produced and potentially exported versus present as buoyant organic matter. While some studies have quantified TEP-C relative to ρC, no research has been published that has done so across the same spatial and temporal scale I present in this thesis. I further relate the concentration of TEP-C (and estimated TEP-C turnover rates) to ρC and NP to help increase our understanding of how surface C export efficiency may vary across the same large gradients in space and time. And finally, this thesis helps to quantify the role of small-celled phytoplankton to nutrient cycling, TEP-C production, and provides one of the first assessments of small cell contributions to Si uptake. It also investigates how environmental variation may affect small cell contributions to nutrient

uptake, which helps further our understanding of the consequences of shifting phytoplankton assemblages.

## 5.2 Main Findings and Implications

*Chapter 2: Estimating the concentration of transparent exopolymer particles in Arctic and Subarctic Oceans using in situ measurements and model predictions*

- TEP concentrations ranged from < 5 – 138 µg XG eq $L^{-1}$ across Subarctic and Arctic regions, with the lowest and highest concentrations observed in the low productivity HNLC regions of the Subarctic and in the productive Bering Strait, respectively. Spatial variation in TEP concentrations was much stronger than seasonal or annual variation.
- The major predictors of TEP concentrations, as determined from MLR and RFR analyses, were biological variables, and included chl-*a*, POC and AOU rates.
- Accurate TEP predictions are improved when secondary environmental predictors, that influence TEP concentrations relative to total biomass, are included in multivariate modelling approaches. These strong environmental TEP predictors include temperature, MLD, salinity, and nutrient concentrations.
- Statistical models, including MLR or RFR techniques, can accurately predict TEP concentrations in the upper mixed layer if biological and environmental predictors (direct and indirect) are considered. A model should include parameters that capture variation in TEP concentrations relative to chl-*a* or POC during periods when these variables may be decoupled (such as in late summer). Environmental conditions such as high temperatures, strong stratification, and nutrient limitation result in increases in TEP relative to

phytoplankton biomass. Therefore, these conditions must be accounted for in statistical models.

- When using historical datasets from Line P, TEP predictions made by MLRs and RFRs suggest that C in the form of TEP (TEP-C) can be estimated to be ~5-15 µg C $L^{-1}$ throughout the low-chl-*a* regions (i.e., transition and HNLC regions) of the oceanic Subarctic year-round. This demonstrates that a large portion (~5-15%) of the standing organic C pool in these region is composed of TEP and may be responsible for decoupling between primary production and C export.
- This thesis provides the first attempt at estimating surface TEP-C using statistical models.

*Chapter 3: Spatiotemporal trends in carbon export potential in the Eastern Subarctic North Pacific estimated from transparent exopolymer particles, carbon uptake and new production*

- Concentrations of TEP-C were highly correlated with C uptake (ρC), and to a lesser degree to $NO_3^-$ uptake (ρ$NO_3$), while they were not significantly correlated with Si uptake (ρSi) across the entire spatiotemporal range of this study. These findings agree with experimental work that suggests TEP production is primarily a product of cellular C uptake and exudation and provides the first large scale spatiotemporal demonstration of a link between TEP-C and ρC.
- In the oceanic regions of the ESNP (i.e., HNLC and transition regions), TEP-C represented a significantly larger fraction relative to total ρC and new production when compared to productive coastal stations. In highly productive samples, TEP-C concentrations were low relative total primary production. This finding provides

additional support for i) the hypotheses proposed by Mari et al., (2017), who attributes the frequently observed decoupling between primary production and C export to elevated ratios of TEP-C: primary production, and ii) to the results of Buesseler (1998), who demonstrated that much of the ocean is characterized by low efficiency of C export (relative to ρC), apart from highly efficient episodic pulses during phytoplankton blooms.

- This thesis provides the first estimates of daily TEP-C turnover rates by building off work done by Wurl et al., (2011), who calculated TEP-C residence times in the upper mixed layer along Line P. Ranges in TEP-C turnover rates were directly compared with rates of ρC, to ascertain the relative magnitude of C fluxes from primary production and TEP-C turnover rates.
- Carbon flux from primary productivity (ρC) was approximately 20x higher than TEP-$C_{turnover}$ rates in coastal regions, while in low productivity HNLC regions TEP-$C_{turnover}$ rates were higher compared to primary production, with the relative C fluxes from TEP-$C_{turnover}$ being approximately 5x lower than primary productivity.
- Excess C consumption by phytoplankton was calculated as measured ρC minus expected ρC from $\rho NO_3^-$, using three different approaches (measured, maximum, and minimum approaches using ranges in *f*-ratios. All approaches to estimating C overconsumption were significantly correlated with TEP-C concentrations across the range of this study, providing the first *in situ* evidence, which builds off a large body of experimental evidence, of a relationship between TEP-C and excess C consumption by phytoplankton.

*Chapter 4: Quantifying spatiotemporal trends in the contributions of small-cell phytoplankton to biogeochemical cycles in the Northeast Pacific Ocean*

- Small cell phytoplankton (<5µm) dominated ρC and $\rho NO_3^-$ in shelf-break, transition, and HNLC regions, while larger cells (>5µm) were responsible for the majority of ρC and $\rho NO_3^-$ in coastal regions. In transition and HNLC regions, small cell ρC and $\rho NO_3^-$ did not vary significantly across seasons or years, and consistently contributed ~78% and 76% to both rates, respectively. Uptake and particulate ratios of C:N did not vary significantly between size classes.
- Small cell phytoplankton contributed significantly less to ρSi compared to ρC or $\rho NO_3^-$; however, they were still responsible for ~20% and ~10% of ρSi in oceanic (transition and HNLC) and coastal regions, respectively. The small cell size fraction was characterized by lower (although not significant) ρSi:ρC ratios, and significantly lower Si:C particulate ratios across all regions.
- Uptake rates of C, $NO_3^-$, and Si by small cells did not appear to be correlated with any of the environmental variables measured over the spatiotemporal range of this study, apart from the depth of the mixed layer and distance from shore.
- The production of TEP-C by both small and large cell size fractions displayed notable differences. Smaller cells were responsible for the majority of TEP-C production along Line P in an experiment conducted in May 2021. Additionally, TEP-C production rates in the small cell fraction experiment represented a much larger fraction of total ρC and NP than compared to the larger fraction.
- This chapter provides one of the first assessments of small cell Si uptake and is the first to do so over large gradients in space and time. It provides a quantitative assessment of

small cell contributions to nutrient uptake in the ESNP and highlights the importance of this size fraction to nutrient cycling (and TEP-C production) in the region.

## 5.3 Future Studies

There are multiple new research directions that emerge from the work in this thesis.

- *Further development of multivariate modelling approaches for TEP.* This study is the first of its kind to attempt to predict TEP-C concentrations. As a result, it provides the foundation for future work to build off, and to develop more refined approaches for predicting TEP in the ocean. New environmental and biological variables could be identified as TEP predictors from large datasets with more complete coverage of variables not investigated in this thesis. Vertical profiles of TEP and associated environmental/biological variables may be able to capture more variation in what drives TEP in the water column (which is especially relevant given that it is a buoyant substance). This may include better parametrization of physical processes that may promote TEP aggregation and formation, such as mixing. Secondly, larger datasets may be able to train more advanced models, including more sophisticated machine learning models (such as neural networks) to predict TEP more accurately and to utilize trends in the data that may not be identified by basic techniques such as MLR or RFR. This would complement the works of this thesis, as more advanced models provide the added benefit of increased predictive power, but typically lack the ability to identify the most significant predictor variables. As such, this thesis provides the framework for future modelling work and could inspire more advanced approaches.

- *Predicting large-scale surface TEP concentrations from remote sensors.* This thesis identified variables such as chl-*a*, AOU, temperature, and MLD as significant predictors of TEP. Some of these variables, and their proxies can be obtained from remote sensors such as satellites or ARGO floats. Obtaining predictions of TEP concentrations from remote sensors in the future would be particularly useful in studies that utilize such sensors for estimating total primary productivity and/or C export. Therefore, the ratio of TEP-C to total productivity or export could be estimated for greater expanses in the ocean.
- *TEP production and primary production experiments.* Future work could build off the methods and results used in this thesis to further understand and quantify the relationship between TEP-C production and total primary production. As Mari et al. (2017) discusses, the relative magnitude of TEP-C production to primary production has very important implications for C export efficiency. Therefore, future studies should measure *in situ* TEP-C production and primary production with larger samples sizes and spatial coverage to further understand how the ratio of TEP-C to primary production varies as a function of environmental or biological conditions.

# Bibliography


Agawin, N. S. R., Duarte, C. M., & Agustí, S. (1998). Growth and abundance of Synechococcus sp. in a Mediterranean Bay: Seasonality and relationship with temperature. *Marine Ecology Progress Series*, *170*, 45–53. https://doi.org/10.3354/meps170045

Agawin, N. S. R., Duarte, C. M., & Agustí, S. (2000). Nutrient and temperature control of the contribution of picoplankton to phytoplankton biomass and production. *Limnology and Oceanography*, *45*(3), 591–600. https://doi.org/10.4319/lo.2000.45.3.0591

Albertano, P., Somma, D. D., & Capucci, E. (1997). Cyanobacterial picoplankton from the Central Baltic Sea: Cell size classification by image-analyzed fluorescence microscopy. *Journal of Plankton Research*, *19*(10), 1405–1416. https://doi.org/10.1093/plankt/19.10.1405

Alonso-Sáez, L., Gasol, J. M., Arístegui, J., Vilas, J. C., Vaqué, D., Duarte, C. M., & Agustí, S. (2007). Large-scale variability in surface bacterial carbon demand and growth efficiency in the subtropical northeast Atlantic Ocean. *Limnology and Oceanography*, *52*(2), 533–546. https://doi.org/10.4319/lo.2007.52.2.0533

Armstrong, R. A., Lee, C., Hedges, J. I., Honjo, S., & Wakeham, S. G. (2001). A new, mechanistic model for organic carbon fluxes in the ocean based on the quantitative association of POC with ballast minerals. *Deep Sea Research Part II: Topical Studies in Oceanography*, *49*(1), 219–236. https://doi.org/10.1016/S0967-0645(01)00101-1

Azetsu-Scott, K., & Passow, U. (2004). Ascending marine particles: Significance of transparent exopolymer particles (TEP) in the upper ocean. *Limnology and Oceanography*, *49*(3), 741–748. https://doi.org/10.4319/lo.2004.49.3.0741

Baines, S. B., Twining, B. S., Brzezinski, M. A., Krause, J. W., Vogt, S., Assael, D., & McDaniel, H. (2012). Significant silicon accumulation by marine picocyanobacteria. *Nature Geoscience*, *5*(12), Article 12. https://doi.org/10.1038/ngeo1641

Ball, S. G., & Morell, M. K. (2003). From Bacterial Glycogen to Starch: Understanding the Biogenesis of the Plant Starch Granule. *Annual Review of Plant Biology*, *54*(1), 207–233. https://doi.org/10.1146/annurev.arplant.54.031902.134927

Banse, K. (1990). New views on the degradation and disposition of organic particles as collected by sediment traps in the open sea. *Deep Sea Research Part A. Oceanographic Research Papers*, *37*(7), 1177–1195. https://doi.org/10.1016/0198-0149(90)90058-4

Barwell-clarke, J., Whitney, F., Sciences, O., J., & Whitney, F. (1996). *Nutrient Methods and Analysis*.

Bar-Zeev, E., Berman-Frank, I., Stambler, N., Domínguez, E. V., Zohary, T., Capuzzo, E., Meeder, E., Suggett, D. J., Iluz, D., Dishon, G., & Berman, T. (2009). Transparent exopolymer particles (TEP) link phytoplankton and bacterial production in the Gulf of Aqaba. *Aquatic Microbial Ecology*, *56*(2–3), 217–225. https://doi.org/10.3354/ame01322

Beattie, A., Hirst, E. L., & Percival, E. (1961). Studies on the metabolism of the Chrysophyceae. Comparative structural investigations on leucosin (chrysolaminarin) separated from diatoms and laminarin from the brown algae. *Biochemical Journal*, *79*(3), 531–537.

Beaugrand, G., Edwards, M., & Legendre, L. (2010). Marine biodiversity, ecosystem functioning, and carbon cycles. *Proceedings of the National Academy of Sciences*, *107*(22), 10120–10124. https://doi.org/10.1073/pnas.0913855107

Beauvais, S., Pedrotti, M. L., Egge, J., Iversen, K., & Marrasé, C. (2006). Effects of turbulence on TEP dynamics under contrasting nutrient conditions: Implications for aggregation and

sedimentation processes. *Marine Ecology Progress Series*, *323*, 47–57. https://doi.org/10.3354/meps323047

Benner, R., Pakulski, J. D., McCarthy, M., Hedges, J. I., & Hatcher, P. G. (1992). Bulk Chemical Characteristics of Dissolved Organic Matter in the Ocean. *Science*, *255*(5051), 1561–1564. https://doi.org/10.1126/science.255.5051.1561

Bhavya, P. S., Lee, J. H., Lee, H. W., Kang, J. J., Lee, J. H., Lee, D., An, S. H., Stockwell, D. A., Whitledge, T. E., & Lee, S. H. (2018). First in situ estimations of small phytoplankton carbon and nitrogen uptake rates in the Kara, Laptev, and East Siberian seas. *Biogeosciences*, *15*(18), 5503–5517. https://doi.org/10.5194/bg-15-5503-2018

Biddanda, B., & Benner, R. (1997). Carbon, nitrogen, and carbohydrate fluxes during the production of particulate and dissolved organic matter by marine phytoplankton. *Limnology and Oceanography*, *42*(3), 506–518. https://doi.org/10.4319/lo.1997.42.3.0506

Biermann, A., Engel, A., & Riebesell, U. (2014). Changes in organic matter cycling in a plankton community exposed to warming under different light intensities. *Journal of Plankton Research*, *36*(3), 658–671. https://doi.org/10.1093/plankt/fbu005

Bijma, J., Pörtner, H.-O., Yesson, C., & Rogers, A. D. (2013). Climate change and the oceans – What does the future hold? *Marine Pollution Bulletin*, *74*(2), 495–505. https://doi.org/10.1016/j.marpolbul.2013.07.022

Bittar, T. B., Passow, U., Hamaraty, L., Bidle, K. D., & Harvey, E. L. (2018). An updated method for the calibration of transparent exopolymer particle measurements. *Limnology and Oceanography: Methods*, *16*(10), 621–628. https://doi.org/10.1002/lom3.10268

Booth, B. C., Lewin, J., & Postel, J. R. (1993). Temporal variation in the structure of autotrophic and heterotrophic communities in the subarctic Pacific. *Progress in Oceanography*, *32*(1), 57–99. https://doi.org/10.1016/0079-6611(93)90009-3

Boyce, D. G., Lewis, M. R., & Worm, B. (2010). Global phytoplankton decline over the past century. *Nature*, *466*(7306), Article 7306. https://doi.org/10.1038/nature09268

Boyd, P., & Harrison, P. J. (1999). Phytoplankton dynamics in the NE subarctic Pacific. *Deep Sea Research Part II: Topical Studies in Oceanography*, *46*(11), 2405–2432. https://doi.org/10.1016/S0967-0645(99)00069-7

Boyd, P., Muggli, D., Varela, D., Goldblatt, R., Chretien, R., Orians, K., & Harrison, P. (1996). In vitro iron enrichment experiments in the NE subarctic Pacific. *Marine Ecology Progress Series*, *136*, 179–193. https://doi.org/10.3354/meps136179

Boyd, P. W. (2015). Toward quantifying the response of the oceans' biological pump to climate change. *Frontiers in Marine Science*, *2*. https://www.frontiersin.org/articles/10.3389/fmars.2015.00077

Boyd, P. W., Strzepek, R., Takeda, S., Jackson, G., Wong, C. S., McKay, R. M., Law, C., Kiyosawa, H., Saito, H., Sherry, N., Johnson, K., Gower, J., & Ramaiah, N. (2005). The evolution and termination of an iron-induced mesoscale bloom in the northeast subarctic Pacific. *Limnology and Oceanography*, *50*(6), 1872–1886. https://doi.org/10.4319/lo.2005.50.6.1872

Boyd, P. W., Watson, A. J., Law, C. S., Abraham, E. R., Trull, T., Murdoch, R., Bakker, D. C. E., Bowie, A. R., Buesseler, K. O., Chang, H., Charette, M., Croot, P., Downing, K., Frew, R., Gall, M., Hadfield, M., Hall, J., Harvey, M., Jameson, G., … Zeldis, J. (2000).

A mesoscale phytoplankton bloom in the polar Southern Ocean stimulated by iron fertilization. *Nature*, *407*(6805), Article 6805. https://doi.org/10.1038/35037500

Breiman, L. (2001). Random Forests. *Machine Learning*, *45*(1), 5–32. https://doi.org/10.1023/A:1010933404324

Brzezinski, M. A. (1985). THE Si:C:N RATIO OF MARINE DIATOMS: INTERSPECIFIC VARIABILITY AND THE EFFECT OF SOME ENVIRONMENTAL VARIABLES1. *Journal of Phycology*, *21*(3), 347–357. https://doi.org/10.1111/j.0022-3646.1985.00347.x

Brzezinski, M. A., & Phillips, D. R. (1997). Evaluation of $^{32}$Si as a tracer for measuring silica production rates in marine waters. *Limnology and Oceanography*, *42*(5), 856–865. https://doi.org/10.4319/lo.1997.42.5.0856

Brzezinski, M. A., Varela, D. E., Jenkins, B. D., Buck, K. N., Kafrissen, S. M., & Jones, J. L. (2022). The upper ocean silicon cycle of the subarctic Pacific during the EXPORTS field campaign. *Elementa: Science of the Anthropocene*, *10*(1), 00087. https://doi.org/10.1525/elementa.2021.00087

Buesseler, K. O. (1998). The decoupling of production and particulate export in the surface ocean. *Global Biogeochemical Cycles*, *12*(2), 297–310. https://doi.org/10.1029/97GB03366

Buesseler, K. O., & Boyd, P. W. (2009). Shedding light on processes that control particle export and flux attenuation in the twilight zone of the open ocean. *Limnology and Oceanography*, *54*(4), 1210–1232. https://doi.org/10.4319/lo.2009.54.4.1210

Burns, W. G., Marchetti, A., & Ziervogel, K. (2019). Enhanced formation of transparent exopolymer particles (TEP) under turbulence during phytoplankton growth. *Journal of Plankton Research*, *41*(3), 349–361. https://doi.org/10.1093/plankt/fbz018

Busch, K., Endres, S., Iversen, M. H., Michels, J., Nöthig, E.-M., & Engel, A. (2017). Bacterial Colonization and Vertical Distribution of Marine Gel Particles (TEP and CSP) in the Arctic Fram Strait. *Frontiers in Marine Science*, *4*. https://www.frontiersin.org/articles/10.3389/fmars.2017.00166

Callieri, C., Sathicq, M. B., Cabello-Yeves, P. J., Eckert, E. M., & Hernández-Avilés, J. S. (2019). TEP production under oxidative stress of the picocyanobacterium Synechococcus: Synechococcus TEP production. *Journal of Limnology*, *78*(3). https://doi.org/10.4081/jlimnol.2019.1907

Carmack, E., & McLaughlin, F. (2011). Towards recognition of physical and geochemical change in Subarctic and Arctic Seas. *Progress in Oceanography*, *90*(1), 90–104. https://doi.org/10.1016/j.pocean.2011.02.007

Claquin, P., Probert, I., Lefebvre, S., & Veron, B. (2008). Effects of temperature on photosynthetic parameters and TEP production in eight species of marine microalgae. *Aquatic Microbial Ecology*, *51*(1), 1–11. https://doi.org/10.3354/ame01187

Collins, M., Knutti, R., Arblaster, J., Dufresne, J.-L., Fichefet, T., Friedlingstein, P., Gao, X., Gutowski, W. J., Johns, T., Krinner, G., Shongwe, M., Tebaldi, C., Weaver, A. J., & Wehner, M. (2013). *Chapter 12 - Long-term climate change: Projections, commitments and irreversibility* (IPCC, Ed.). Cambridge University Press. http://www.climatechange2013.org/images/report/WG1AR5_Chapter12_FINAL.pdf

Collins, S., Rost, B., & Rynearson, T. A. (2014). Evolutionary potential of marine phytoplankton under ocean acidification. *Evolutionary Applications*, *7*(1), 140–155. https://doi.org/10.1111/eva.12120

Corzo, A., Morillo, J. A., & Rodríguez, S. (2000). Production of transparent exopolymer particles (TEP) in cultures of Chaetoceros calcitrans under nitrogen limitation. *Aquatic Microbial Ecology*, *23*(1), 63–72. https://doi.org/10.3354/ame023063

Corzo, A., Rodríguez-Gálvez, S., Lubian, L., Sangrá, P., Martínez, A., & Morillo, J. A. (2005). Spatial distribution of transparent exopolymer particles in the Bransfield Strait, Antarctica. *Journal of Plankton Research*, *27*(7), 635–646. https://doi.org/10.1093/plankt/fbi038

de Boyer Montégut, C., Madec, G., Fischer, A. S., Lazar, A., & Iudicone, D. (2004). Mixed layer depth over the global ocean: An examination of profile data and a profile-based climatology. *Journal of Geophysical Research: Oceans*, *109*(C12). https://doi.org/10.1029/2004JC002378

De La Rocha, C. L., & Passow, U. (2007). Factors influencing the sinking of POC and the efficiency of the biological carbon pump. *Deep Sea Research Part II: Topical Studies in Oceanography*, *54*(5), 639–658. https://doi.org/10.1016/j.dsr2.2007.01.004

de Vicente, I., Ortega-Retuerta, E., Mazuecos, I. P., Pace, M. L., Cole, J. J., & Reche, I. (2010). Variation in transparent exopolymer particles in relation to biological and chemical factors in two contrasting lake districts. *Aquatic Sciences*, *72*(4), 443–453. https://doi.org/10.1007/s00027-010-0147-6

Dugdale, R. C., & Goering, J. J. (1967). Uptake of New and Regenerated Forms of Nitrogen in Primary Productivity1. *Limnology and Oceanography*, *12*(2), 196–206. https://doi.org/10.4319/lo.1967.12.2.0196

Dugdale, R. C., & Wilkerson, F. P. (1986). The use of $^{15}N$ to measure nitrogen uptake in eutrophic oceans; experimental considerations1,2. *Limnology and Oceanography*, *31*(4), 673–689. https://doi.org/10.4319/lo.1986.31.4.0673

Emerson, S. R., & Hamme, R. C. (2022). *Chemical Oceanography*. Cambridge University Press.

Engel, A. (2002a). Direct relationship between $CO_2$ uptake and transparent exopolymer particles production in natural phytoplankton. *Journal of Plankton Research*, *24*(1), 49–53. https://doi.org/10.1093/plankt/24.1.49

Engel, A. (2002b). Direct relationship between CO2 uptake and transparent exopolymer particles production in natural phytoplankton. *Journal of Plankton Research*, *24*(1), 49–53. https://doi.org/10.1093/plankt/24.1.49

Engel, A. (2004). Distribution of transparent exopolymer particles (TEP) in the northeast Atlantic Ocean and their potential significance for aggregation processes. *Deep Sea Research Part I: Oceanographic Research Papers*, *51*(1), 83–92. https://doi.org/10.1016/j.dsr.2003.09.001

Engel, A., Goldthwait, S., Passow, U., & Alldredge, A. (2002a). Temporal decoupling of carbon and nitrogen dynamics in a mesocosm diatom bloom. *Limnology and Oceanography*, *47*(3), 753–761. https://doi.org/10.4319/lo.2002.47.3.0753

Engel, A., Goldthwait, S., Passow, U., & Alldredge, A. (2002b). Temporal decoupling of carbon and nitrogen dynamics in a mesocosm diatom bloom. *Limnology and Oceanography*, *47*(3), 753–761. https://doi.org/10.4319/lo.2002.47.3.0753

Engel, A., Händel, N., Wohlers, J., Lunau, M., Grossart, H.-P., Sommer, U., & Riebesell, U. (2011). Effects of sea surface warming on the production and composition of dissolved

organic matter during phytoplankton blooms: Results from a mesocosm study. *Journal of Plankton Research*, *33*(3), 357–372. https://doi.org/10.1093/plankt/fbq122

Engel, A., & Passow, U. (2001). Carbon and nitrogen content of transparent exopolymer particles (TEP) in relation to their Alcian Blue adsorption. *Marine Ecology Progress Series*, *219*, 1–10. https://doi.org/10.3354/meps219001

Eppley, R. W., & Peterson, B. J. (1979). Particulate organic matter flux and planktonic new production in the deep ocean. *Nature*, *282*(5740), Article 5740. https://doi.org/10.1038/282677a0

Favorite, R. (1976). Oceanography of the Subarctic Pacific region, 1960-71. *International North Pacific Fisheries Commission Bulletin*, *33*, 1–187.

Field, C., Behrenfeld, M., Randerson, J., & Falkowski, P. (1998). *Primary Production of the Biosphere: Integrating Terrestrial and Oceanic Components*. https://doi.org/10.1126/science.281.5374.237

Firme, G. F., Rue, E. L., Weeks, D. A., Bruland, K. W., & Hutchins, D. A. (2003). Spatial and temporal variability in phytoplankton iron limitation along the California coast and consequences for Si, N, and C biogeochemistry. *Global Biogeochemical Cycles*, *17*(1). https://doi.org/10.1029/2001GB001824

Franck, V. M., Bruland, K. W., Hutchins, D. A., & Brzezinski, M. A. (2003). Iron and zinc effects on silicic acid and nitrate uptake kinetics in three high-nutrient, low-chlorophyll (HNLC) regions. *Marine Ecology Progress Series*, *252*, 15–33. https://doi.org/10.3354/meps252015

Franck, V. M., Smith, G. J., Bruland, K. W., & Brzezinski, M. A. (2005). Comparison of size-dependent carbon, nitrate, and silicic acid uptake rates in high- and low-iron waters.

*Limnology and Oceanography*, *50*(3), 825–838. https://doi.org/10.4319/lo.2005.50.3.0825

Fukao, T., Kimoto, K., & Kotani, Y. (2012). Effect of temperature on cell growth and production of transparent exopolymer particles by the diatom Coscinodiscus granii isolated from marine mucilage. *Journal of Applied Phycology*, *24*(2), 181–186. https://doi.org/10.1007/s10811-011-9666-3

Gargett, A. E. (1991). Physical processes and the maintenance of nutrient-rich euphotic zones. *Limnology and Oceanography*, *36*(8), 1527–1545. https://doi.org/10.4319/lo.1991.36.8.1527

Goldman, J. C., & Mann, R. (1980). Temperature-influenced variations in speciation and chemical composition of marine phytoplankton in outdoor mass cultures. *Journal of Experimental Marine Biology and Ecology*, *46*(1), 29–39. https://doi.org/10.1016/0022-0981(80)90088-X

Graham, M. H. (2003). Confronting Multicollinearity in Ecological Multiple Regression. *Ecology*, *84*(11), 2809–2815.

Guo, K., Chen, J., Yuan, J., Wang, X., Xu, S., Hou, S., & Wang, Y. (2022). Effects of Temperature on Transparent Exopolymer Particle Production and Organic Carbon Allocation of Four Marine Phytoplankton Species. *Biology*, *11*(7), Article 7. https://doi.org/10.3390/biology11071056

Guo, S., Wu, Y., Zhu, M., & Sun, X. (2022). Concentrations of transparent exopolymer particles (TEPs) and their role in the carbon export in the South China Sea and western tropical North Pacific. *Marine Environmental Research*, *179*, 105699. https://doi.org/10.1016/j.marenvres.2022.105699

Hama, T., Miyazaki, T., Ogawa, Y., Iwakuma, T., Takahashi, M., Otsuki, A., & Ichimura, S. (1983). Measurement of photosynthetic production of a marine phytoplankton population using a stable 13C isotope. *Marine Biology*, *73*(1), 31–36. https://doi.org/10.1007/BF00396282

Hansell, D. A., Carlson, C. A., & Schlitzer, R. (2012). Net removal of major marine dissolved organic carbon fractions in the subsurface ocean. *Global Biogeochemical Cycles*, *26*(1). https://doi.org/10.1029/2011GB004069

Hansell, D. A., & Waterhouse, T. Y. (1997). Controls on the distributions of organic carbon and nitrogen in the eastern Pacific Ocean. *Deep Sea Research Part I: Oceanographic Research Papers*, *44*(5), 843–857. https://doi.org/10.1016/S0967-0637(96)00128-8

Harris, S. L., Varela, D. E., Whitney, F. W., & Harrison, P. J. (2009). Nutrient and phytoplankton dynamics off the west coast of Vancouver Island during the 1997/98 ENSO event. *Deep Sea Research Part II: Topical Studies in Oceanography*, *56*(24), 2487–2502. https://doi.org/10.1016/j.dsr2.2009.02.009

Harrison, P. J., Whitney, F. A., Tsuda, A., Saito, H., & Tadokoro, K. (2004). Nutrient and Plankton Dynamics in the NE and NW Gyres of the Subarctic Pacific Ocean. *Journal of Oceanography*, *60*(1), 93–117. https://doi.org/10.1023/B:JOCE.0000038321.57391.2a

Harrison, W. G., & Wood, L. J. E. (1988). Inorganic nitrogen uptake by marine picoplankton: Evidence for size partitioning. *Limnology and Oceanography*, *33*(3), 468–475. https://doi.org/10.4319/lo.1988.33.3.0468

Herndl, G. J., & Reinthaler, T. (2013). Microbial control of the dark end of the biological pump. *Nature Geoscience*, *6*(9), Article 9. https://doi.org/10.1038/ngeo1921

Hodal, H., & Kristiansen, S. (2008). The importance of small-celled phytoplankton in spring blooms at the marginal ice zone in the northern Barents Sea. *Deep Sea Research Part II: Topical Studies in Oceanography*, *55*(20), 2176–2185. https://doi.org/10.1016/j.dsr2.2008.05.012

Hong, Y., Smith Jr., W. O., & White, A.-M. (1997). Studies on Transparent Exopolymer Particles (tep) Produced in the Ross Sea (antarctica) and by Phaeocystis Antarctica (prymnesiophyceae)1. *Journal of Phycology*, *33*(3), 368–376. https://doi.org/10.1111/j.0022-3646.1997.00368.x

Irion, S., Christaki, U., Berthelot, H., L'Helguen, S., & Jardillier, L. (2021). Small phytoplankton contribute greatly to CO2-fixation after the diatom bloom in the Southern Ocean. *The ISME Journal*, *15*(9), Article 9. https://doi.org/10.1038/s41396-021-00915-z

Islam, M. S., Sun, J., Zhang, G., Chen, Z., & Zhou, H. (2021). Environmental influences on sinking rates and distributions of transparent exopolymer particles after a typhoon surge at the Western Pacific. *Scientific Reports*, *11*(1), Article 1. https://doi.org/10.1038/s41598-021-88477-0

Iuculano, F., Mazuecos, I. P., Reche, I., & Agustí, S. (2017). Prochlorococcus as a Possible Source for Transparent Exopolymer Particles (TEP). *Frontiers in Microbiology*, *8*. https://www.frontiersin.org/articles/10.3389/fmicb.2017.00709

Jahnke, R. A. (1996). The global ocean flux of particulate organic carbon: Areal distribution and magnitude. *Global Biogeochemical Cycles*, *10*(1), 71–88. https://doi.org/10.1029/95GB03525

Karl, D. M., Hebel, D. V., Björkman, K., & Letelier, R. M. (1998). The role of dissolved organic matter release in the productivity of the oligotrophic North Pacific Ocean. *Limnology and Oceanography*, *43*(6), 1270–1286. https://doi.org/10.4319/lo.1998.43.6.1270

Kiørboe, T., Tiselius, P., Mitchell-Innes, B., Hansen, J. L. S., Visser, A. W., & Mari, X. (1998). Intensive aggregate formation with low vertical flux during an upwelling-induced diatom bloom. *Limnology and Oceanography*, *43*(1), 104–116. https://doi.org/10.4319/lo.1998.43.1.0104

Kodama, T., Kurogi, H., Okazaki, M., Jinbo, T., Chow, S., Tomoda, T., Ichikawa, T., & Watanabe, T. (2014). Vertical distribution of transparent exopolymer particle (TEP) concentration in the oligotrophic western tropical North Pacific. *Marine Ecology Progress Series*, *513*, 29–37. https://doi.org/10.3354/meps10954

Krause, J. W., Brzezinski, M. A., Baines, S. B., Collier, J. L., Twining, B. S., & Ohnemus, D. C. (2017). Picoplankton contribution to biogenic silica stocks and production rates in the Sargasso Sea. *Global Biogeochemical Cycles*, *31*(5), 762–774. https://doi.org/10.1002/2017GB005619

La Roche, J., Boyd, P. W., McKay, R. M. L., & Geider, R. J. (1996). Flavodoxin as an in situ marker for iron stress in phytoplankton. *Nature*, *382*(6594), Article 6594. https://doi.org/10.1038/382802a0

Lee, S. H., Joo, H. M., Liu, Z., Chen, J., & He, J. (2012). Phytoplankton productivity in newly opened waters of the Western Arctic Ocean. *Deep Sea Research Part II: Topical Studies in Oceanography*, *81–84*, 18–27. https://doi.org/10.1016/j.dsr2.2011.06.005

Lee, S. H., Sun Yun, M., Kyung Kim, B., Joo, H., Kang, S.-H., Keun Kang, C., & Whitledge, T. E. (2013). Contribution of small phytoplankton to total primary production in the

Chukchi Sea. *Continental Shelf Research*, *68*, 43–50. https://doi.org/10.1016/j.csr.2013.08.008

Legendre, L., Gosselin, M., Hirche, H.-J., Kattner, G., & Rosenberg, G. (1993). Environmental control and potential fate of size-fractionated phytoplankton production in the Greenland Sea (75° N). *Marine Ecology Progress Series*, *98*, 297–313. https://doi.org/10.3354/meps098297

Legendre, L., & Rivkin, R. B. (2002). Fluxes of carbon in the upper ocean: Regulation by food-web control nodes. *Marine Ecology Progress Series*, *242*, 95–109. https://doi.org/10.3354/meps242095

Li, J., Xu, M., Wang, J., Lan, C., & Lai, J. (2023). Effects of nutrient limitation on cell growth, exopolysaccharide secretion and TEP production of Phaeocystis globosa. *Marine Environmental Research*, *183*, 105801. https://doi.org/10.1016/j.marenvres.2022.105801

Li, W. K. W., McLaughlin, F. A., Lovejoy, C., & Carmack, E. C. (2009). Smallest Algae Thrive As the Arctic Ocean Freshens. *Science*, *326*(5952), 539–539. https://doi.org/10.1126/science.1179798

Llopis Monferrer, N., Leynaert, A., Tréguer, P., Gutiérrez-Rodríguez, A., Moriceau, B., Gallinari, M., Latasa, M., L'Helguen, S., Maguer, J.-F., Safi, K., Pinkerton, M. H., & Not, F. (2021). Role of small Rhizaria and diatoms in the pelagic silica production of the Southern Ocean. *Limnology and Oceanography*, *66*(6), 2187–2202. https://doi.org/10.1002/lno.11743

López-Sandoval, D. C., Fernández, A., & Marañón, E. (2011). Dissolved and particulate primary production along a longitudinal gradient in the Mediterranean Sea. *Biogeosciences*, *8*(3), 815–825. https://doi.org/10.5194/bg-8-815-2011

M. Franck, V., Brzezinski, M. A., Coale, K. H., & Nelson, D. M. (2000). Iron and silicic acid concentrations regulate Si uptake north and south of the Polar Frontal Zone in the Pacific Sector of the Southern Ocean. *Deep Sea Research Part II: Topical Studies in Oceanography*, *47*(15), 3315–3338. https://doi.org/10.1016/S0967-0645(00)00070-9

Marañón, E., Cermeño, P., Fernández, E., Rodríguez, J., & Zabala, L. (2004). Significance and mechanisms of photosynthetic production of dissolved organic carbon in a coastal eutrophic ecosystem. *Limnology and Oceanography*, *49*(5), 1652–1666. https://doi.org/10.4319/lo.2004.49.5.1652

Mari, X., Beauvais, S., Lemée, R., & Pedrotti, M. L. (2001). Non-Redfield C:N ratio of transparent exopolymeric particles in the northwestern Mediterranean Sea. *Limnology and Oceanography*, *46*(7), 1831–1836. https://doi.org/10.4319/lo.2001.46.7.1831

Mari, X., & Burd, A. (1998). Seasonal size spectra of transparent exopolymeric particles (TEP) in a coastal sea and comparison with those predicted using coagulation theory. *Marine Ecology Progress Series*, *163*, 63–76. https://doi.org/10.3354/meps163063

Mari, X., Passow, U., Migon, C., Burd, A. B., & Legendre, L. (2017). Transparent exopolymer particles: Effects on carbon cycling in the ocean. *Progress in Oceanography*, *151*, 13–37. https://doi.org/10.1016/j.pocean.2016.11.002

Mari, X., Rassoulzadegan, F., Brussaard, C. P. D., & Wassmann, P. (2005). Dynamics of transparent exopolymeric particles (TEP) production by Phaeocystis globosa under N- or P-limitation: A controlling factor of the retention/export balance. *Harmful Algae*, *4*(5), 895–914. https://doi.org/10.1016/j.hal.2004.12.014

Marinov, I., Doney, S. C., & Lima, I. D. (2010). Response of ocean phytoplankton community structure to climate change over the 21st century: Partitioning the effects of nutrients,

temperature and light. *Biogeosciences*, *7*(12), 3941–3959. https://doi.org/10.5194/bg-7-3941-2010

Martin, J. H., Knauer, G. A., Karl, D. M., & Broenkow, W. W. (1987). VERTEX: Carbon cycling in the northeast Pacific. *Deep Sea Research Part A. Oceanographic Research Papers*, *34*(2), 267–285. https://doi.org/10.1016/0198-0149(87)90086-0

McCarthy, M., Hedges, J., & Benner, R. (1996). Major biochemical composition of dissolved high molecular weight organic matter in seawater. *Marine Chemistry*, *55*(3), 281–297. https://doi.org/10.1016/S0304-4203(96)00041-2

Meyer, M. G., Gong, W., Kafrissen, S. M., Torano, O., Varela, D. E., Santoro, A. E., Cassar, N., Gifford, S., Niebergall, A. K., Sharpe, G., & Marchetti, A. (2022). Phytoplankton size-class contributions to new and regenerated production during the EXPORTS Northeast Pacific Ocean field deployment. *Elementa: Science of the Anthropocene*, *10*(1), 00068. https://doi.org/10.1525/elementa.2021.00068

Michaels, A. F., & Silver, M. W. (1988). Primary production, sinking fluxes and the microbial food web. *Deep Sea Research Part A. Oceanographic Research Papers*, *35*(4), 473–490. https://doi.org/10.1016/0198-0149(88)90126-4

Morán, X. A. G., López-Urrutia, Á., Calvo-Díaz, A., & Li, W. K. W. (2010). Increasing importance of small phytoplankton in a warmer ocean. *Global Change Biology*, *16*(3), 1137–1144. https://doi.org/10.1111/j.1365-2486.2009.01960.x

Morán, X. A. G., Sebastián, M., Pedrís-Alií, C., & Estrada, M. (2006). Response of Southern Ocean phytoplankton and bacterioplankton production to short-term experimental warming. *Limnology and Oceanography*, *51*(4), 1791–1800. https://doi.org/10.4319/lo.2006.51.4.1791

Mühlenbruch, M., Grossart, H.-P., Eigemann, F., & Voss, M. (2018). Mini-review: Phytoplankton-derived polysaccharides in the marine environment and their interactions with heterotrophic bacteria. *Environmental Microbiology*, *20*(8), 2671–2685. https://doi.org/10.1111/1462-2920.14302

Nagata, T. (2000). Production mechanisms of dissolved organic matter. *Microbial Ecology of the Oceans*, 121–152.

Nodder, S. D., & Waite, A. M. (2001). Is Southern Ocean organic carbon and biogenic silica export enhanced by iron-stimulated increases in biological production? Sediment trap results from SOIREE. *Deep Sea Research Part II: Topical Studies in Oceanography*, *48*(11), 2681–2701. https://doi.org/10.1016/S0967-0645(01)00014-5

Ohnemus, D. C., Rauschenberg, S., Krause, J. W., Brzezinski, M. A., Collier, J. L., Geraci-Yee, S., Baines, S. B., & Twining, B. S. (2016). Silicon content of individual cells of Synechococcus from the North Atlantic Ocean. *Marine Chemistry*, *187*, 16–24. https://doi.org/10.1016/j.marchem.2016.10.003

Olli, K., & Heiskanen, A.-S. (1999). Seasonal stages of phytoplankton community structure and sinking loss in the Gulf of Riga. *Journal of Marine Systems*, *23*(1), 165–184. https://doi.org/10.1016/S0924-7963(99)00056-1

Ortega-Retuerta, E., Duarte, C. M., & Reche, I. (2010). Significance of Bacterial Activity for the Distribution and Dynamics of Transparent Exopolymer Particles in the Mediterranean Sea. *Microbial Ecology*, *59*(4), 808–818. https://doi.org/10.1007/s00248-010-9640-7

Ortega-Retuerta, E., Marrasé, C., Muñoz-Fernández, A., Sala, M. M., Simó, R., & Gasol, J. M. (2018). Seasonal dynamics of transparent exopolymer particles (TEP) and their drivers in

the coastal NW Mediterranean Sea. *Science of The Total Environment*, *631–632*, 180–190. https://doi.org/10.1016/j.scitotenv.2018.02.341

Ortega-Retuerta, E., Mazuecos, I. P., Reche, I., Gasol, J. M., Álvarez-Salgado, X. A., Álvarez, M., Montero, M. F., & Arístegui, J. (2019). Transparent exopolymer particle (TEP) distribution and in situ prokaryotic generation across the deep Mediterranean Sea and nearby North East Atlantic Ocean. *Progress in Oceanography*, *173*, 180–191. https://doi.org/10.1016/j.pocean.2019.03.002

Ortega-Retuerta, E., Passow, U., Duarte, C. M., & Reche, I. (2009b). Effects of ultraviolet B radiation on (not so) transparent exopolymer particles. *Biogeosciences*, *6*(12), 3071–3080. https://doi.org/10.5194/bg-6-3071-2009

Ortega-Retuerta, E., Reche, I., Pulido-Villena, E., Agustí, S., & Duarte, C. M. (2009). Uncoupled distributions of transparent exopolymer particles (TEP) and dissolved carbohydrates in the Southern Ocean. *Marine Chemistry*, *115*(1), 59–65. https://doi.org/10.1016/j.marchem.2009.06.004

Ortega-Retuerta, E., Sala, M. M., Borrull, E., Mestre, M., Aparicio, F. L., Gallisai, R., Antequera, C., Marrasé, C., Peters, F., Simó, R., & Gasol, J. M. (2017). Horizontal and Vertical Distributions of Transparent Exopolymer Particles (TEP) in the NW Mediterranean Sea Are Linked to Chlorophyll a and O2 Variability. *Frontiers in Microbiology*, *7*. https://www.frontiersin.org/article/10.3389/fmicb.2016.02159

Parsons, T. (2013). *A Manual of Chemical & Biological Methods for Seawater Analysis*. Elsevier.

Passow, U. (2000). Formation of transparent exopolymer particles, TEP, from dissolved precursor material. *Marine Ecology Progress Series*, *192*, 1–11. https://doi.org/10.3354/meps192001

Passow, U. (2002a). Production of transparent exopolymer particles (TEP) by phyto- and bacterioplankton. *Marine Ecology Progress Series*, *236*, 1–12. https://doi.org/10.3354/meps236001

Passow, U. (2002b). Transparent exopolymer particles (TEP) in aquatic environments. *Progress in Oceanography*, *55*(3), 287–333. https://doi.org/10.1016/S0079-6611(02)00138-6

Passow, U., & Alldredge, A. L. (1995a). A dye-binding assay for the spectrophotometric measurement of transparent exopolymer particles (TEP). *Limnology and Oceanography*, *40*(7), 1326–1335. https://doi.org/10.4319/lo.1995.40.7.1326

Passow, U., & Alldredge, A. L. (1995b). Aggregation of a diatom bloom in a mesocosm: The role of transparent exopolymer particles (TEP). *Deep Sea Research Part II: Topical Studies in Oceanography*, *42*(1), 99–109. https://doi.org/10.1016/0967-0645(95)00006-C

Passow, U., & Carlson, C. A. (2012). The biological pump in a high $CO_2$ world. *Marine Ecology Progress Series*, *470*, 249–272. JSTOR.

Pauly, D., & Cheung, W. W. L. (2018). Sound physiological knowledge and principles in modeling shrinking of fishes under climate change. *Global Change Biology*, *24*(1), e15–e26. https://doi.org/10.1111/gcb.13831

Pedrotti, M. L., Peters, F., Beauvais, S., Vidal, M., Egge, J., Jacobsen, A., & Marrasé, C. (2010). Effects of nutrients and turbulence on the production of transparent exopolymer particles: A mesocosm study. *Marine Ecology Progress Series*, *419*, 57–69. https://doi.org/10.3354/meps08840

Peña, M. A., Nemcek, N., & Robert, M. (2019). Phytoplankton responses to the 2014–2016 warming anomaly in the northeast subarctic Pacific Ocean. *Limnology and Oceanography*, *64*(2), 515–525. https://doi.org/10.1002/lno.11056

Peña, M. A., & Varela, D. E. (2007a). Seasonal and interannual variability in phytoplankton and nutrient dynamics along Line P in the NE subarctic Pacific. *Progress in Oceanography*, *75*(2), 200–222. https://doi.org/10.1016/j.pocean.2007.08.009

Peña, M. A., & Varela, D. E. (2007b). Seasonal and interannual variability in phytoplankton and nutrient dynamics along Line P in the NE subarctic Pacific. *Progress in Oceanography*, *75*(2), 200–222. https://doi.org/10.1016/j.pocean.2007.08.009

Piontek, J., Händel, N., Langer, G., Wohlers, J., Riebesell, U., & Engel, A. (2009). Effects of rising temperature on the formation and microbial degradation of marine diatom aggregates. *Aquatic Microbial Ecology*, *54*(3), 305–318. https://doi.org/10.3354/ame01273

Pitcher, G. C., Walker, D. R., Mitchell-Innes, B. A., & Moloney, C. L. (1991). Short-term variability during an anchor station study in the southern Benguela upwelling system: Phytoplankton dynamics. *Progress in Oceanography*, *28*(1), 39–64. https://doi.org/10.1016/0079-6611(91)90020-M

Polimene, L., Sailley, S., Clark, D., Mitra, A., & Allen, J. I. (2017). Biological or microbial carbon pump? The role of phytoplankton stoichiometry in ocean carbon sequestration. *Journal of Plankton Research*, *39*(2), 180–186. https://doi.org/10.1093/plankt/fbw091

Polovina, J. J., Howell, E. A., & Abecassis, M. (2008). Ocean's least productive waters are expanding. *Geophysical Research Letters*, *35*(3). https://doi.org/10.1029/2007GL031745

Prieto, L., Navarro, G., Cózar, A., Echevarría, F., & García, C. M. (2006). Distribution of TEP in the euphotic and upper mesopelagic zones of the southern Iberian coasts. *Deep Sea Research Part II: Topical Studies in Oceanography*, *53*(11), 1314–1328. https://doi.org/10.1016/j.dsr2.2006.03.009

Probyn, T. (1985). Nitrogen uptake by size-fractionated phytoplankton populations in the southern Benguela upwelling system. *Marine Ecology Progress Series*, *22*, 249–258. https://doi.org/10.3354/meps022249

Radić, T., Ivančić, I., Fuks, D., & Radić, J. (2006). Marine bacterioplankton production of polysaccharidic and proteinaceous particles under different nutrient regimes. *FEMS Microbiology Ecology*, *58*(3), 333–342. https://doi.org/10.1111/j.1574-6941.2006.00176.x

Ramaiah, N., & Furuya, K. (2002). Seasonal variations in phytoplankton composition and transparent exopolymer particles in a eutrophicated coastal environment. *Aquatic Microbial Ecology*, *30*, 69–82. https://doi.org/10.3354/ame030069

Ramus, J. (1977). Alcian Blue: A Quantitative Aqueous Assay for Algal Acid and Sulfated Polysaccharides1. *Journal of Phycology*, *13*(4), 345–348. https://doi.org/10.1111/j.1529-8817.1977.tb02939.x

Raven, J. A. (1998). The twelfth Tansley Lecture. Small is beautiful: The picophytoplankton. *Functional Ecology*, *12*(4), 503–513. https://doi.org/10.1046/j.1365-2435.1998.00233.x

Richardson, T. (2019). Mechanisms and Pathways of Small-Phytoplankton Export from the Surface Ocean. *Annual Review of Marine Science*, *11*. https://doi.org/10.1146/annurev-marine-121916-063627

Richardson, T. L., & Jackson, G. A. (2007). Small Phytoplankton and Carbon Export from the Surface Ocean. *Science*, *315*(5813), 838–840. https://doi.org/10.1126/science.1133471

Rinaldi, A., Vollenweider, R. A., Montanari, G., Ferrari, C. R., & Ghetti, A. (1995). Mucilages in Italian seas: The Adriatic and Tyrrhenian Seas, 1988–1991. *Science of The Total Environment*, *165*(1), 165–183. https://doi.org/10.1016/0048-9697(95)04550-K

Romanelli, E., Sweet, J., Giering, S. L. C., Siegel, D. A., & Passow, U. (2023). The importance of transparent exopolymer particles over ballast in determining both sinking and suspension of small particles during late summer in the Northeast Pacific Ocean. *Elementa: Science of the Anthropocene*, *11*(1), 00122. https://doi.org/10.1525/elementa.2022.00122

Rost, B., Zondervan, I., & Wolf-Gladrow, D. (2008). Sensitivity of phytoplankton to future changes in ocean carbonate chemistry: Current knowledge, contradictions and research directions. *Marine Ecology Progress Series*, *373*, 227–237. https://doi.org/10.3354/meps07776

Russell, P., Hertz, P., & Mcmillan, B. (2010). *Biology: Exploring the Diversity of Life.* (1st ed., Vol. 1). Toronto:Nelson College Indigenous.

Sambrotto, R. N., Savidge, G., Robinson, C., Boyd, P., Takahashi, T., Karl, D. M., ... & Codispoti, L. (1993). Elevated consumption of carbon relative to nitrogen in the surface ocean. *Nature*, *363*(6426), 248-250.

Sambrotto, R. N., Niebauer, H. J., Goering, J. J., & Iverson, R. L. (1986). Relationships among vertical mixing, nitrate uptake, and phytoplankton growth during the spring bloom in the southeast Bering Sea middle shelf. *Continental Shelf Research*, *5*(1), 161–198. https://doi.org/10.1016/0278-4343(86)90014-2

Sanders, R., Henson, S. A., Koski, M., De La Rocha, C. L., Painter, S. C., Poulton, A. J., Riley, J., Salihoglu, B., Visser, A., Yool, A., Bellerby, R., & Martin, A. P. (2014). The Biological Carbon Pump in the North Atlantic. *Progress in Oceanography*, *129*, 200–218. https://doi.org/10.1016/j.pocean.2014.05.005

Seebah, S., Fairfield, C., Ullrich, M. S., & Passow, U. (2014). Aggregation and Sedimentation of Thalassiosira weissflogii (diatom) in a Warmer and More Acidified Future Ocean. *PLOS ONE*, *9*(11), e112379. https://doi.org/10.1371/journal.pone.0112379

Springer, A. M., & McRoy, C. P. (1993). The paradox of pelagic food webs in the northern Bering Sea—III. Patterns of primary production. *Continental Shelf Research*, *13*(5), 575–599. https://doi.org/10.1016/0278-4343(93)90095-F

Staats, N., Stal, L. J., & Mur, L. R. (2000). Exopolysaccharide production by the epipelic diatom Cylindrotheca closterium: Effects of nutrient conditions. *Journal of Experimental Marine Biology and Ecology*, *249*(1), 13–27. https://doi.org/10.1016/S0022-0981(00)00166-0

Steinacher, M., Joos, F., Frölicher, T. L., Bopp, L., Cadule, P., Cocco, V., Doney, S. C., Gehlen, M., Lindsay, K., Moore, J. K., Schneider, B., & Segschneider, J. (2010). Projected 21st century decrease in marine productivity: A multi-model analysis. *Biogeosciences*, *7*(3), 979–1005. https://doi.org/10.5194/bg-7-979-2010

Steinberg, D. K., Van Mooy, B. A. S., Buesseler, K. O., Boyd, P. W., Kobari, T., & Karl, D. M. (2008). Bacterial vs. Zooplankton control of sinking particle flux in the ocean's twilight zone. *Limnology and Oceanography*, *53*(4), 1327–1338. https://doi.org/10.4319/lo.2008.53.4.1327

Sun, C.-C., Wang, Y.-S., Li, Q. P., Yue, W.-Z., Wang, Y.-T., Sun, F.-L., & Peng, Y.-L. (2012). Distribution characteristics of transparent exopolymer particles in the Pearl River estuary,

China. *Journal of Geophysical Research: Biogeosciences*, *117*(G4). https://doi.org/10.1029/2012JG001951

Tabata, S. (1975). The general circulation of the Pacific Ocean and a brief account of the oceanographic structure of the North Pacific Ocean Part I - circulation and volume transports. *Atmosphere*, *13*(4), 133–168. https://doi.org/10.1080/00046973.1975.9648394

Tabata, S. (1976). The general circulation of the pacific ocean and a brief account of the oceanographic structure of the north pacific ocean: Part II — Thermal regime and influence on the climate. *Atmosphere*, *14*(1), 1–27. https://doi.org/10.1080/00046973.1976.9648398

Tang, T., Kisslinger, K., & Lee, C. (2014). Silicate deposition during decomposition of cyanobacteria may promote export of picophytoplankton to the deep ocean. *Nature Communications*, *5*(1), Article 1. https://doi.org/10.1038/ncomms5143

Taucher, J., Schulz, K. G., Dittmar, T., Sommer, U., Oschlies, A., & Riebesell, U. (2012). Enhanced carbon overconsumption in response to increasing temperatures during a mesocosm experiment. *Biogeosciences*, *9*(9), 3531–3545. https://doi.org/10.5194/bg-9-3531-2012

Thomalla, S. J., Poulton, A. J., Sanders, R., Turnewitsch, R., Holligan, P. M., & Lucas, M. I. (2008). Variable export fluxes and efficiencies for calcite, opal, and organic carbon in the Atlantic Ocean: A ballast effect in action? *Global Biogeochemical Cycles*, *22*(1). https://doi.org/10.1029/2007GB002982

Thornton, D. C. O. (2014). *Dissolved organic matter (DOM) release by phytoplankton in the contemporary and future ocean*. *European Journal of Phycology*, *49*(1), 20-46.

Thornton, D. C. O., & Chen, J. (2017). Exopolymer production as a function of cell permeability and death in a diatom (Thalassiosira weissflogii) and a cyanobacterium (Synechococcus elongatus). *Journal of Phycology*, *53*(2), 245–260. https://doi.org/10.1111/jpy.12470

Toggweiler, J. R. (1993). Carbon overconsumption. *Nature*, *363*(6426), Article 6426. https://doi.org/10.1038/363210a0

Tréguer, P., Bowler, C., Moriceau, B., Dutkiewicz, S., Gehlen, M., Aumont, O., Bittner, L., Dugdale, R., Finkel, Z., Iudicone, D., Jahn, O., Guidi, L., Lasbleiz, M., Leblanc, K., Levy, M., & Pondaven, P. (2018). Influence of diatom diversity on the ocean biological carbon pump. *Nature Geoscience*, *11*(1), 27–37. https://doi.org/10.1038/s41561-017-0028-x

Tréguer, P. J. (2014). The Southern Ocean silica cycle. *Comptes Rendus Geoscience*, *346*(11), 279–286. https://doi.org/10.1016/j.crte.2014.07.003

Van Oostende, N., Harlay, J., Vanelslander, B., Chou, L., Vyverman, W., & Sabbe, K. (2012). Phytoplankton community dynamics during late spring coccolithophore blooms at the continental margin of the Celtic Sea (North East Atlantic, 2006–2008). *Progress in Oceanography*, *104*, 1–16. https://doi.org/10.1016/j.pocean.2012.04.016

Varela, D. E., Crawford, D. W., Wrohan, I. A., Wyatt, S. N., & Carmack, E. C. (2013). Pelagic primary productivity and upper ocean nutrient dynamics across Subarctic and Arctic Seas. *Journal of Geophysical Research: Oceans*, *118*(12), 7132–7152. https://doi.org/10.1002/2013JC009211

Varela, D. E., & Harrison, P. J. (1999). Seasonal variability in nitrogenous nutrition of phytoplankton assemblages in the northeastern subarctic Pacific Ocean. *Deep Sea*

*Research Part II: Topical Studies in Oceanography*, *46*(11), 2505–2538. https://doi.org/10.1016/S0967-0645(99)00074-0

Verdugo, P., Alldredge, A. L., Azam, F., Kirchman, D. L., Passow, U., & Santschi, P. H. (2004). The oceanic gel phase: A bridge in the DOM–POM continuum. *Marine Chemistry*, *92*(1), 67–85. https://doi.org/10.1016/j.marchem.2004.06.017

Wei, Y., Sun, J., Chen, Z., Zhang, Z., Zhang, G., & Liu, X. (2021). Significant contribution of picoplankton size fraction to biogenic silica standing stocks in the Western Pacific Ocean. *Progress in Oceanography*, *192*, 102516. https://doi.org/10.1016/j.pocean.2021.102516

Wei, Y., Wang, X., Gui, J., & Sun, J. (2021). Significant Pico- and Nanoplankton Contributions to Biogenic Silica Standing Stocks and Production Rates in the Oligotrophic Eastern Indian Ocean. *Ecosystems*, *24*(7), 1654–1669. https://doi.org/10.1007/s10021-021-00608-w

Wetz, M. S., Robbins, M. C., & Paerl, H. W. (2009). Transparent Exopolymer Particles (TEP) in a River-Dominated Estuary: Spatial–Temporal Distributions and an Assessment of Controls upon TEP Formation. *Estuaries and Coasts*, *32*(3), 447–455. https://doi.org/10.1007/s12237-009-9143-2

Whitney, F. A., & Freeland, H. J. (1999). Variability in upper-ocean water properties in the NE Pacific Ocean. *Deep Sea Research Part II: Topical Studies in Oceanography*, *46*(11), 2351–2370. https://doi.org/10.1016/S0967-0645(99)00067-3

Wohlers, J., Engel, A., Zöllner, E., Breithaupt, P., Jürgens, K., Hoppe, H.-G., Sommer, U., & Riebesell, U. (2009). Changes in biogenic carbon flow in response to sea surface

warming. *Proceedings of the National Academy of Sciences*, *106*(17), 7067–7072. https://doi.org/10.1073/pnas.0812743106

Woodgate, R. A., Aagaard, K., & Weingartner, T. J. (2006). Interannual changes in the Bering Strait fluxes of volume, heat and freshwater between 1991 and 2004. *Geophysical Research Letters*, *33*(15). https://doi.org/10.1029/2006GL026931

Wurl, O., Miller, L., & Vagle, S. (2011). Production and fate of transparent exopolymer particles in the ocean. *Journal of Geophysical Research: Oceans*, *116*(C7). https://doi.org/10.1029/2011JC007342

Yamada, Y., Fukuda, H., Uchimiya, M., Motegi, C., Nishino, S., Kikuchi, T., & Nagata, T. (2015). Localized accumulation and a shelf-basin gradient of particles in the Chukchi Sea and Canada Basin, western Arctic. *Journal of Geophysical Research: Oceans*, *120*(7), 4638–4653. https://doi.org/10.1002/2015JC010794

Yamada, Y., Yokokawa, T., Uchimiya, M., Nishino, S., Fukuda, H., Ogawa, H., & Nagata, T. (2017). Transparent exopolymer particles (TEP) in the deep ocean: Full-depth distribution patterns and contribution to the organic carbon pool. *Marine Ecology Progress Series*, *583*, 81–93. https://doi.org/10.3354/meps12339

Zamanillo, M., Ortega-Retuerta, E., Nunes, S., Estrada, M., Sala, M. M., Royer, S.-J., López-Sandoval, D. C., Emelianov, M., Vaqué, D., Marrasé, C., & Simó, R. (2019). Distribution of transparent exopolymer particles (TEP) in distinct regions of the Southern Ocean. *Science of The Total Environment*, *691*, 736–748. https://doi.org/10.1016/j.scitotenv.2019.06.524

Zamanillo, M., Ortega-Retuerta, E., Nunes, S., Rodríguez-Ros, P., Dall'Osto, M., Estrada, M., Montserrat Sala, M., & Simó, R. (2019). Main drivers of transparent exopolymer particle

distribution across the surface Atlantic Ocean. *Biogeosciences*, *16*(3), 733–749. https://doi.org/10.5194/bg-16-733-2019

Zäncker, B., Engel, A., & Cunliffe, M. (2019). Bacterial communities associated with individual transparent exopolymer particles (TEP). *Journal of Plankton Research*, *41*(4), 561–565. https://doi.org/10.1093/plankt/fbz022

# Appendix A: Quantifying %TEP-C in the Eastern Subarctic Northeast Pacific and Arctic regions

## A.1 Objective

The ratio of C in the form of TEP relative to total POC concentrations (%TEP-C) is a biogeochemically important fraction, as discussed in *General Introduction: Variation in the efficiency of the biological carbon pump.* Therefore, samples of C in the form of TEP (TEP-C), alongside total POC measurements were taken over the entire spatiotemporal range of this study. This appendix seeks to evaluate the overall distribution of these ratios, and to determine spatial and temporal variation. This section demonstrates the relative consistency of TEP based C to total POC across the Subarctic and Arctic, with limited spatial variation.

## A.2 Methods

Samples were collected in the same fashion as *Chapter 1: Estimating the concentration of transparent exopolymer particles (TEP) in Arctic and Subarctic Oceans using in situ measurements and model predictions*. This involved sampling across the ESNP and Arctic regions, with sample collection occurring on the Line P and La Perouse programs from 2019 – 2022, and on the DBO and JOIS throughout 2022-2023. Measurements for TEP and POC were taken as outlined in the same chapter. A two-way ANOVA was used to estimate significant differences across regions and seasons.

## A.3 Results and Implications

The fraction of POC composed of TEP-C, or the %TEP-C, was relatively consistent across both the ESNP and Arctic regions. Lowest values of %TEP-C were observed during

winter seasons in the ESNP, with values of <1% observed. Highest %TEP-C values were observed in off-shelf regions of the ESNP in the summer, with a maximum value of 33.2% recorded (Figure A.1). Ranges and median values of %TEP-C are shown in Figure A.1, for each region and season sampled.

Little spatiotemporal variability was observed in %TEP-C values. A two-way ANOVA, using region (ESNP on-shelf, ESNP off-shelf, BE-CH, BS-CB), and season (spring, summer, fall, winter) as independent variables revealed only significantly higher values of %TEP-C in summer versus winter seasons. These results suggest that C in the form of TEP can consistently represent ~5-15% of total POC in the Subarctic and Arctic regions.

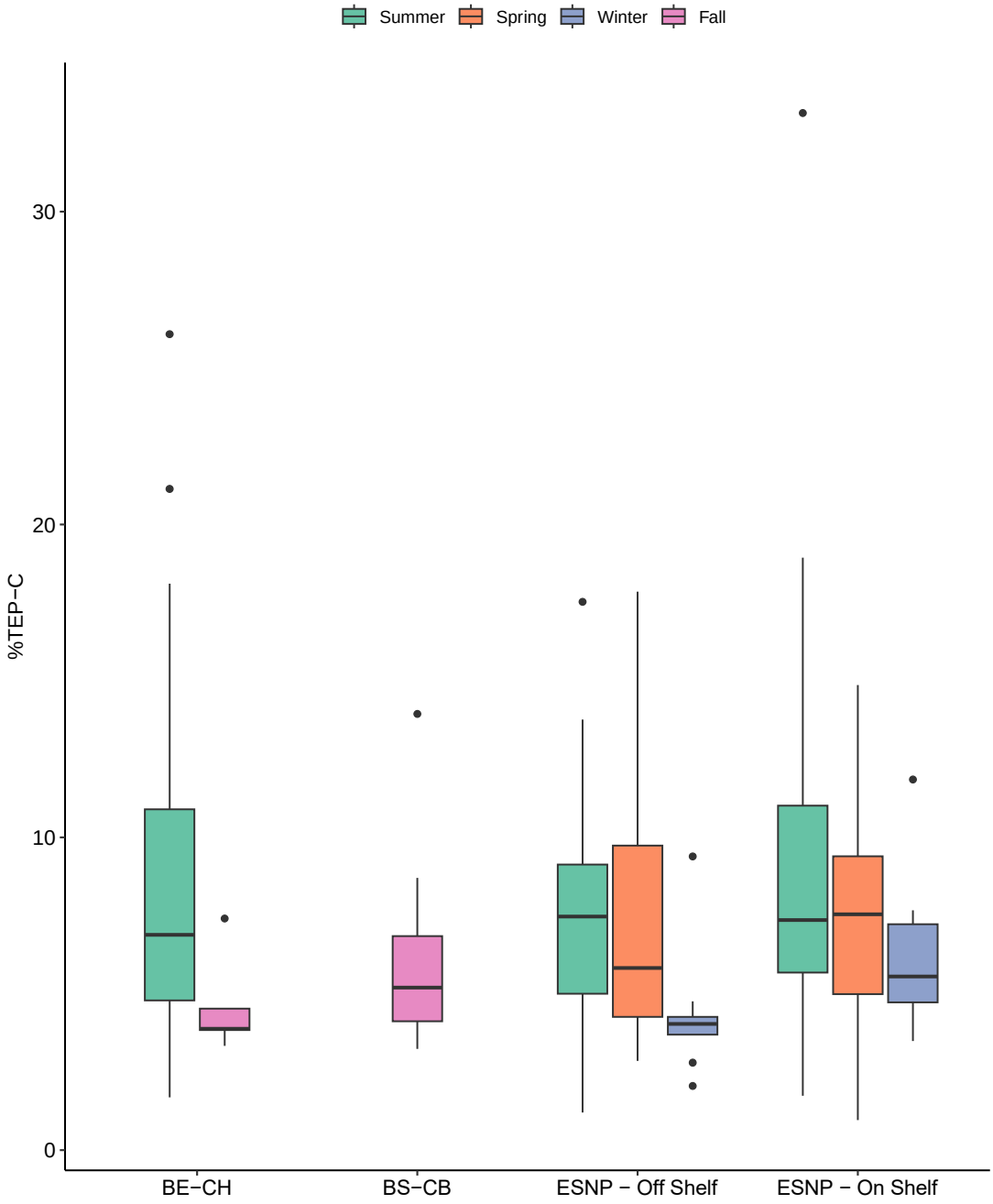


**Figure A.1.** The ratio (%) of POC composed of TEP-C across each subregion and season examined in this thesis. Boxplots displays means and ranges in the dataset, with single points representing outliers and the boxes representing the 50% interquartile range.

# Appendix B: Main predictors of %TEP-C ratios in the Subarctic and Arctic regions

## B.1. Objective

This thesis dedicated a major portion of its work to understanding the main predictors of TEP in marine environments, however, I did not include an analysis of the main biological or environmental factors that influence the relative concentration of TEP-C to POC (%TEP-C). Thus, this appendix section aims to provide a brief overview of the main variables that explained variance in %TEP-C ratios. I demonstrate that the %TEP-C was not associated with any biological variables (in direct contrast to total TEP concentrations), but instead, was highly correlated with environmental conditions including temperature, nutrient concentrations, and mixed layer depth.

## B.2. Methods

Sampling locations and chemical analyses for this section were performed in the same fashion as *Chapter 3.3.5,* and as *Appendix A.* Linear regression analyses were used to determine significant relationships between %TEP-C and independent variables.

## B.3. Results and Implications

The %TEP-C was generally not correlated with any biological metrics. Instead, significant positive correlations were observed with temperature, salinity, and 24h averaged PAR in the ESNP. Significant negative correlations were also observed in the ESNP with all nutrient concentrations ($NO_3^-$; $PO_4^{3-}$; $Si(OH)_4^-$) and the depth of the mixed layer (Table A1) (MLD).

Regression analyses in the Arctic revealed similar, but overall weaker trends. Of note is the same coefficient direction between %TEP-C and temperature, MLD, and nutrient concentrations across both regions.

These results suggest that the fraction of total POC composed of TEP-C is primarily driven by the environment, and not total biomass or productivity. Of particular interest is the negative associations with nutrient concentrations, as EPS exudation/TEP production by phytoplankton is known to increase under conditions of nutrient limitation through a process known as carbon overconsumption (see *Chapter 1.5* for more detail and references). Temperature is also known to have a stimulatory effect on EPS production by phytoplankton, and thus may explain why the %TEP-C is positively correlated with temperature across both the Subarctic and Arctic region (see *Chapter 2.5.3* for more detail and references).

**Table B.1.** Linear regression statistics between %TEP-C and independent biological or environmental variables (Ind. Var.) in the Eastern Subarctic North Pacific and Arctic. Bold font denotes statistical significance ($p < 0.05$).

| Ind. Var. | Region | $R^2$ | $p$ | Coefficient | Region | $R^2$ | $p$ | Coefficient |
|---|---|---|---|---|---|---|---|---|
| Chlorophyll *a* | ESNP | 0.00 | 0.65 | | Arctic (BE-CH + BS-CB) | 0.00 | 0.51 | |
| POC | | 0.00 | 0.79 | | | 0.03 | 0.10 | |
| DO | | 0.00 | 0.55 | | | **0.05** | **0.05** | **-0.40** |
| Fluorescence | | 0.00 | 0.85 | | | 0.01 | 0.21 | |
| C uptake | | 0.00 | 0.31 | | | N/A | | |
| $NO_3^-$ uptake | | 0.00 | 0.56 | | | N/A | | |
| New production | | 0.00 | 0.34 | | | N/A | | |
| Silica uptake | | 0.01 | 0.22 | | | N/A | | |
| Nitrate conc. | | **0.08** | **<<0.01** | **-0.22** | | **0.03** | **0.08** | **-0.27** |
| Silica conc. | | **0.04** | **<<0.01** | **-0.10** | | 0.00 | 0.24 | |
| Phosphate conc. | | **0.02** | **0.04** | **-1.92** | | **0.03** | **0.10** | **-1.78** |
| Temperature | | **0.06** | **<<0.01** | **0.35** | | **0.06** | **0.01** | **0.42** |
| MLD | | **0.02** | **0.04** | **-0.04** | | **0.03** | **0.07** | **-0.18** |
| Density | | 0.00 | 0.15 | 0.34 | | | | |
| Salinity | | **0.03** | **0.04** | **0.85** | | | | |
| 24h-PAR | | **0.03** | **0.01** | **0.005** | | | | |

# Appendix C: Remote-sensing derived TEP predictions using chlorophyll *a* and temperature as predictors

## C.1. Objective

The results from *Chapter 1: Estimating the concentration of transparent exopolymer particles (TEP) in Arctic and Subarctic Oceans using in situ measurements and model predictions* indicate that TEP can be accurately predicted from chlorophyll *a*, temperature, MLD and nutrient concentrations within the upper mixed layer of the ESNP. These findings, coupled with recent work by Ortega-Retuerta et al., (2017), who suggest that TEP can be predicted using satellite derived chlorophyll *a*, provided motivation for this appendix section. Here, I aimed to derive large scale predictions of TEP at the ocean's surface across the ESNP using chlorophyll *a* and temperature as predictors (i.e., dependent variables) of TEP. First, I show cross validation results of MLR and RFR that demonstrates the utility of these variables as TEP predictors in the region. Second, I apply a RFR model to satellite derived chlorophyll *a* and temperature products to provide a large-scale visualization of surface TEP.

## C.2. Methods

Sampling locations, chemical analyses, and statistical analyses for this appendix were performed in the same fashion as *Chapter 2.3.* However, multiple linear regression (MLR) and random forest regression (RFR) analyses were instead only composed of chl-*a* and temperature as TEP predictors. All other methods, statistical analyses, and cross validation techniques were performed in the same fashion. The models were only trained on data from the ESNP, as described in *Chapter 2.3.* The model was trained on TEP data in units of XG eq $L^{-1}$, and the model predictions were subsequently converted to TEP-C (µg C $L^{-1}$).

The RFR model was used to derive predictions from remote sensing of chlorophyll *a* and temperature as it was more accurate in predicting TEP compared to the MLR when evaluated using cross validation techniques. Data for satellite derived estimates of surface TEP was obtained from the *Ocean Color* NASA database from the instrument *Modis-Aqua*. This instrument is part of both the *Terra* and *Aqua* satellites. Data for chlorophyll *a* and SST were collected from this database at level L3 8-day 4km resolution, from August 24$^{th}$ – September 2$^{nd}$, 2021 (the same temporal range as the sampling occurrences of Line P 2021-008). The *Modis* chl-*a* concentration algorithm returns near surface concentration of chl-*a*, calculated from derived empirical relationships from *in situ* measurements and blue to green band ratios of *in situ* remote sensing reflectance (doi:10.5067/AQUA/MODIS/L3M/POC/2018).

## C.3. Results and Implications

The use of chl-*a* and temperature as model inputs of surface TEP-C provided accurate TEP predictions when cross validated on new data inputs, with a MAE of 10.8 and 12.2 for RFRs and MLRs, respectively (Figure C.1). The MLR regression had an $R^2 = 0.67$, while the RFR had an $R^2 = 0.74$. While these results are less accurate, and explain less variance, than the model results from *Chapter 2.4.5* for both MLRs and RFRs, they still provided accurate predictions of TEP as shown in Figure C.1. Additionally, the MLR still satisfied linear modelling assumptions (including normal distribution of residuals and lack of multicollinearity between dependent variables). These results demonstrate that TEP (TEP-C) can be predicted at the oceans surfaces using chl-*a* and temperature and RFR modelling techniques. While the MLR provided some promising results, there is evidence of increased error rates (i.e., larger residuals) at higher concentrations of TEP (Figure C.1).

I applied the RFR model derived in this section to surface chl-*a* and temperature data obtained from the *Modis-Aqua* algorithm to predict TEP-C concentrations across the ESNP, including the entire spatial range of Line P and La Perouse programs from which the model data is based off. This data was taken as an 8-day average, covering the same temporal range as the Summer 2021 Line P cruise (ID: 2021-008). This provides the first large scale visualizations and estimations of TEP-C to date (Figure C.2).

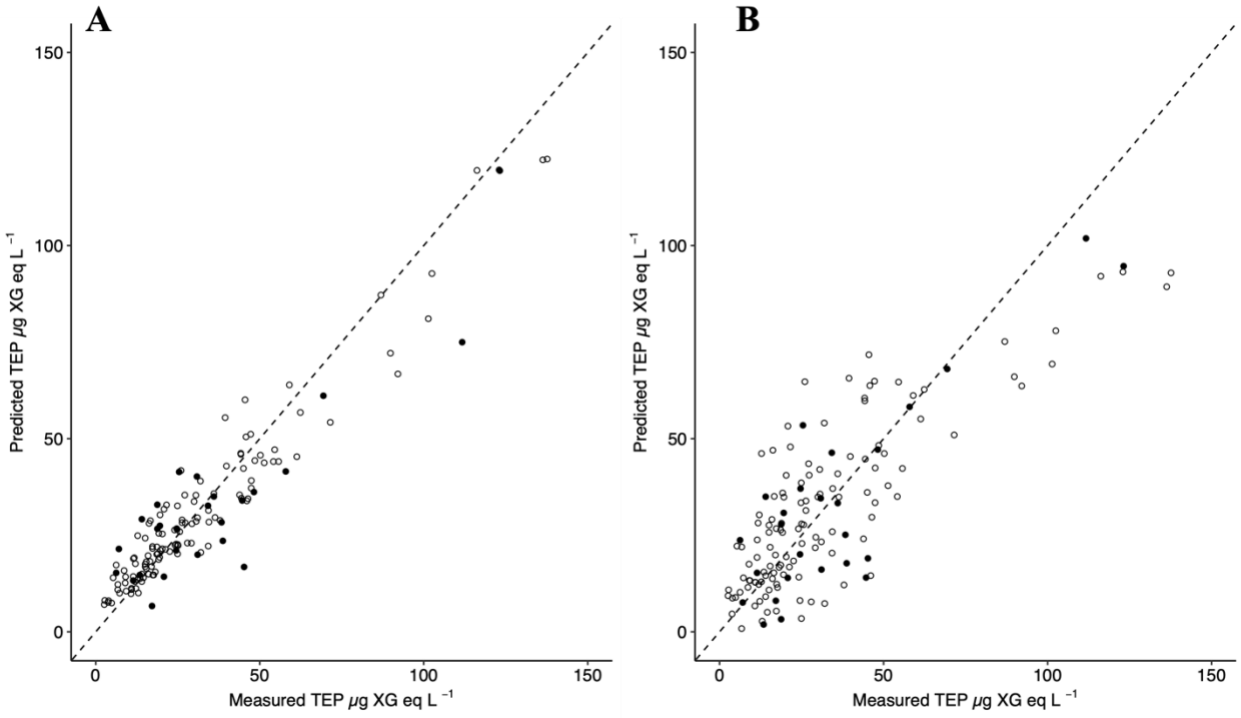


**Figure C.1.** Comparison between observed and predicted values by both Random Forest Regression (RFR) (**A**) and Multiple Linear Regression (MLR) (**B**) models in the ESNP. The models were trained on 80% of the data (open circles) and tested on the "hold-out" 20% (filled circles). Dashed lines indicate a 1:1 slope between measured and predicted values.

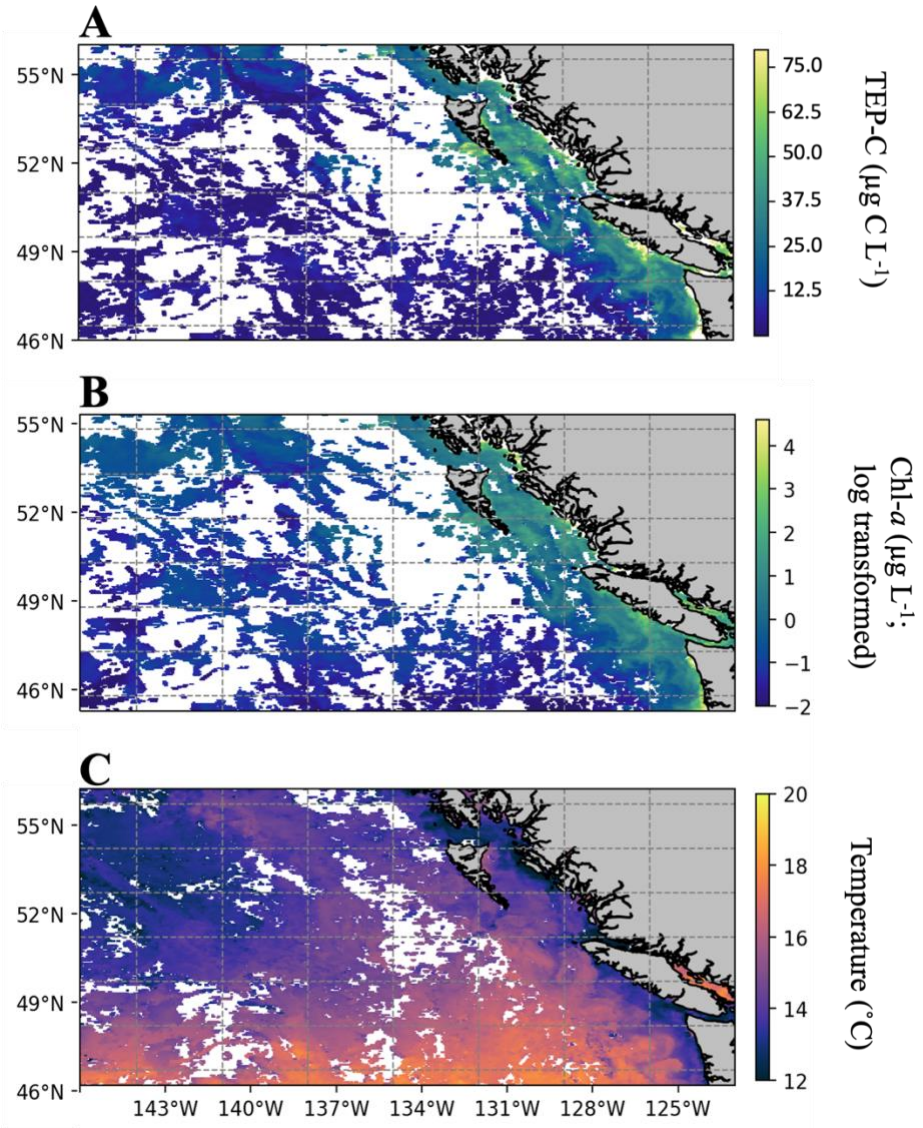


**Figure C.2.** Random Forest Regression predictions of TEP-C (**A**), using dependent variables from satellite derived products of chlorophyll-a (**B;** log transformed), and temperature (**C**). Model predictions and satellite products cover an 8-day period from August 24$^{th}$ – September 2$^{nd}$, 2021, corresponding to the Line P 2021-008 cruise period.

# Appendix D: Size-fractionated Chlorophyll-*a* and Biogenic Silica Across the Eastern Subarctic North Pacific

## D.1. Objective

The objective of this section was to quantify chlorophyll-*a* (chl-*a*) and biogenic silica (bSi) in different phytoplankton size fractions across the ESNP. Proxies of phytoplankton and diatom biomass (chl-*a* and bSi, respectively) were measured in >5µm and <5µm size fractions across multiple seasons throughout 2019-2021 in coastal, shelf-break, transition, and HNLC regions of the ESNP. In 2021, size fractions >5µm, <5µm, and <2µm were measured.

## D.2. Methods

Samples for this section were taken at the same stations as in *Chapter 3.3.1* and analyzed in the same fashion as *Chapter 4.3.3* (in the case of bSi), and *Chapter 2.3.4* (for chl-*a*). Size fractionated chl-*a* samples were taken by sequentially filtering 500ml seawater through 5µm (>5µm samples), 2µm (>2µm samples), and 0.7µm filters (total samples) (2x polycarbonate and glass fiber filter, respectively). Size fractionated bSi samples were taken in the same fashion, but with all polycarbonate filters. All samples were immediately frozen onboard the vessel at -20˚C. Regional characterization was defined as in *Chapter 3.3.1*. Three way ANOVAs were used to compute statistical differences between subregions, seasons, and years for both chl-*a* and bSi and all relevant size fractions.

## D.3. Results and Implications

Total chl-*a* was significantly higher in coastal regions compared to shelf-break, transition, and HNLC regions ($p < 0.05$); no significant differences were observed among shelf-break, transition, and HNLC regions, and no seasonal significance was detected (Figure D.1.) Chl-*a* <5 µm was significantly lowest in transition regions compared to all other regions ($p < 0.05$), and coastal regions were significantly higher in <5 µm chl-*a* compared to HNLC regions ($p < 0.05$). No seasonal variation was also observed in <5 µm chl-*a*. The <2 µm chl-*a* fraction was only measured on shelf-break, transition and HNLC regions, and was only significantly higher in shelf-break vs HNLC regions ($p < 0.05$). No significant annual variation was observed in total or size fractionated chl-*a*. The fraction of total chl-*a* composed of <5 µm chl-*a* did vary significantly in space, with all oceanic regions (shelf-break, transition, and HNLC) characterized by significantly higher fractions of small chl-*a* ($p < 0.05$).

Trends in total bSi mirrored that of chl-*a*. Total bSi was significantly higher in coastal regions compared to shelf-break, transition, and HNLC regions ($p < 0.05$), with some evidence of seasonally higher values in summer compared to spring ($p = 0.07$; winter data not available). However, size fractionated bSi (both <5µm and <2µm) did not vary significantly in space or time.

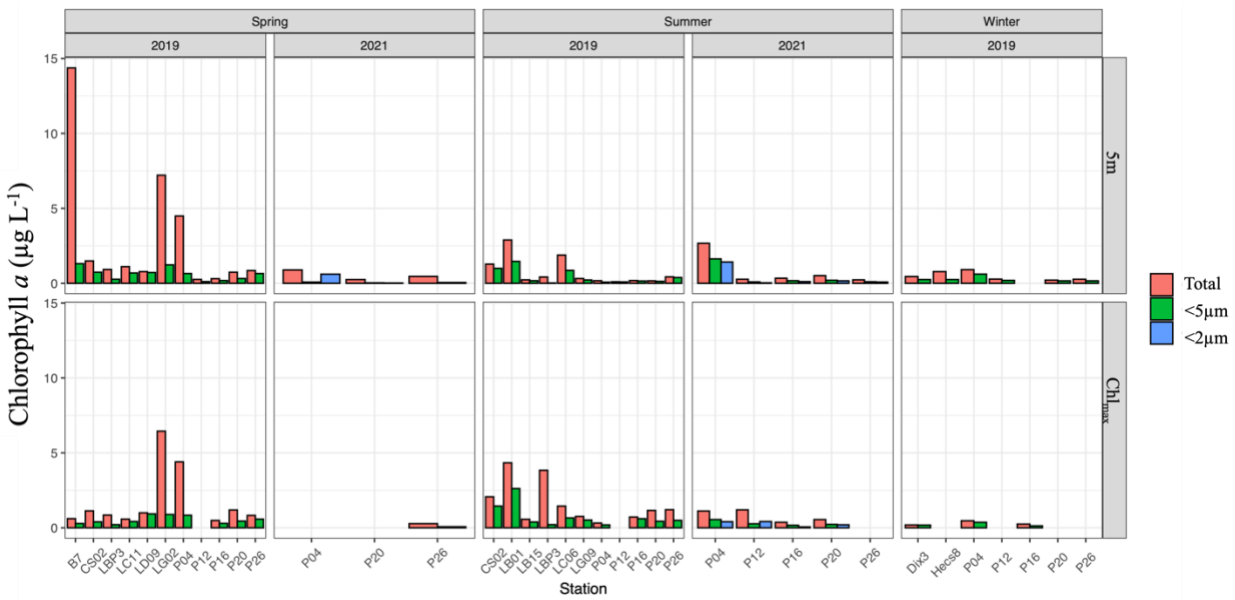


**Figure D.1.** Total, <5 µm, and <2 µm chlorophyll-a across the Eastern Subarctic North Pacific during spring and summer of 2019, winter 2020, and spring and summer of 2021. Samples were taken at both 5m and the chlorophyll max ($Chl_{max}$). Not all stations shown have size fractionated values available across all years, seasons, or depths. Samples for <2 µm chlorophyll *a* were only taken in 2021.

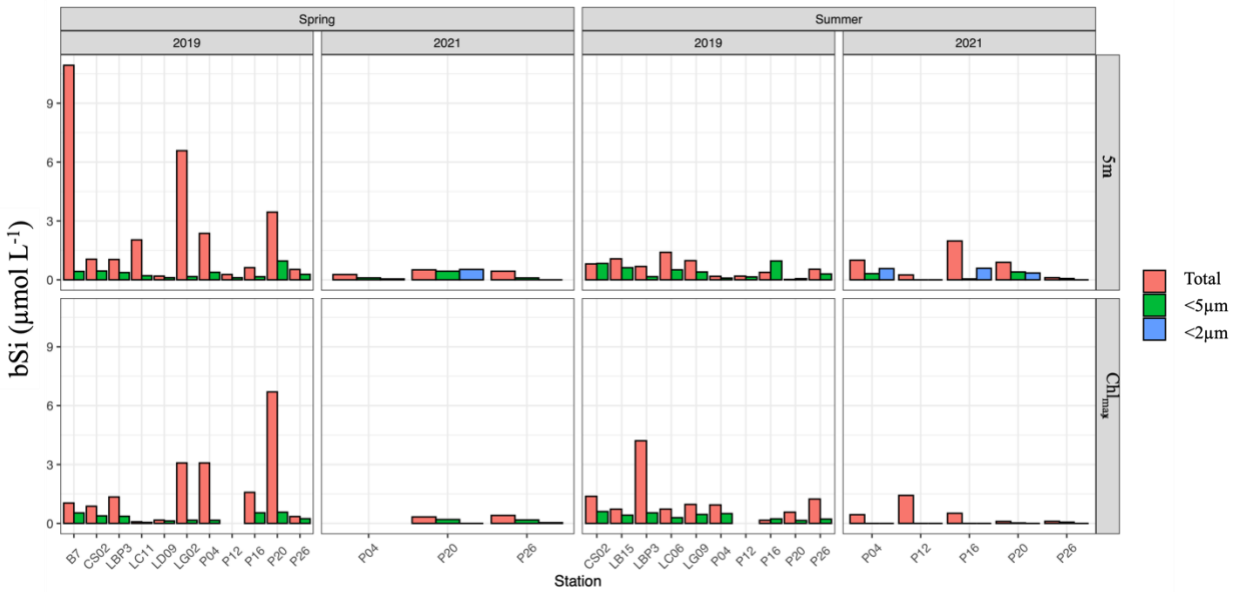


**Figure D.2.** Total, <5 µm, and <2 µm biogenic silica across the Eastern Subarctic North Pacific during spring and summer of 2019, winter 2020, and spring and summer of 2021. Samples were taken at both 5m and the chlorophyll max ($Chl_{max}$). Not all stations shown have size fractionated values available across all years, seasons, or depths. Samples for <2 µm biogenic silica were only taken in 2021.

# Appendix E: The contributions of picophytoplankton to carbon, nitrate, and silicic acid uptake in the Eastern Subarctic North Pacific

## Objective

The objective of this section was to quantify the contributions of picophytoplankton (<2 µm) to nutrient uptake rates along Line P in the ESNP. Few studies have simultaneously measured ρC, $\rho NO_3^-$, and ρSi in picophytoplankton size fractions; to my knowledge, this is only one of a few studies to quantify picophytoplankton contributions to ρSi.

## Methods

Nutrient uptake experiments for ρC, $\rho NO_3^-$, and ρSi were conducted in the spring and summer of 2021, along Line P cruises 2021-006 and 2021-008 (as described in *Table 4.1*). Nutrient uptake experiments for ρC, $\rho NO_3^-$, and ρSi was performed using the same methodology as described in *Chapter 4.3.3*. For size fractionation, in the case of ρC and $\rho NO_3^-$, seawater was filtered through a 2 µm polycarbonate filter (to remove particles >2 µm), and the filtrate was collected onto a 0.75 µm glass fiber filter. In the case of ρSi, seawater was filtered through both 2 µm and 0.6 µm polycarbonate filters; the contribution of <2 µm size fraction was then calculated as the difference between ρSi on the 0.6 µm and 2 µm filters. Samples analyses and rate calculations were performed as outlined in *Chapter 4.3.3*.

## Results and Implications

Picophytoplankton ρC and $\rho NO_3^-$ ranged from 0.02-6.6 µmol C $L^{-1}$ $d^{-1}$, and <0.01 – 0.72 µmol N $L^{-1}$ $d^{-1}$, respectively. Very low values for ρC and $\rho NO_3$ by picophytoplankton were

observed at the chlorophyll max compared to 5m. Summer values were generally higher than spring values, although no statistical tests were performed due to low sample sizes.

Picophytoplankton ρSi were very low (<0.0001 – 0.003 μmol Si $L^{-1}$ $d^{-1}$), and much lower than what would be expected from Redfield Stoichiometry if compared to ρC and $\rho NO_3^-$ by phytoplankton. Nonetheless, I provide evidence of very small contributions of picophytoplankton to ρSi in the ESNP.

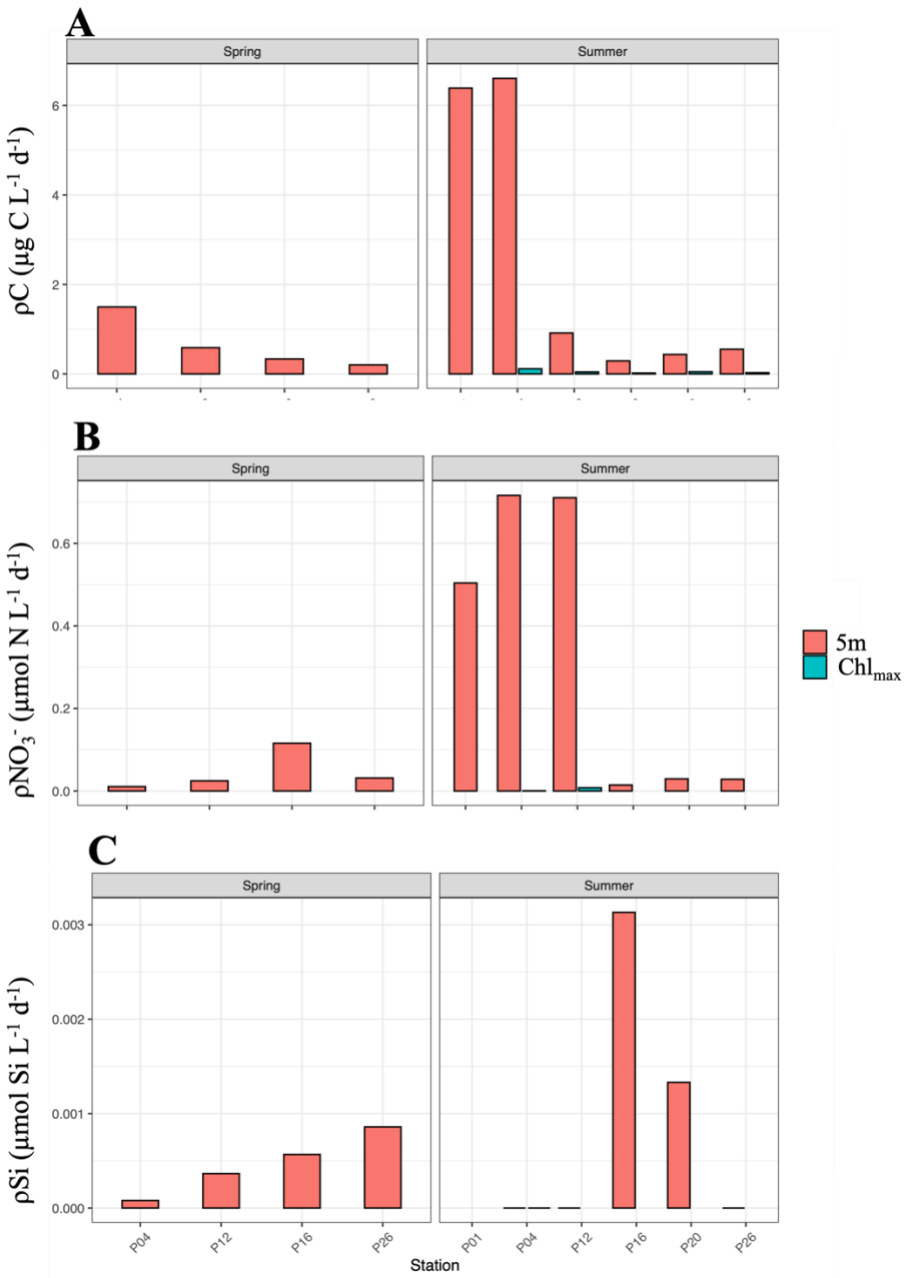


**Figure E.1.** Picophytoplankton nutrient uptake rates, including C uptake (ρC; **A**), $NO_3^-$ uptake (ρ $NO_3^-$; **B**), and silicic acid uptake (ρSi, **C**). Samples were taken during spring and summer 2021 along Line P in the Eastern Subarctic North Pacific. Nutrient uptake rates were taken at 5m, and in summer 2021, at the chlorophyll max depth ($Chl_{max}$).